

UNCLASSIFIED

AD NUMBER: AD0481550

LIMITATION CHANGES

TO:

Approved for public release; distribution is unlimited.

FROM:

Distribution authorized to US Government Agencies only; Proprietary Information; Export Controlled; 1 Mar 1966. Other requests shall be referred to Air Force Weapons Laboratory, Kirtland AFB, NM 87117.

AUTHORITY

AFWL ltr dtd 30 Nov 1971

AFWL-TR-64-169

AFWL-TR
64-169

481550

**A MODELING HANDBOOK INCLUDING
EXPERIMENTS ON INELASTIC DEFORMATIONS
OF CONICAL SHELLS**

**Carl G. Langner
Wilfred E. Baker**

**Southwest Research Institute
San Antonio, Texas
Contract No. AF 29(601)-6033**



TECHNICAL REPORT NO. AFWL-TR-64-169

March 1966

**AIR FORCE WEAPONS LABORATORY
Research and Technology Division
Air Force Systems Command
Kirtland Air Force Base
New Mexico**

AFWL-TR-64-169

Research and Technology Division
AIR FORCE WEAPONS LABORATORY
Air Force Systems Command
Kirtland Air Force Base
New Mexico

When U. S. Government drawings, specifications, or other data are used for any purpose other than a definitely related Government procurement operation, the Government thereby incurs no responsibility nor any obligation whatsoever, and the fact that the Government may have formulated, furnished, or in any way supplied the said drawings, specifications, or other data, is not to be regarded by implication or otherwise, as in any manner licensing the holder or any other person or corporation, or conveying any rights or permission to manufacture, use, or sell any patented invention that may in any way be related thereto.

This report is made available for study with the understanding that proprietary interests in and relating thereto will not be impaired. In case of apparent conflict or any other questions between the Government's rights and those of others, notify the Judge Advocate, Air Force Systems Command, Andrews Air Force Base, Washington, D. C. 20331.

This document is subject to special export controls and each transmittal to foreign governments or foreign nationals may be made only with prior approval of AFWL (WLRP), Kirtland AFB, NM. Distribution is limited because of the technology discussed in the report.

AFWL-TR-64-169

A MODELING HANDBOOK
INCLUDING EXPERIMENTS ON INELASTIC
DEFORMATIONS OF CONICAL SHELLS

Carl G. Langner
Wilfred E. Baker

Southwest Research Institute
San Antonio, Texas
Contract No. AF29(601)-6033

TECHNICAL REPORT NO. AFWL-TR-64-169

This document is subject to special export controls and each transmittal to foreign governments or foreign nationals may be made only with prior approval of AFWL (WLRP), Kirtland AFB, NM. Distribution is limited because of the technology discussed in the report.

FOREWORD

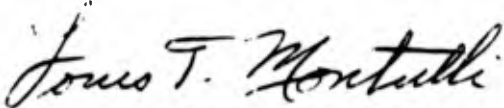
This report was prepared by the Southwest Research Institute (SwRI Project 02-1361) San Antonio, Texas, under Contract AF29(601)-6033. The work represents an extension of SwRI Project 96-1151-2 under Contract AF29(601)-4923.

The research was performed under Program Element 7.60.06.01.D, Project 5776, Task 15.029, and was funded by the Defense Atomic Support Agency (DASA) under DASA MIPR 541-63.

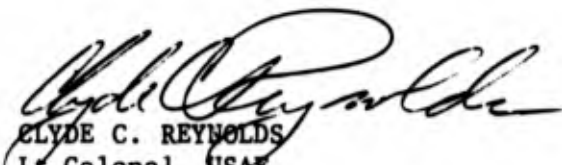
Inclusive dates of research were June 1963 through October 1965. The report was submitted 9 February 1966 by the AFWL Project Officer, 1Lt Louis T. Montulli (WLRP).

The authors wish to acknowledge the contributions of the following persons to this report: Dr. G. E. Nevill, formerly with SwRI, now with the University of Florida (Gainesville), initiated the project and directed most of the work. Mr. Fred O. Hoese conducted the materials development program, fabricated the models, and helped in conducting the model and prototype tests. The authors also wish to thank the project officers, Lt Richard Brightman and Lt Louis Montulli, for their patient supervision of this work.

This report has been reviewed and is approved.



LOUIS T. MONTULLI
1Lt USAF
Project Officer



ELYDE C. REYNOLDS
Lt Colonel USAF
Chief, Physics Branch



WILLIAM H. STEPHENS
Colonel USAF
Chief, Research Division

ABSTRACT

The results of model studies and experiments related to response of truncated conical shells to impulsive loading are presented. Theory of modeling is discussed in some detail, with particular emphasis on scaling of elastic and plastic response of shell structures when these structures are made of material different from those in a prototype structure (dissimilar materials). Work on development of dissimilar model materials and techniques for fabrication of conical shell models is then presented. Next, the experimental phase of the program, including test arrangement and instrumentation for both shock-tube and sprayed-explosive loadings, and results for maximum transient and residual displacements of the conical shells are discussed. The report is completed with conclusions on the study, and recommendations for further work to corroborate the concept of modeling of dynamic structural response using dissimilar materials. The report also includes supporting theoretical analyses as appendices.

CONTENTS

<u>Section</u>		<u>Page</u>
I.	INTRODUCTION	1
	1. The Modeling Approach	1
	2. The Model Law	2
	3. Advantages of Modeling with Dissimilar Materials	3
	4. Disadvantages of Modeling with Dissimilar Materials	4
II.	MODELING ANALYSIS	6
	1. Specification of Independent and Dependent Variables	6
	2. Dimensional Analysis	8
	3. Derivation of the Model Law	10
	4. Implications of the Model Law	11
	5. Subjective Aspects of Modeling	14
III.	ERRORS IN MODELING	16
	1. Classification of Modeling Investigations	16
	2. Sources of Modeling Errors	18
	3. Error Predictions and Corrections	20
IV.	MATERIALS DEVELOPMENT AND MODEL FABRICATION	23
	1. Chronological Summary of Developments	23
	2. Material Tests and Properties	24
	3. Corrections for Strain-Rate Effects	25
	4. Selection of the Model Materials	27
	5. Production of the Model Materials	29
	6. Fabrication of the Models	30
V.	EXPERIMENTS	32
	1. Definitions of the Variables	32
	2. The Prototype Variables	34
	3. Scale Factors	36
	4. The Model Variables	37
	5. The Shock Tube Model Test Facility	40
	6. Model Test Procedure	42
	7. Model Test Results	45
	8. The Sprayed Explosive Loading Technique	49
	9. The Prototype Tests	50

CONTENTS (Cont'd)

<u>Section</u>		<u>Page</u>
VI.	CONCLUSIONS AND RECOMMENDATIONS	52
	1. Conclusions	52
	2. Recommendations	53
	REFERENCES	55
	APPENDICES	57
	A. A Brief Review of Continuum Mechanics	58
	B. Dimensional Analysis (Abstract Treatment)	62
	C. Theory of Modeling (Abstract Treatment)	65
	D. Solid Material Behavior and Constitutive Equations	67
	TABLES AND ILLUSTRATIONS	79
	Distribution	108

LIST OF ILLUSTRATIONS

<u>Figure</u>		<u>Page</u>
1	Compression Test Specimens	88
2	Interpretation of Uniaxial Compression Test Data	89
3	Shell Geometry	90
4	Idealized Impulsive Load Distribution and Transient Displacements of a Conical Frustrum Shell	91
5	Schematic Diagram of Model Test Facility	92
6	Shock Tube Model Test Facility	94
7	Model Shell Mounted on the Test Stand	95
8	Sprayed Explosives Test Facility	96
9	Calibration and Test Records	97
10	Impulse-Deformation Characteristics of the Models, I	98
11	Impulse-Deformation Characteristics of the Models, II	99
12	Standard Cone Model M1, Before and After Testing	100
13	Standard Cylinder Model M7, Before and After Testing	101
14	Thick Cone Model M6 and Heat Shield Model M2	102
15	Sandwich Model M3 and Foam-Filled Model M4	103
16	Prototype Test Facility	104
17	Sandwich Prototype Shell, After Receiving an Impulse of 14,000 Dyne-Sec/Cm ²	105
18	Heat-Shield Prototype Shell, After Receiving an Impulse of 3500 Dyne-Sec/Cm ²	106
19a	Stress Vectors Associated with Uniaxial Stress	107
19b	Strain Vectors Associated with Uniaxial Stress	107

LIST OF TABLES

<u>Table</u>		<u>Page</u>
I	Measured Properties of Prototype Materials	80
II	"Static" Properties of the Model Materials	80
III	"Dynamic" Properties of the Model Materials	80
IV	Compositions of Prototype and Model Materials	81
V	Pertinent Shell Variables	82
VI	Scale Factors and Modeling Relationships	83
VII	Prototype Specifications	84
VIII	Model Specifications	84
IX	Shock Tube Loading Characteristics	85
X	Model Test Results	86
XI	Model Test Results in Dimensionless Form	87

SECTION I

INTRODUCTION

Scaled models have been used extensively as a tool for analysis of structures. Examples of modeling investigations can be found in Langhaar's book [2] and in the ASME publication [3] on "Use of Models and Scaling in Shock and Vibration". The latter also contains numerous references to recent literature on modeling. The class of structural problems to which the theory of modeling has been applied has been restricted largely to determination of static or steady-amplitude vibrational forces and displacements in elastic structures.

As the science of mechanics progresses to include more complicated material effects, the possibility of modeling these effects arises. Recently the plastic and viscous regimes of solid material behavior have received widespread attention [4-11]. The eventual generalization from modeling elastic response of structures due to static loads is modeling elastic, plastic, viscous, and inertial response of structures due to transient loads. Baker [4] presented a modeling investigation of large deformations of structures subjected to transient loads; this investigation was similar to the present investigation but differed in that the same materials were used in the models and prototypes, and strain-rate (viscous) effects were neglected.

1. The Modeling Approach

This report describes a novel approach to the problem of predicting permanent deformations of full-scale structures (hereafter called prototypes) subjected to transient pressure loadings. The method involves building small-scale (geometrically similar) models of the prototypes, and testing these models using pressure loadings that are scaled from the corresponding full-scale pressure loadings, according to a certain model law. The model law also provides the means of predicting the deformations of the prototypes from the observed deformations of the models.

The novel feature of the approach presented in this report is the use of dissimilar materials for constructing the models. (The word dissimilar as used throughout this report conveys the meaning "different but similar", and may be properly considered as a contraction of this phrase.) The model materials are specifically tailored so that the mass densities and the deformation properties are scaled from the corresponding properties of the prototype materials. As with the geometric and loading variables, the material properties must be scaled according to the model law.

The basic principle of modeling is similarity: a model is made to function with length, force, and time scales which are linearly related to

(but not identical with) the length, force, and time scales in which the prototype functions.

Many of the model and prototype variables are field quantities, which means that the quantities are distributed continuously throughout certain regions of space and time. A field variable in a model is said to be similar (or homologous) to the corresponding prototype variable if the model variable bears a constant ratio to the prototype variable for all corresponding points of space and time. For instance, the distributed transient pressure loadings on the prototype and the model are required to be similar in the above sense. If the model is properly constructed and tested, then the resulting transient displacements will also be similar.

The present investigation is restricted to prototypes and models which are classical mechanical systems of macroscopic size, for which the fundamental concepts of force (or mass), length, and time have independent dimensions. Appendix A presents a brief review of classical continuum mechanics. Thermodynamic and electromagnetic phenomena and chemical reactions are assumed to have negligible effect on the response of the prototype and the model. Furthermore, gravitational forces are not important for the application of modeling considered in this report, and are therefore omitted.

2. The Model Law

The model law referred to above is a set of relationships between the model variables and the corresponding prototype variables. Although the model law derives its validity from the equations of mechanics, it is usually studied under the separate disciplines of dimensional analysis and the theory of models.

Dimensional analysis is the method of deducing information about a phenomenon by considering solely relationships between the dimensions of the relevant physical quantities. The theory of models is the application of dimensional analysis to a prototype and a model. The fundamental result of dimensional analysis is the Buckingham (Pi) theorem, which establishes necessary and sufficient conditions for similarity between two or more systems. The result of the theory of models is the model law. Langhaar [2] provides an excellent introduction to dimensional analysis and the theory of models. Appendices B and C of this report present abstract treatments of dimensional analysis and the theory of models, respectively, which illustrate the logical structure of these two subjects.

The following properties of the model law are results derived from dimensional analysis and the theory of models:

- (1) all variables in either the prototype or the model which affect the response (in this case, deformation) are significant and must be included in the model law;
- (2) for every significant variable in the prototype there is a corresponding significant variable in the model, and vice versa;
- (3) all corresponding model and prototype variables must have the same physical dimensions (length, mass, time, etc.);
- (4) all model variables which have the same dimension must bear the same constant ratio (called the scale factor) to the corresponding prototype variables; and
- (5) all scale factors will be fixed and can be determined once the scale factors of three dimensionally independent quantities have been fixed.*

These five properties completely determine the model law except for choosing the three dimensionally independent scale factors and calculating the remaining scale factors. The usual dimensionally independent scale factors are: (1) length; (2) force or pressure; and (3) mass, mass density, or time. The equations for calculating the various scale factors in terms of the three dimensionally independent scale factors are given in Appendix C. Section II of this report illustrates the modeling procedure by determining the model law for a class of structural prototypes subjected to distributed impulsive loadings.

3. Advantages of Modeling with Dissimilar Materials

If the same materials are used in the model as in the prototype, then the pressure (stress) scales and the mass-density scales will be the same for both the prototype and the model. For dynamic structural modeling, the choice of only one scale factor — usually the length scale factor — is permitted, and the time scale is found to vary directly with the length scale. Thus, all natural times of the model will be reduced from the prototype in the same ratio as all lengths. If the duration of the transient pressure loading for the prototype is fairly short (an impulsive loading, say) and if the model is much smaller than the prototype, then the duration of the loading for the model must be very short. Experimental difficulties may arise either in applying the high-pressure, short-duration loading or in measuring the rapid response of the model.

* More than three dimensionally independent quantities would be required if the prototype were governed by thermodynamic or electromagnetic phenomena in addition to purely mechanical effects.

The main advantage of using dissimilar materials for the models is that each of the three dimensionally independent scale factors can be chosen independently. Thus, in addition to using a reduced length scale for the models (because of reduced cost), the pressure (stress) scale and the mass-density scale can be chosen arbitrarily. A convenient combination of scale factors for modeling transient deformations of structural prototypes involves a greatly reduced pressure scale and an increased mass-density scale. With this combination the time scale of the model can be made approximately the same as the time scale of the prototype.

The experimental difficulties encountered in modeling with the same materials for the prototype and the model can be overcome by using dissimilar materials. If the prototype is loaded by a high-pressure, short-duration pulse, then the model can be loaded using a low-pressure pulse of approximately the same duration as the prototype loading pulse. Such a loading pulse is easier to produce than the high-pressure, extremely short-duration pulse required when the prototype and the model are made from the same materials. Also, the response of a model using dissimilar materials can be made much less rapid than the response of a model made from the same materials as the prototype, for convenience in measurements.

A further advantage of modeling with dissimilar materials concerns strain-rate effects. Strain-rate (or viscosity) effects cannot be modeled if the same materials are used in the prototype and the model, since the strains are the same and the time scales are necessarily different. This deficiency can be overcome using dissimilar materials, since the time scale factor can be made unity by properly adjusting the length, pressure, and mass-density scales. However, new problems arise if the strain-rate properties of the model materials differ significantly from the corresponding properties of the prototype materials, as explained in Sections I.4 and IV.3.

4. Disadvantages of Modeling with Dissimilar Materials

Modeling with dissimilar materials has certain disadvantages as well as advantages. The main disadvantage of using dissimilar materials is the difficulty of finding (or creating) model materials which accurately model the stress-deformation (constitutive) properties of the prototype materials. Whereas the use of the same materials for the prototype and the model automatically assures accurate modeling of the elastic and plastic response characteristics*; the elastic, plastic, and viscous response characteristics of dissimilar materials have to be specifically tailored to model the corresponding properties in the prototype materials.

* Viscous response characteristics cannot be modeled using the same materials for the prototype and the model, as explained previously.

In general, it is no simple task even to determine the stress-deformation properties of the prototype and model materials, and it is still more difficult to find materials in which these properties match. Appendix D describes the stress-deformation characteristics of a typical solid material. The discussion in Appendix D provides an indication of the complexity of solid material behavior. In fact, there does not yet exist a satisfactory theory of stress-deformation characteristics of solid materials which includes elastic, plastic, viscous, and inertial effects. Such a theory is necessary in order to define the properties which are to be measured in a material test.

The only recourse in the absence of a satisfactory theory — which is the one taken in this report — is to define certain pseudo-properties based on a simple material test. The use of pseudo-properties does not necessarily imply inaccurate modeling. If the material test has been designed so that the major deformation effects are included, then the pseudo-properties will sometimes provide a sound basis for modeling. The compression test used for determining material properties in the present investigation (see Section IV.2) was considered adequate in this respect.

The main faults with using such pseudo-properties are that: (1) they do not strictly characterize the material, since they may depend on such factors as the size, shape, orientation, and mechanical history of the test specimens and the rates at which the particular tests were performed; and (2) they do not completely describe the stress-deformation properties of the materials. Even though these pseudo-properties might be matched according to the model law, there remains an uncertainty as to how well the model materials actually model the prototype materials. This uncertainty results in loss of confidence in the model test results. Section III deals with the problem of estimating errors in model tests.

In summary, modeling of deformation properties using dissimilar materials is a complicated science, which has not yet reached a satisfactory state of development. Until a satisfactory theory of solid material behavior is developed and until material constants appearing in these theories have been evaluated for common materials, modeling with dissimilar materials can only give approximate results in predicting inelastic deformations. Once a satisfactory theory has been developed, the use of pseudo-properties and various correction factors could be abandoned, and the model test results would undoubtedly be more nearly accurate.

It should be mentioned that the inertial (mass) characteristics of dissimilar materials are not nearly as difficult to model as the stress-deformation characteristics. This is true because mass density is simply a scalar quantity — in contrast with the tensor quantities that are involved in specifying the deformation properties. Mass density is easily measured (by weighing and measuring volume) and easily controlled for model materials. In the present investigation, mass density was controlled simply by varying the percentage of lead powder in the composition of the model materials.

SECTION II

MODELING ANALYSIS

This section presents an analysis for modeling inelastic deformations of a structural prototype subjected to a distributed impulsive load. For independent geometric variables we use characteristic lengths and angles. For independent material variables we use the constants appearing in the general constitutive equation for solids presented in Appendix A; these constants may be interpreted alternatively as the elastic and plastic moduli defined in Section IV.2. For loading variables we use the duration and the spatial distribution of the total impulse. For dependent variables we consider total weight, natural period (reciprocal of natural frequency), and the maximum transient and residual displacements at a finite number of points on the external surface of the prototype.

This analysis follows the derivations of dimensional analysis and modeling theory presented in Appendices B and C. The analysis could be readily extended, of course, to include more general transient loadings and more complete descriptions of the resulting transient response. The model law derived in this analysis will be used in Sections IV and V.

1. Specification of Independent and Dependent Variables

Consider a structural prototype S consisting of N distinct material regions R_n connected at a finite number of contact surfaces by perfect bonds. Let each region consist of an initially uniform, deformable solid material. The structural prototype described above must satisfy Equations (A.4) - (A.9) of Appendix A, generalized to N solid bodies.

Let the stresses and strains at all points in S be initially zero (at time $t = t_0$), and let the initial geometry of S be completely described by a finite number of lengths l_i and angles θ_i . As expressed by Equations (A.7) and (A.8) of Appendix A, any solid material (occupying a region R_n of S) can be completely specified by the mass density ρ_n ; three constitutive constants μ_n, λ_n, τ_n with dimensions of stress, length, and time, respectively; and a finite number of dimensionless constitutive constants $c_{mn}, m = 1, 2, \dots, M$. Since we have no occasion to use characteristic length λ_n as a material property, we hereby omit it from the analysis. The materials are assumed to be initially uniform (or homogeneous), so that spatial distributions of the material constants need not be considered.

Specification of geometric and material variables gives rise to certain gross properties of the structural prototype. For instance, the prototype will have a certain weight W in a gravitational field with constant acceleration g . The mass and elastic properties will combine with the geometry and the boundary conditions to determine a series of natural frequencies f_1, f_2, \dots

for the prototype. Let $T_1 = (4f_1)^{-1}$ denote the quarter period corresponding to the lowest natural frequency. Intermediate dependent variables such as the weight W and the natural period T_1 can be used for checking how well a given prototype has been modeled, as discussed in Section IV.3.

Consider a pressure loading applied to the external surface of the prototype; let its distribution in space and time be given by

$$P(\underline{X}, t) = \begin{cases} 0, & t < t_0 \text{ and } t > t_0 + T_0 \\ P'(\underline{X}, t), & t_0 < t < t_0 + T_0 \end{cases} \quad (2.1.1)$$

where \underline{X} are coordinates of points on the surface of S , t is time, and T_0 is the duration of the pressure pulse. The resulting transient impulse is given by

$$I(\underline{X}, t) = \begin{cases} 0, & t < t_0 \\ \int_{t_0}^t P'(\underline{X}, t) dt, & t_0 < t < t_0 + T_0 \\ I_0 \Psi(\underline{X}), & t > t_0 + T_0 \end{cases} \quad (2.1.2)$$

Here I_0 is the total impulse and $\Psi(\underline{X})$ is the normalized impulse distribution over the external surface of the prototype.

Assume that the pressure pulse $P'(\underline{X}, t)$ is sufficiently regular that the response of the prototype to this pulse consists primarily of the first few modes of natural vibration. Furthermore, assume that one or the other of the two conditions

$$T_0 \ll T_1 \text{ or } T_0 \approx T_1 \quad (2.1.3)$$

on the load duration is valid. The consequence of these assumptions is to reduce the number of load distribution variables to three: I_0 , $\Psi(\underline{X})$, and T_0 .

If $T_0 \ll T_1$, then the response of S will be essentially independent of the pressure distribution, and will depend only on the total impulse distribution $I_0 \Psi(\underline{X})$. This result follows from the observation that the majority of the deformation will occur after the loading pulse has been applied, so that the overall loading is equivalent to specifying an initial velocity distribution. If $T_0 \approx T_1$, then the response of S will depend primarily on $I_0 \Psi(\underline{X})$ and T_0 . The extent to which the response of S is independent of the form of the pressure distribution when $T_0 \approx T_1$ is critically dependent on the regularity of the pressure distribution.*

* Chapter 4 of Jacobsen and Ayre [12] gives a detailed discussion of the effect of pulse shape on the response of a simple oscillator.

Assume that the prototype S is rigidly attached (clamped) to an inertial frame over a part of its external surface. This boundary condition can be expressed mathematically as

$$\underline{U}(\underline{X}^A, t) = 0 \quad (2.1.4)$$

where \underline{U} is the displacement (vector) of a point \underline{X}^A on the clamped surface of S . Let the transient displacements of points on the remaining external surface of S :

$$\underline{U}(\underline{X}, t), t > t_0 \quad (2.1.5)$$

represent the response of S to the transient pressure loading described above. For dependent variables we consider the maximum transient displacements U_j^T and the maximum residual (permanent) displacements U_j^R at a finite number of points \underline{X}_j on the external surface of S .

2. Dimensional Analysis

The dimensional analysis developed in Appendix B will now be specialized to the class of impulsively loaded, structural prototypes described in Section II.1. The physical dimensions of the mechanical variables are enclosed in brackets.

Suppose there exist deterministic relationships between the dependent variables

$$\pi_j = W/g [M], T_1 [T], U_j^T [L], U_j^R [L] \quad (2.2.1)$$

and the complete set of independent variables

$$\pi_i = \left\{ \begin{array}{l} \ell_i [L], \theta_i [-] \\ \rho_n [ML^{-3}], \mu_n [ML^{-1}T^{-2}], \tau_n [T], c_{mn} \\ T_0 [T], I_0 [ML^{-1}T^{-1}], \Psi(\underline{X}) [-] \end{array} \right\} \quad (2.2.2)$$

for the class of mechanical systems considered in Section II.1. In analogy with Equations (B.5) these relationships can be written as

$$W/g, T_1, U_j^T, U_j^R = \pi_j(\ell_i, \theta_i, \rho_n, \mu_n, \tau_n, c_{mn}, T_0, I_0, \Psi(\underline{X})) \quad (2.2.3)$$

Our purpose in what follows is to select a set of primary independent variables, and then to reduce the deterministic relationship (2.2.3) to a relationship between dimensionless products based on these primary independent variables.

Select as primary independent variables the three quantities

$$\pi_{s=1} = l_1 [L], \pi_{s=2} = \rho_1 [ML^{-3}], \pi_{s=3} = \mu_1 [ML^{-1}T^{-1}] \quad (2.2.4)$$

where l_1 is a convenient characteristic length, and ρ_1 and μ_1 are the density and the stress constant for the material which contributes the greatest strength to the prototype. These quantities are dimensionally independent, since the exponents

$$\left. \begin{aligned} p_1 = 0, q_1 = 1, r_1 = 0 \\ p_2 = 1, q_2 = -3, r_2 = 0 \\ p_3 = 1, q_3 = -1, r_3 = -2 \end{aligned} \right\} \quad (2.2.5)$$

obey the necessary Equations (B.7). The quantities (2.2.4) are not unique; other sets of independent variables might also serve as the primary independent variables. However, the set of π_s selected above are the most convenient, since these quantities are the least likely to be changed during tests involving parametric variations of the independent variables. The secondary independent variables

$$\pi_k = l_{i+1}, \theta_i, \rho_{n+1}, \mu_{n+1}, \tau_n, c_{mn}, T_o, I_o, \Psi(\underline{X}) \quad (2.2.6)$$

are the quantities which remain after the primary independent variables have been deleted from the complete set of independent variables.

The dependent variables π_j and the secondary independent variables π_k can be transformed into dimensionless products based on the primary independent variables π_s according to Equations (B.9) and (B.10). These dimensionless products are

$$\pi_j' = W/g\rho_1 l_1^3, T_1/l_1(\rho_1/\mu_1)^{1/2}, U_j^T/l_1, U_j^R/l_1 \quad (2.2.7)$$

and

$$\pi_k' = \left\{ \begin{aligned} & l_{i+1}/l_1, \theta_i \\ & \rho_{n+1}/\rho_1, \mu_{n+1}/\mu_1, \tau_n/l_1(\rho_1/\mu_1)^{1/2}, c_{mn} \\ & T_o/l_1(\rho_1/\mu_1)^{1/2}, I_o/l_1(\rho_1\mu_1)^{1/2}, \Psi(\underline{X}) \end{aligned} \right\} \quad (2.2.8)$$

According to the Buckingham theorem Equation (B.11) there exists a set of relationships:

$$\frac{W}{g\rho_1 l_1^3}, \frac{T_1}{l_1 (\rho_1/\mu_1)^{1/2}}, \frac{U_j^T}{l_1}, \frac{U_j^R}{l_1} = \pi_j' \left[\frac{l_{i+1}}{l_1}, \theta_i, \frac{\rho_{n+1}}{\rho_1}, \frac{\mu_{n+1}}{\mu_1}, \right. \\ \left. \frac{\tau_n}{l_1 (\rho_1/\mu_1)^{1/2}}, c_{lm}, \frac{T_o}{l_1 (\rho_1/\mu_1)^{1/2}}, \frac{I_o}{l_1 (\rho_1\mu_1)^{1/2}}, \psi(\underline{X}) \right] \quad (2.2.9)$$

among the dimensionless products (2.2.7, 2.2.8) which is equivalent to the original set of deterministic Equations (2.2.3). These functional relationships are valid for all values of the dimensionless products permitted by physical considerations, and so generate a class of mechanical systems.

Without knowing the functional form of Equation (2.2.9), if the dimensionless independent variables (2.2.8) have exactly the same values for each of two mechanical systems, then the dimensionless dependent variables (2.2.7) will also have the same values. The equality of the dimensionless independent variables provides a set of similarity conditions between my two mechanical systems, and equality of the dimensionless dependent variables provides similarity relations by which the response of one mechanical system can be predicted from the response of the other.

3. Derivation of the Model Law

The modeling theory developed in Appendix C will now be specialized to the class of prototypes described in the two preceding sections. Consider a second mechanical system governed by the dependent and independent variables in Equations (2.2.1, 2.2.2). We call this mechanical system a model, and we seek relationships which will insure that the model is similar to the prototype. Variables referred to the prototype and the model will be distinguished by the subscripts p and m, respectively.

We seek relationships between the corresponding prototype and model variables π_{jp} , π_{jm} and π_{kp} , π_{km} which depend on the scale factors

$$\lambda \equiv l_{1m}/l_{1p}, \gamma \equiv \rho_{1m}/\rho_{1p}, \mu \equiv \mu_{1m}/\mu_{1p} \quad (2.3.1)$$

of length, density, and stress. The desired relationships are presented in Appendix C; thus, Equations (C.7) of Appendix C can be written as

$$\left. \begin{aligned} \pi_{km}/\pi_{kp} &= (\lambda)^{d_{k1}} (\gamma)^{d_{k2}} (\mu)^{d_{k3}} \\ \pi_{jp}/\pi_{jm} &= (\lambda)^{-c_{j1}} (\gamma)^{-c_{j2}} (\mu)^{-c_{j3}} \end{aligned} \right\} \quad (2.3.2)$$

Here c_{js} and d_{ks} are the exponents of l_1 , ρ_1 , and μ_1 in Equations (2.2.7) and (2.2.8) respectively. Written out, Equations (2.3.2) become

$$\left. \begin{aligned} \frac{l_{i+1,m}}{l_{i+1,p}} &= \lambda, & \frac{\theta_{i,m}}{\theta_{i,p}} &= 1 \\ \frac{\rho_{n+1,m}}{\rho_{n+1,p}} &= \gamma, & \frac{\mu_{n+1,m}}{\mu_{n+1,p}} &= \mu, & \frac{\tau_{n,m}}{\tau_{n,p}} &= \tau, & \frac{c_{mn,m}}{c_{mn,p}} &= 1 \\ \frac{T_{o,m}}{T_{o,p}} &= \tau, & \frac{I_{o,m}}{I_{o,p}} &= \lambda(\mu\gamma)^{1/2}, & \Psi_m(X_m) &= \Psi_p(X_p) \end{aligned} \right\} \quad (2.3.3)$$

and

$$\frac{W_p}{W_m} = \frac{1}{\gamma\lambda^3}, \quad \frac{T_{lp}}{T_{lm}} = \frac{1}{\tau}, \quad \frac{U_{jp}^T}{U_{jm}^T} = \frac{U_{jp}^R}{U_{jm}^R} = \frac{1}{\lambda} \quad (2.3.4)$$

where $\tau = \lambda(\gamma/\mu)^{1/2}$ is the time scale factor. (2.3.5)

Equations (2.3.3) are modeling conditions, which together with appropriately chosen scale factors (2.3.1) can be used to determine (ideal) model independent variables from the given prototype independent variables. Scale models of the prototype can be built and tested in accordance with these model independent variables. Equations (2.3.4) are modeling relations by which the response of the given prototype can be predicted from the measured response of the models. When considered together, Equations (2.3.1), (2.3.3), and (2.3.4) are known as the model law.

4. Implications of the Model Law

The implications of the model law developed in Section II.3 will now be examined. We first remark that, in general, the three scale factors

$$\lambda \equiv l_{1m}/l_{1p}, \quad \gamma \equiv \rho_{1m}/\rho_{1p}, \quad \mu \equiv \mu_{1m}/\mu_{1p} \quad (2.4.1)$$

are independent; that is, the length, density, and stress scales in the model can be selected arbitrarily within the limits imposed by available materials and fabrication techniques. Selecting values for these three scale factors automatically fixes the ratios of all corresponding variables in the prototype and the model, by Equations (2.3.3) and (2.3.4).

The modeling conditions

$$\frac{l_{i,m}}{l_{i,p}} = \lambda, \quad \frac{\theta_{i,m}}{\theta_{i,p}} = 1, \quad i = 1, 2, \dots, I \quad (2.4.2)$$

imply geometric similarity between the prototype and the model. That is, if all lengths are scaled in a constant ratio λ and all angles remain the same, then the model will be a scale replica of the prototype.

The modeling conditions

$$\left. \begin{aligned} \frac{\rho_{n,m}}{\rho_{n,p}} = \gamma, \quad \frac{\mu_{n,m}}{\mu_{n,p}} = \mu \\ \frac{\tau_{n,m}}{\tau_{n,p}} = \tau \equiv \lambda \left(\frac{\gamma}{\mu} \right)^{1/2}, \quad \frac{c_{mn,m}}{c_{mn,p}} = 1 \end{aligned} \right\} n = 1, 2, \dots, N \quad (2.4.3)$$

imply scaled material properties between the prototype and the model. If the densities, stress constants, and time constants of all materials comprising a prototype are scaled in the constant ratios γ , μ , and τ , respectively, and if the corresponding dimensionless material constants are equal, then the model materials will be similar to the prototype materials. Note that the time constants must be scaled in a ratio which depends on the scale factors of length, density, and stress.

We mention here that the ideal program of matching exact material constants cannot be attained in practice, since as yet there does not exist a completely satisfactory theory of stress-deformation relations for solids materials which undergo large deformations. Therefore, it becomes necessary to use certain engineering properties to describe the approximate behavior of the solids, as discussed Section I.4. Such approximation does not extend to mass density, since density can be easily obtained for any material.

The material properties E_n , Y_n , and E'_n used in this investigation, as defined in Section IV.2, have the dimensions of stress. To model these properties, it is necessary simply to replace the characteristic stress constant μ_n with E_n , and to define the dimensionless constants as $c_{1n} = E_n/Y_n$ and $c_{2n} = E'_n/E_n$. No time constant was included in this set of properties because "dynamic" values were used; that is, the values of E_n , Y_n , E'_n were "corrected" to eliminate the effects of strain rate, as described in Section IV.3.

The modeling conditions

$$\frac{T_{o,m}}{T_{o,p}} = \tau, \quad \frac{I_{o,m}}{I_{o,p}} = \lambda(\gamma\mu)^{1/2}, \quad \Psi_m(\underline{X}_m) = \Psi_p(\underline{X}_p) \quad (2.4.4)$$

imply similarity of the impulsive loadings applied to the prototype and the model. If the load duration, peak impulse, and impulse distribution are scaled according to Equation (2.4.4), then the impulsive load applied to the model will be similar to that applied to the prototype. The stipulation that

$$T_0 \ll T_1 \text{ or } T_0 = T_1 \quad (2.4.5)$$

stated in Section II. 1, must hold for both the prototype and the model if the impulsive loading is to be accurately modeled.

A model and a prototype which belong to the class of mechanical systems considered in this section will be mechanically similar only if they possess geometric similarity, similarity of material properties, and similarity of impulsive loading. For a prototype and a model which are mechanically similar, the following scaling laws apply

$$\left. \begin{aligned} \frac{W_p}{W_m} &= \frac{1}{\gamma \lambda^3}, \quad \frac{T_{1p}}{T_{1m}} = \frac{1}{\tau} \\ \frac{U_{jp}^T}{U_{jm}^T} &= \frac{U_{jp}^R}{U_{jm}^R} = \frac{1}{\lambda}, \quad j = 1, 2, \dots, J \end{aligned} \right\} \quad (2.4.6)$$

The ratios of weight, quarter period, and transient and residual displacements depend only on the length, density, and stress scale factors.

Two types of modeling involving inelastic deformations are possible. For the first type, the same materials are used for both the prototype and the model. Thus, the density and stress scale factors are simply unity, and the time scale varies directly as the length scale [because $\tau = \lambda(\gamma/\mu)^{1/2}$]. Elastic and plastic characteristics of material behavior are automatically satisfied for this type of modeling, provided the materials are not very rate-sensitive.* This type of modeling is ideally suited for a material such as aluminum which is very insensitive to strain rate. For materials in which the characteristic constants of stress and time both have a significant effect on the response, then the use of the same materials for the prototype and the model will result in inaccurate modeling.

The second type of modeling, which was used in the experimental portion of this investigation, involves the use of different materials in the

* An exception to this statement can be made when the model scale is so small that critical parts of the structure have thicknesses of the order of the grain size of the material.

prototype and the model. The density and stress scale factors, as well as the length scale factor, can be varied arbitrarily for this type of modeling. This makes possible modeling the density, stress, and time constants of the prototype materials. It is doubtful however, whether a given prototype material can ever be modeled completely using a different material; this would require equating simultaneously all the dimensionless material constants.

For economic reasons the length scale factor λ is usually made less than unity (between one-tenth and one-half is typical). It is often desirable that the time scales remain about the same. These conditions can be met by using a density scale factor γ greater than unity, and a stress scale factor μ much less than unity. (Advantages and disadvantages of modeling with "dissimilar" materials are discussed in Sections I. 3 and I. 4.)

5. Subjective Aspects of Modeling

The modeling procedure outlined above is not nearly so rigidly specified as it first appears; rather it entails many choices which can only be settled through the judgment and experience of the model engineer. The first problem confronting the engineer is that of choosing a finite set of dependent variables which will adequately describe the behavior of the model and the prototype. This choice is often relatively easy to make, but it is certainly not trivial.

The second problem is that of choosing the important independent variables - those quantities which significantly affect the behavior of the model and the prototype. This choice is much more difficult to make than the first. It depends on the particular class of mechanical systems to which the model and prototype belong, the type of behavior which the model is expected to simulate, and the accuracy with which the model is supposed to simulate the prototype behavior. Moreover, in making this choice the engineer is required to know, in general, how changes in certain quantities affect certain other quantities in a mechanical system. In particular, the engineer should recognize effects which are not present in the prototype, can seriously affect the behavior of the model, and vice versa.

In so far as geometric and loading variables are concerned, experience is usually a fair guide in helping to decide upon the detail and accuracy of the variables necessary to determine a given mechanical system. For many mechanical systems there exists a sufficiently accurate underlying mathematical theory, such as the Navier-Stokes equations for problems involving fluid flow, that a complete set of material variables, likewise, can readily be obtained. However, in certain cases, such as those in which large plastic deformations of solids are involved, the problem of specifying material properties is greatly complicated by the lack of a satisfactory theoretical foundation. The modeling program associated with this report involved large transient deformations of solids, and was hampered considerably by

this lack of a satisfactory theory from which to derive material constants. A preliminary analysis of the problem of specifying properly invariant constants for determining solid material behavior is given in Appendix D.

The third problem facing the model engineer is that of choosing scale factors between the model and the prototype; appropriate ratios must be selected for the three, dimensionally independent variables which most directly affect the behavior of the model and the prototype. This choice usually involves a compromise between the desired accuracy of modeling and the cost of the model, and it depends largely on the facilities available for building and testing the model, and the materials available for constructing the models. Personal preferences of the engineer can again enter into making this decision; he may prefer some particular size of model, or favor some particular range of the time or load scales. In general, however, the model should be made as small and otherwise as cheaply as possible, without impairing the accuracy of modeling.

Finally, it is often necessary to deliberately "distort" the model, i. e., abandon some of the dimensionless independent variables. Choice of appropriate scale factors and transformation of the variables into dimensionless form will show those variables for which it is either impossible or prohibitively expensive to maintain exact similarity between the model and the prototype. Examples of such variables are: (1) those which determine interactions with auxiliary equipment, such as the flexibility of a test stand; (2) details in constructing the model which would be extremely difficult to fabricate, such as very thin sections of material, or tiny welds, rivets, and other fasteners; and (3) material constants for which model materials do not exist.

Although these dimensionless variables are known to have a significant effect on the model and prototype behavior, they are deliberately given different values for the model, and an attempt is then made to correct the dependent variables accordingly. Obviously this process is one which must rely heavily on the experience of the engineer. To accurately account for the effects of deliberately distorting a model of a given prototype would require the results of many simple experiments on models in which each of these independent variables are varied separately. An analysis of this subject is presented in Section III. 3.

SECTION III

ERRORS IN MODELING

Parts 2 through 4 of Section II dealt with exact simulation between mechanical systems. That is, the independent variables of a model were assumed to satisfy exactly a set of modeling conditions based on the independent variables of a prototype; and, consequently, the response of the model was assumed to be exactly similar to the response of the prototype. In this section we consider the case, which invariably occurs in practice, in which certain of the independent variables fail to satisfy the modeling conditions, and the responses of the model and the prototype are not exactly similar. The difference between the measured response of the model and actual response of the prototype, as compared on a common scale (such as, in terms of dimensionless variables), is called the modeling error.

1. Classification of Modeling Investigations

Before embarking on a detailed account of errors in modeling, we should review briefly the specific goals of modeling. Engineers are frequently concerned with predicting the behavior of a proposed structure or other mechanical system, commonly referred to as a prototype. In some cases, basic information is required before a hypothetical prototype can be designed. In other cases, prior information is desired to insure that a proposed prototype will operate properly once built. In still other cases, additional information about an existing prototype is desired in order to improve its operation in a subsequent design.

A modeling investigation is undertaken to supply the desired information because a model test can usually be performed for a fraction of the cost of a prototype test. Model tests are feasible in many cases where testing one or more prototypes would be prohibitively expensive or otherwise unfeasible. A modeling investigation usually consists of several model tests and perhaps a few prototype tests. Because cost considerations enter into the decision of how many prototype tests can be performed, it is convenient to classify modeling investigations by the number of prototype tests compared with the number of model tests.

For example, a modeling investigation undertaken simply to verify the possibility of modeling a certain phenomenon might consist of one prototype test for each model test. In this case the modeling errors are directly accessible, consisting simply of comparisons between the response of the corresponding prototypes and models. However, for an investigation in which the ratio of model tests to prototype tests is unity, the model tests are entirely redundant; they provide no new information about the response of the prototypes.

A more useful type of modeling investigation consists of making several model tests for each prototype test. A few typical prototype tests are made, which provide standards for checking the model tests; the majority of the tests are model tests. A few of the model tests are specifically designed to predict the results of the prototype tests. The modeling errors observed from these few tests are then used as indications of the modeling errors which probably occur for the remaining model tests. The modeling errors for this type of analysis can be described either by "most probable" errors or by "error bounds." The concept of error bounds is developed in part 4 of this section.

This type of modeling investigation is very practical, in that control over the independent variables can be relaxed to a large extent without loss of confidence in the test results. For example, pseudo-properties such as described in Section I.4 and II.4 can be used to specify the material properties instead of more exact properties. Also, dimensional tolerances, methods of loading, and methods of measuring response need not be as strict as for pure modeling. The modeling conditions can be relaxed for this type of modeling because the specific comparisons of prototype and model test results prevent the error estimates from becoming totally uncertain. Naturally, the more prototype tests, and the better correlation between the model and prototype test results, the more confidence can be placed in the remaining model tests.

A third type of modeling investigation, which we shall call "pure modeling," involves testing models without testing any prototypes. This type of modeling investigation is conducted when a prototype is, for some reason, inaccessible. Since there are no prototype tests by which to compare the model test results, pure modeling must be performed with meticulous care using methods well proven by past experience. Pure modeling is very useful for supplying information in cases where the modeling techniques are known to be accurate. Modeling of elastic vibrations is an example where pure modeling can be used with virtual impunity.

For modeling techniques in which "modeling accuracy" (modeling errors invariably small) has not yet been verified, the use of pure modeling requires that strict control be maintained over the model variables. Even with strict control over the model variables, the accuracy of the model test results often remains uncertain, since modeling errors can arise from any of several sources, as described in the next section. It is for pure modeling that error prediction techniques, as described in Section III.3, can be used with advantage.

When prototype test results are not available for a modeling investigation, it is often desirable to build and test an intermediate structure which has the same general characteristics as the prototype. Comparison of the test results of this structure with results from a corresponding model test establishes confidence in the modeling technique. The technique of using an intermediate structure is not feasible in modeling large structures such as dams or tall buildings, since scale models are already expensive items. For such cases the results of pure modeling must be relied upon, perhaps with the aid of auxiliary analyses and calculations.

One further situation may occur. Consider the case where a prototype exists, but where the desired test on the prototype is somehow prohibitive. In this case certain intermediate dependent variables may be used (instead of the desired dependent variables) to provide corrections leading to more accurate test results. Two examples come to mind. First, suppose the length scale factor and the weights of the prototype and model are known. These quantities can be combined to provide a check on the density scale factor. Second, suppose the length and density scale factors are known, and suppose, in addition, that the fundamental natural frequency of the prototype and the model has been measured. A "dynamic" stress scale factor can be calculated from this information. The latter method was employed in Section IV. 3.

2. Sources of Modeling Errors

The problem of predicting the errors associated with a model test is complicated because errors can arise from any of several sources. Among these sources are:

- (1) The modeling analysis may be based on an inexact or inappropriate theory, in which case certain controlling variables may be overlooked or misinterpreted.
- (2) The accuracy of measuring the controlling variables or the response of the model may be poor.
- (3) It may be impossible or unfeasible within the scope of a modeling investigation to satisfy all the modeling conditions. This is usually the most drastic source of modeling errors.

The first source of modeling errors listed above is dependent on the experience of the modeling practitioner and the existing theories which can be used to describe a phenomenon, and is outside the realm of error prediction techniques. Likewise, the second source of errors is outside the realm of error predictions, except when a large number of observations are made, in which case the theory of probability can sometimes be brought to bear.* The usual result of the first two sources of error is simply uncertainty as to the accuracy of model test results. The first source of error mentioned above was significant in the present investigation.

The third source of modeling errors is the one most frequently encountered, and it is usually the source of the largest errors, as suggested above. Error prediction techniques can sometimes be used with this source

* Chapter 1 of Murphy [13] provides a good introduction to use of probability methods for interpreting experimental observations.

of errors, if modeling errors from other sources are negligible. The remainder of this section is concerned primarily with the third source of modeling errors.

Because strict control can never be maintained over the independent variables of a model, the response of the model will never exactly predict the response of the prototype. For most engineering applications an exact model is not necessary; there usually exists a finite tolerance on the accuracy of results from a modeling investigation which will be acceptable.

The problem of controlling the independent variables of a model becomes practically significant when, as often happens, a conflict arises when trying to satisfy two or more variables which significantly affect the response of the model. In this case a "distorted" model must be considered.* Compromises of this kind occur in virtually every modeling investigation. In each case, an engineer must judge from his experience, using whatever experimental or theoretical results are available, in deciding the best way to perform a model test.

The most fundamental principle to be observed in conducting a model test is that important variables — i. e., variables which most directly affect the response of the model — must be controlled more carefully than less important variables. Because this principle is of fundamental importance in modeling, it warrants further elaboration.

Let the independent variables of the model be divided into three classes: the most important variables, the intermediate variables, and the unimportant variables. The most important variables, such as the characteristic lengths and the characteristic density and stress constants, must be modeled exactly. The scale factors are always based on the most important variables. If it is impossible to model exactly one of the variables considered to be most important, then this variable must be considered as an intermediate variable, and given special attention.

The intermediate variables usually constitute the majority of the independent variables. They are the variables which affect the response of the model, but cannot necessarily be made to satisfy the modeling conditions. It is the intermediate variables for which error predictions or corrections must be made. The unimportant variables, such as material constants which have very little effect on the response of the model, and insignificant geometric variables, can be ignored. No attempt should be made to model the unimportant variables until the more important variables have first been modeled.

* A model test is called "distorted" if one or more of the independent variables are deliberately made to deviate from the modeling conditions required for exact simulation.

3. Error Predictions and Corrections

One of the most serious problems in modeling occurs when no prototype results are available; thus all results, including error estimates, etc., must be established from model test results alone. To analyze this problem we must first assume that all sources of modeling errors are negligible except one, namely errors caused by differences between certain of the model independent variables and the modeling conditions.

We shall use the following notation: Let

$$\pi_{rp} = f(\pi_{ip}) \text{ and } \pi_{rm} = f(\pi_{im}) \quad (3.3.1)$$

represent unique dimensionless functional relationships between the response of the prototype π_{rp} and the prototype independent variables π_{ip} , and between the response of the model π_{rm} and the model independent variables π_{im} . If the same physical laws govern the behavior of the model and the prototype and if the same independent variables are significant, then the function f in both of Equations (3.3.1) will be identical.

If π_{im} are equal to the corresponding π_{ip} , then exact simulation will have been achieved, and π_{rp} will exactly equal π_{rm} . In practice this situation is rarely achieved. Consider the more common situation in which

$$\pi_{im} = \pi_{ip} + \delta_i \quad (3.3.2)$$

that is, where the model independent variables deviate from the modeling conditions by a known amount δ_i . When this situation occurs

$$\pi_{rm} = f(\pi_{ip} + \delta_i) \quad (3.3.3)$$

and the modeling error is given by

$$\delta_r = \pi_{rm} - \pi_{rp} = f(\pi_{ip} + \delta_i) - f(\pi_{ip}) \quad (3.3.4)$$

The problem of interest is to determine δ_r in terms of δ_i .

In the past, techniques utilizing auxiliary mathematical analysis and comparison of model test results with selected prototype results have been successfully used to develop correction factors.* Here, however, we shall treat the situation in which no useful analyses can be performed and no prototype results are available. We consider those situations in which only model test information is available.

If the function $f(\pi_{ip} + \delta_i)$ has continuous partial derivatives through order n , then it may be expanded in a finite Taylor series as:

* Refer to Chapters 6 and 7 of Murphy [13], and the paper in the ASME Symposium [3] by Ezra.

$$f(\pi_{ip} + \delta_i) = \left[1 + \frac{1}{1!} \sum_i \delta_i D_i + \dots + \frac{1}{(n-1)!} \left(\sum_i \delta_i D_i \right)^{n-1} \right] f(\pi_{ip}) + \frac{1}{n!} \left(\sum_i \delta_i D_i \right)^n f(\pi_{ip} + \theta \delta_i), \quad 0 < \theta < 1 \quad (3.3.5)$$

where D_i is the operator $\frac{\partial}{\partial \pi_i}$ and $D_i^l D_j^m = \frac{\partial^l}{\partial \pi_i^l} \frac{\partial^m}{\partial \pi_j^m}$, etc.* The proposed

approach is to experimentally determine from model tests alone the values of the necessary partial derivatives occurring in Equation (3.3.5), and then to use this relation to establish bounds on the errors and to make corrections.

In view of the difficulty of experimentally determining higher derivatives, we consider establishing a first order correction as follows. Keeping only the first order terms in (3.4.5) results in

$$\delta_r = f(\pi_{ip} + \delta_i) - f(\pi_{ip}) = \sum_i \delta_i D_i f(\pi_{ip} + \theta \delta_i) \quad (3.3.6)$$

Thus, bounds on the maximum error can be written as

$$\left. \begin{aligned} \delta_r^+ &= \sum_i \delta_i \left[\max D_i f_i(\pi_{ip} + \theta \delta_i) \right] \\ \delta_r^- &= \sum_i \delta_i \left[\min D_i f_i(\pi_{ip} + \theta \delta_i) \right] \end{aligned} \right\} \quad 0 < \theta < 1 \quad (3.3.7)$$

and corrections for the model test results are given approximately by

$$\pi_{rp} \approx \pi_{rm} - \sum_i \delta_i \left[\text{avg } D_i f_i(\pi_{ip} + \theta \delta_i) \right] \quad (3.3.8)$$

We conclude from Equations (3.3.7) and (3.3.8) that prediction of error bounds and error corrections can be obtained from knowledge of the various first partial derivatives of the response variables π_r with respect to the independent variables π_i . These partial derivatives presumably can be obtained from the results of an extensive model test program. In those cases where it is impossible to cover the entire range $0 < \theta < 1$ for each of the π_i , sufficient results are required to allow meaningful extrapolation over this range.

The error bounds expressed by Equation (3.3.7) require knowledge of first derivatives only. A closer bound may be obtained if second derivative information is available, since

$$\delta_r = \sum_i \delta_i D_i f(\pi_{ip}) + \frac{1}{2} \left(\sum_i \delta_i D_i \right)^2 f(\pi_{ip} + \theta \delta_i) \quad (3.3.9)$$

* See Pipes [14], p. 25.

provides the next level of sophistication over Equation (3.3.6). However, it seems unlikely that second order corrections based on Equation (3.3.9) would ever be used, since a model test program required to evaluate the first partial derivatives may in itself be a prohibitive undertaking.

The method of error prediction described above would be of use primarily for model tests in which only one (or at most two) of the model independent variables is "distorted," and a correction for this distorted variable is sought. The method is most promising for the case of one or two "distorted" variables, since the number of model tests needed to evaluate the partial derivatives in this method increases rapidly with the number of distorted variables.*

* The analysis cannot be applied to the model test results presented later in this report because, within the framework of the assumption of our model analysis, we had no distorted variables.

SECTION IV

MATERIALS DEVELOPMENT AND MODEL FABRICATION

A large part of the effort expended in this program was directed toward development of suitable "dissimilar" model materials. The model materials finally used were epoxy resins and polyurethane foams combined with lead powder, all of which were much weaker and considerably more dense than the corresponding prototype materials. These model materials were tailored specifically to model certain materials used in the construction of re-entry vehicles (hereafter referred to as RVs). This section describes the development of the model materials, and the techniques used to fabricate small-scale models from these materials. Included in this section are descriptions of the mechanical properties of the model materials and the tests used to obtain the material properties.

1. Chronological Summary of Developments

At the beginning of this program, the dissimilar materials technique had been advanced to the point where a reasonably good, weak, dense model material simulating the properties of 6061-T6 aluminum alloy, designated as AL, had been developed using epoxy plastics and lead powder [1]. This material, however, had several drawbacks. The most serious of these was the necessity for testing the material before it had completely aged and, therefore, before the properties had ceased changing significantly with time. A second serious problem was the relatively large strain rate sensitivity of the material. In addition, there was the general need for improved fabrication techniques to be used with the unusual materials being developed.

The first stage in the materials development program was therefore directed to eliminating the ageing problem by the development of material formulations having constant, predictable properties when fully cured. This goal was satisfactorily accomplished by use of a combination of flexible epoxy resin with the more rigid resins which had been used. In particular, the original formulation of Epon 828 plus Thiokol LP3 plus curing agent D was replaced by the combination of Epon 828, Epon 871, and curing agent CL. Appropriate quantities of unoxidized lead powder were included in each mixture. The problem of strain rate sensitivity was not eliminated by this change, however, and an attempt was made to partially account for this effect by testing the materials at each of two strain rates.

The second stage of this program involved devising a better technique for fabricating the models. In view of the settlement problems which had been encountered with attempts to mould lead-plastics mixtures, an attempt was made to develop a spray technique for application of the model materials. Since the materials of greatest interest contain on the order of 10 to 1, by

weight, of lead to plastic, they could hardly be called liquids and would not even pour satisfactorily. It was necessary, therefore, to add a solvent to these mixtures in order that they be sprayable. After some experimentation, methylene chloride was selected as a satisfactory solvent. This development plus the invention of a continuous mixing cup and an investigation of different types of spray nozzles, made it possible to apply the model material to a mandrel or other form by spraying.

With the basic spray application technique thus developed, the next stage of the program was concerned with developing material formulations having sets of properties which properly simulate the prototype material properties. Included in this exploratory stage of the program was the use of various metal powders such as pure aluminum and lead-tin alloys in place of pure lead. Since none of these powders seemed to offer any advantage over lead, they were not investigated in detail. However, should models be desired with significantly less mass density than the lead-plastic materials, use of aluminum or other light metal powders in conjunction with the plastic might be desirable.

Once an accurate model material, designated MAL, for 6061-T6 aluminum had been developed, work was begun on the feasibility of modeling typical RV heat shield materials. Since new heat shield materials are being developed continually, and since their properties vary rather widely, it was not considered possible to cover the range of properties of current interest for heat shield materials. The approach taken was to recognize that heat shield materials are characterized by low strength and medium density, and to select a typical material for use as prototype heat shield. The prototype ablator selected was castable C-124 epoxy, designated HS. This stage of the materials development program was concentrated on developing a material to simulate C-124. The resulting material was designated MHS.

In view of the prevalence of the use of very lightweight core or filler materials, such as honeycomb and foams, a final stage of materials development, namely development of materials to model weak and very lightweight prototype materials, was initiated. Here again, the wide variety of materials and the associated wide range of properties which might be used for stiffening or as fillers, led to simplification of the problem by selecting a single material. Keeping in mind the modeling requirements, a standard urethane foam (Emerson and Cummings FPH - 10H), designated PF, was selected as the prototype material to be modeled. The problem remaining was to develop a relatively dense, extremely weak foam with small cell size for use as the model material. This problem was solved by the addition of moderate amounts of lead powder plus very small quantities of water to a weak foam resin (FPH - 4H), the resulting material being designated MPF.

2. Material Tests and Properties

In arriving at the final selection of model materials, batches of more than fifty combinations of epoxy resin and urethane foam with lead powder

were made and tested. In addition, numerous specimens of the prototype materials were tested to insure that the material properties were properly matched. This section describes the material tests and material properties used in this investigation.

Cylindrical specimens of each material were machined to one of three standard sizes. The specimens of AL and HS and the candidates for MAL model material were 0.25-in. diameter by 0.50-in. long; the candidates for the MHS model material were 0.50-in. diameter by 0.50-in. long; and specimens of PF and MPF were 1.00-in. diameter by 1.00-in. long. Figure 1 shows a representative sampling of the material specimens tested in this investigation. An average (weight) density ρ_g was obtained by weighing each test specimen, and then comparing the weight of the specimen to its original volume.

The basic test for determining stress-deformation properties of the materials was a compression test. The cylindrical specimens were lubricated at each end with a special grease, to prevent generation of shear stresses. The specimens were then tested in compression on an Instron machine at strain rates of approximately 0.1 to 2.0 min^{-1} . The Instron machine was instrumented with a load cell of proper capacity placed in series with the specimen, and a strain-gage extensometer placed in parallel with the specimen. For some of the material tests, a device for measuring transverse strains was attached to the test specimen.

For tests in which only axial load p and axial extension δ_l were measured, the output was recorded on the Instron chart recorder, which plots data directly as load versus extension. For the tests in which transverse extension δ_t , as well as axial load and axial extension, were measured, the results were recorded on a Sandborn three-channel pen recorder, as plots of the three quantities measured versus time.

The data from all the material tests were reduced to plots of stress (based on the original cross-sectional area) versus strain (based on the original length and diameter), as shown in Figure 2. The following "pseudoproperties" were estimated from the axial-stress versus axial-strain curve: the initial (elastic) slope E ; the eventual (plastic) slope E' ; and the point Y at which the asymptote to the plastic portion of the stress strain curve intersects the stress axis. Each of these pseudoproperties has the dimension of stress. Attempts to measure transverse strain with sufficient accuracy to evaluate the pseudoproperties ν , ν' , and Y' , defined in Figure 2, were not successful; consequently, these properties were not used in specifying material behavior.

3. Corrections for Strain-Rate Effects

The results of compression tests of the final MAL material and the AL prototype material showed that the elastic and plastic properties of the

prototype material were modeled quite accurately at the so-called "static" loading rates (on the order of minutes). However, the model material was found to be much more sensitive to variations in strain rate than the prototype materials. Although exact modeling of transient deformations is not possible when model materials exhibit strain-rate effects to a different extent than the corresponding prototype materials, inexact modeling can be justified if the strain-rate effects do not predominantly control the response of the models. All that is needed is some method of correction.

One method of obtaining more accurate test results in this case involves testing the model materials at one strain rate: an average of all strain rates which occur during a model test. The "pseudoproperties" obtained at this strain rate represent average properties for the model test, and are thus improvements over the "static" values. Because of the lack of high-speed testing facilities at SwRI, the material tests were limited to the "static" range—much slower than the average strain rate during a model test. It was necessary, therefore, to consider some other method of compensating for the strain-rate sensitivity of the model materials.

A simple correction for strain-rate effects can be made by comparing the natural frequencies of corresponding prototypes and models. This correction can be used to transform the "static" properties into "dynamic" properties. The natural frequencies of a structure which deforms primarily by stretching and one which deforms primarily by bending are given, respectively, by the formulas*

$$f = \frac{\lambda}{l} \left[\frac{E}{\rho} \right]^{1/2} \text{ and } f = \frac{\lambda}{l^2} \left[\frac{EF}{\rho} \right]^{1/2} \quad (4.3.1)$$

where λ is a dimensionless mode number, and F is a shape factor with the dimension of length squared.

For a geometrically similar model and prototype, the ratio of frequencies for either stretching or bending deformations is given by the single expression

$$\frac{f_m}{f_p} = \frac{l_p}{l_m} \left[\frac{E_m \rho_p}{E_p \rho_m} \right]^{1/2} \quad (4.3.2)$$

Inverting this expression, we get

$$\frac{E_m}{E_p} = \frac{\rho_m}{\rho_p} \left(\frac{l_m f_m}{l_p f_p} \right)^2 \quad (4.3.3)$$

* See pages 467 and 484 of Reference [12].

Thus, a "dynamic" modulus E_m for the model material can be calculated from the modulus E_p of the prototype material, using the ratios of length, density, and natural frequency of the corresponding prototypes and models.

The plastic properties Y and E' are assumed to change from "static" to "dynamic" in the same ratio as the elastic modulus E ; that is, the ratios E/Y and E/E' are assumed to be the same for "static" and "dynamic" loading rates. The above method was used to determine "dynamic" properties of the model materials in this investigation. Though no rigorous proof exists for use of this method, the use of Equation (4.3.3) can be justified for evaluating the dynamic modulus since frequency is determined mainly by inertial and elastic properties.

4. Selection of the Model Materials

The first material considered was the MAL model material; the properties of MAL were required to simulate the properties of the prototype material AL. Since MAL was the strongest and most basic construction material of the three model materials, much more effort was devoted to matching the properties of MAL than with MHS or MPF. The principal criteria used in selecting a suitable model material MAL were that the ratios E/Y and E/E' should be equal for the two materials MAL and AL. Two secondary criteria required that the scale factors of stress and density be approximately 1/20 and 3, respectively.

The properties of the prototype materials are listed in Table I. Thus, the properties of the prototype material AL are

$$E = 1.0 \times 10^7 \text{ psi}, \quad Y = 4 \times 10^4 \text{ psi}, \quad E' = 3 \times 10^5 \text{ psi} \quad (4.4.1)$$

and the ratios E/Y and E/E' for AL are

$$E/Y = 250, \quad E/E' = 33 \quad (4.4.2)$$

The model material MAL was required to have the same values of E/Y and E/E' as listed above for AL. Various combinations of Epon 828, Epon 871, curing agent CL, and lead powder were tried until a satisfactory match of E/Y and E/E' was obtained. The "static" properties of the model material finally selected for MAL are

$$E = 5.5 \times 10^5 \text{ psi}, \quad Y = 2 \times 10^3 \text{ psi}, \quad E' = 1.4 \times 10^4 \text{ psi} \quad (4.4.3)$$

In addition to differences of strain-rate effects, noted in Section IV.3, the MAL material did not have as sharp an initial yield point as the prototype material AL. Thus an effort was made to sharpen the yield point of the MAL model material. Various additives were tried, but none produced the desired effect.

Once the model material MAL had been developed to simulate aluminum reasonably well, development of the materials MHS and MPF was begun. The scale factors of stress and density were fixed by the properties of AL and MAL:

$$\left. \begin{aligned} \mu(\text{static}) &= E_{\text{MAL}}/E_{\text{AL}} = .055 \\ \gamma &= \rho_{\text{MAL}}/\rho_{\text{AL}} = 2.85 \end{aligned} \right\} \quad (4.4.4)$$

Thus, it was necessary to match the ratios

$$\left. \begin{aligned} E_{\text{MHS}}/E_{\text{HS}} &= E_{\text{MPF}}/E_{\text{PF}} = .055 \\ \rho_{\text{MHS}}/\rho_{\text{HS}} &= \rho_{\text{MPF}}/\rho_{\text{PF}} = 2.85 \end{aligned} \right\} \quad (4.4.5)$$

and to consider the ratios E/Y and E/E' as secondary quantities, to be matched only after the Equations (4.4.5) had been satisfied. This procedure was justified since the influence of MHS and MPF on the response of the models was expected to occur mainly through inertial and elastic effects.

Table II lists the properties of the final model materials, including MHS and MPF. We see that, in general, the scaling between the "static" properties of the prototype and model materials is good. The occasional mismatch of properties was considered to be of minor importance. Table IV gives the final compositions used for the model and prototype materials. Space limitations prohibit listing the compositions and properties of all the material combinations tested in this program.

The "static" properties listed in Table II were transformed into "dynamic" properties on the basis of measured natural frequencies of the prototypes and the models, as discussed in part 3 of this section. The ratios of length, density, and natural frequency between the prototypes were approximately

$$l_m/l_p = 0.20, \rho_m/\rho_p = 2.85, f_m/f_p = 0.94 \quad (4.4.5)$$

Equation (4.3.3) provides the dynamic modulus of MAL

$$E_{\text{MAL}} = E_{\text{AL}} \frac{\rho_m}{\rho_p} \left(\frac{l_m f_m}{l_p f_p} \right)^2 = 1.0 \times 10^6 \quad (4.4.6)$$

The "dynamic" stress scale factor is, therefore

$$\mu(\text{dynamic}) = E_{\text{MAL}}/E_{\text{AL}} = 0.10$$

The remaining properties of the model materials were assumed to be transformed in the ratio

$$E_{\text{MAL(dynamic)}} : E_{\text{MAL(static)}} = 1.82 : 1 \quad (4.4.7)$$

Table III lists the "dynamic" properties of the model materials.

5. Production of the Model Materials

The following procedure was used to produce the model material MAL: First, 60 grams Epon 828 and 10 grams curing agent CL were mixed, then thoroughly blended at 100°C. Then, 40 grams Epon 871 and 50 cc's methylene chloride solvent were added to the mixture; the mixture was then poured into the sprayer cup. With the continuous mixer in operation, 1000 grams unoxidized (200 mesh) lead powder was slowly added to the mixture. The material was then ready to be sprayed onto a mandrel or other model form.

As part of this program, two aluminum mandrels were made with dimensions matching the internal configurations of the model shells. The mandrels were made in such a way that they could be collapsed and removed from inside the model shells once the models were completed. Before spraying, the mandrels were coated with fused teflon mold release agent, and then preheated to approximately 60°C to aid evaporation of the methylene chloride solvent. The mandrels were rotated at 18 revolutions per minute while the model material MAL was being sprayed. The spray nozzle was held approximately 18 inches from the mandrel surface.

Once a sufficiently thick layer of MAL had been deposited on the mandrel, the mandrel and shell were placed in an oven, where they were allowed to cure for two hours at 60°C, followed by four hours at 125°C. After curing, the shells were machined to final dimensions in a lathe; then, unless an additional layer of material was to be applied, the mold was collapsed and removed. The models were then stored in a refrigerator at approximately 5°C until testing. Ambient temperature during the tests was generally about 25°C to 28°C.

The material MHS developed for modeling the C-124 ablator material was produced as follows: First, 4.5 grams Epon 828 and 2.0 grams curing agent CL were mixed, then thoroughly blended at 100°C. Then, 15.5 grams Epon 871, 0.4 gram, Cab-O-Sil silicon fibres, and 80 grams unoxidized (200 mesh) lead powder were added to the mixture. The material was then set aside for a few minutes to allow escape of entrapped air bubbles, and then cast into place. After curing for two hours at 60°C, followed by four hours at 125°C, the material was machined to size, and then stored at 5°C until testing.

The prototype foam used in this investigation was Emerson and Cummings FPH-10H. The model foam was a combination of 20 grams Emerson and

Cummings FPH-4H foam resin, 13 grams catalyst, 150 grams unoxidized lead powder, and 2.5 grams distilled water. When mixed at approximately 25°C, this combination grows rapidly in volume. The majority of growth is completed in 20 to 30 seconds and maximum volume is reached in two or three minutes. This material was applied directly to the shells before starting to grow. Once set, the foam was machined and the completed model was stored at 5°C until ready for testing. This material was used both as sandwich core for the models M3 and as filler for the models M4.

6. Fabrication of the Models

This section describes the technique of making the various models. The models were cylindrical and conical shells with the general configuration shown in Figure 3. A total of nine different models with varying geometry and shell compositions were considered. The properties of these models, designated M1-M9, are listed in Table VI. Because of their simplicity, the "plain" models M1 and M5-M9 were made first. The composite models were made last. Several samples of a model were made and tested in cases where more data was desired or where different methods of loading the models were employed.

All models were begun by spraying the basic MAL model material onto a preheated aluminum mandrel, as described in the last section. This spray process was continued until a layer in excess of the final desired thickness had been deposited on the mandrel. The mandrel, with the layer of MAL, was then put into an oven. After the MAL had properly cured, the mandrel was mounted in a lathe and the layer of MAL was machined to the desired thickness. The above procedure was sufficient to fabricate the plain models M1 and M5-M9. All that remained to be done was to collapse and remove the mandrel from the model, and to place the model under refrigeration until testing.

The composite models M2-M4 were each begun according to the above procedure, but they required additional operations before they were finished. The heat shield model M2 was made according to the following procedure: A layer of MAL was applied to the mandrel, then cured and machined. A sheet of mylar was then wrapped around the mandrel to form a mold, and the MHS model heat shield material was cast in the annular space between the MAL and the mylar. This layer of MHS was then cured and machined to final thickness. The finished model was then removed from the mandrel and placed under refrigeration.

For the sandwich model M3, a layer of MPF model foam was spread onto the surface of the original MAL shell, and allowed to grow and become set. This layer of MPF was then machined to the proper thickness, and a second layer of MAL was sprayed onto the MPF. The outside layer of MAL was then cured and machined to the desired thickness. The finished sandwich model was then removed from the mandrel and placed under refrigeration.

Fabrication of the foam-filled model M4 followed the same procedure used to make the plain models, with the exception that after the mandrel was removed, the entire volume inside the model was filled with MPF model foam. After the foam had set, the excess foam was cut off flush with the edge of the model, and the finished model M4 was placed under refrigeration.

After fabrication, the models invariably showed good dimensional tolerances compared with the specified geometric variables. The beautiful finished appearance of these models attested to the care which Mr. F.O. Hoese devoted in making them. Figures 12 through 15 are photographs of the models, showing various stages of deformation. The materials, after fabrication, were considered to be homogeneous and isotropic. In order to prevent effects of strain hardening from entering the data, tests were made on only those faces of the models which had slight previous histories of deformation.

SECTION V

EXPERIMENTS

This section describes an experimental investigation undertaken to demonstrate the technique of modeling inelastic deformations using dissimilar materials. A second purpose of this investigation, as stated in the Foreword, was to generate information about the impulse-deformation characteristics of conical shells. Thus, the structures selected to be modeled were truncated conical shells clamped around the small edge; and the loading selected was an impulse distributed uniformly over a quadrant of the shell. The quantities to be modeled were maximum transient and residual displacements versus impulse.

A series of nine distinct models was tested. Three of these were composite shell models: a heat-shield covered shell model, a sandwich shell model, and a foam-filled model. Six of these were plain shell models: which included various permutations of length, thickness and cone angle. The models were tested in a shock tube and with a recently developed sprayed-explosives loading technique. Each of the models was tested using at least two load durations, in order to test the effect of this parameter on the magnitude of the deformations. In addition to the model tests, a series of four prototype tests was conducted using sheet explosives to provide the load. Unfortunately, the prototype tests were poorly designed and could not be used to verify the model test results.

1. Definitions of the Variables

The prototypes and models in this investigation belong to a class of mechanical systems which can be described by the finite set of mechanical variables listed in Table V. These variables fall naturally into four categories, which are discussed separately in the following paragraphs.

a. Geometry. The prototypes and models were constructed in the form of conical frustrum shells, as illustrated in Figure 3. The geometry of such a shell is completely described by the cone angle α , the mean inner radius a , the axial length b , and the uniform shell thickness h . For a composite shell, consisting of several layers of different materials, the thickness h_n of each layer was considered in addition to the overall thickness h . A cylindrical extension at the small end of the conical shell, referred to as "base" in Figure 3, was built into each of the model shells for the purpose of clamping the models to a rigid frame. Each model and prototype shell was required to conform with this geometry before each test; in particular, initial eccentricities were required to be small.

b. Material properties. The principal phenomena governing the response of the prototypes and models were dynamics and inelastic deformations of solid materials; hence the necessity of modeling inertial and constitutive material properties. The material properties used in this investigation were mass density ρ and the "pseudoproperties" E , Y , and E' , as defined in Section IV.2 for a simple compression test. For a composite shell, the properties ρ_n , E_n , Y_n , E'_n , $n = 1, 2, \dots, N$, which correspond to each of the N layers of material, were considered. The properties E , Y , E' were converted to "dynamic" properties by the method described in Section IV.3. Tables I - III list the properties of the prototype and model materials.

We emphasize that the properties E , Y , and E' do not completely describe the constitutive behavior of solid materials, but merely reflect gross average properties between axial stress and axial strain. Nevertheless, physical intuition prompts us to rely on these properties, especially in lieu of better ones. It is felt that if, in addition to geometric and loading variables, these properties (for corresponding strain rates) satisfy appropriate modeling conditions, then the mechanical response of the prototype and model should be reasonably similar.

c. Impulsive load distribution. The present problem is concerned with determining the response of the prototypes and models to impulsive loads. It is necessary, therefore, to specify the distribution and magnitude of these loads. Assume that all surfaces of the shell are free of stress except the base, which is assumed rigidly clamped to an inertial frame, and the portion of the external surface exposed to a distributed pressure pulse $P(\theta, z, t)$. Figure 4 shows an initially undeformed shell with a distributed load applied to its outer surface, and a typical deformed shape which results from such a load.

We assume this pressure pulse to be distributed uniformly over a quadrant of the shell, and to be uncoupled from the motion of the shell. A typical pressure pulse reaches an instantaneous peak P_0 , and then decays to zero in a finite time T_0 , called the impulse duration, as shown in Figure 4. We may express the idealized impulse mathematically, in cylindrical coordinates, as

$$I(\theta, z) = \int_{t_0}^{t_0 + T_0} P(\theta, z, t) dt = I_0 \Psi(\theta, z) \quad (5.1.1)$$

where $I_0 = P_0 T_0 / 4$ is the peak impulse, and where

$$\Psi(\theta, z) = \left\{ \begin{array}{l} 1, \quad -\pi/4 < \theta < \pi/4 \\ 0, \quad \pi/4 < \theta < 7\pi/4 \end{array} ; 0 < z < b \right\} \quad (5.1.2)$$

is the normalized impulse distribution.

The load distribution defined by Equation (5.1.2) is considered to be sufficiently regular to excite mainly the first few natural vibration modes of the shells. As stated in Section II.1, if either one of the two conditions $T_0 \ll T_1$ or $T_0 = T_1$ is valid, where T_1 is the fundamental quarter period of the shell, and providing the load distribution is sufficiently regular, then the load can be described simply by the variables T_0 , I_0 and $\Psi(\theta, z)$.

d. Response variables. A conical frustrum shell will deform approximately as shown in Figure 4 (the dashed lines) when subjected to an impulsive load such as described above. The initial transient deformation will then disperse rapidly over the entire shell, and the resulting complex shell vibrations will eventually decay, leaving a field of residual displacements. For a given shell, and a given load duration and distribution, the amount of deformation —both transient and residual —increases with the total impulse.

In order to express the impulse-deformation characteristics of a shell quantitatively, it is necessary to define suitable measures of the deformation. Let the radial displacements of the inner surface of a shell be represented by the function $u(\theta, z, t)$, $t > t_0$. Define the quantities

$$\left. \begin{aligned} U^T &\equiv \max u(0, b, t), \quad 0 < t - t_0 < 2T_1 \\ U^R &\equiv \lim u(0, b, t), \quad t - t_0 \rightarrow \infty \end{aligned} \right\} \quad (5.1.3)$$

to be the maximum transient displacement and the maximum residual displacement of the point $\theta = 0$, $z = b$ on the inner surface of the shell. In general, the largest transient and residual displacements will be associated with this point, so that U^T and U^R satisfactorily characterize the extremes of shell deformation for a single test. Therefore, the scalar functions

$$U^T = U^T(I_0, T_0), \quad U^R = U^R(I_0, T_0) \quad (5.1.4)$$

suffice to describe the impulse-deformation characteristics of a given shell with a given normalized load distribution.

It is of interest to determine which shells have the highest resistance to deformation and the lowest weight; thus, we shall determine the total weight W of each shell. Likewise, since the resistance to deformation by impulsive loads is intrinsically related to the fundamental natural frequency f_1 of a given shell, we shall also determine the fundamental quarter period $T_1 \equiv 1/4f_1$ as a dependent variable for each shell.

2. The Prototype Variables

After consulting with the project sponsors, an aluminum alloy (type 6061-T6) was chosen as the primary material to be used in constructing the prototype shells, and the following values were selected for geometric variables:

$$\left. \begin{array}{l} \text{cone angle, } \alpha_p = 12.5^\circ \\ \text{mean inner radius, } a_p = 15 \text{ in.} \\ \text{axial length, } b_p = 30 \text{ in.} \end{array} \right\} \quad (5.2.1)$$

The diameters corresponding to these values are

$$\left. \begin{array}{l} \text{upper diameter} = 36.65 \text{ in.} \\ \text{lower diameter} = 24.35 \text{ in.} \end{array} \right\} \quad (5.2.2)$$

which are typical dimensions of an RV tail section. In addition it was decided to load the shells with sheet explosives obtained from and administered by Stanford Research Institute. The total number of prototypes was limited to four because of costs of building and testing.

Selection of the shell compositions involved a compromise of several factors. The shells were required to be as simple, and to have as many common features, as possible, in order to provide meaningful results. The shells were required to be of fairly light construction in order that manageable explosives would produce deformations of about ten percent, as desired. Yet the shells were required to be thick enough that reduced scale models of the shells could be fabricated without difficulty. Also, the project sponsor requested that the shells be strong enough to reasonably typify RV tail section construction; and that special composite shells be considered having, alternately, a layer of ablative heat shield material; sandwich construction; and some light, shock absorbent material to completely fill the shell.

The final selections of shell compositions are described below. The prototype materials, designated AL, HS, and PF, were described in Section IV. The geometric properties of the prototype shells are also listed in Table VII.

Prototype P1. A plain shell $h_p = 0.125$ -in. thick of aluminum alloy (AL).

Prototype P2. A composite shell, consisting of a layer $h_{2p} = 0.250$ -in. thick of heat shield material (HS) bonded to a layer $h_{1p} = 0.125$ -in. thick of aluminum alloy (AL); total shell thickness $h_p = 0.375$ -in.

Prototype P3. A composite shell, of sandwich type construction, consisting of two layers $h_{1p}, h_{3p} = 0.075$ -in. thick of aluminum alloy (AL) separated by a layer $h_{2p} = 1.00$ -in. thick of plastic foam (PF); total shell thickness $h_p = 1.15$ in.

Prototype P4. A plain shell $h_{1p} = 0.125$ -in. thick of aluminum alloy (AL) completely filled with plastic foam (PF).

We conclude this discussion of prototype variables with a discussion of loading and response variables. The prototype shells were to be rigidly clamped around their bases (small diameter edge) during the prototype tests, and were to be loaded uniformly over a quadrant by means of sheet explosives. The load distribution of the sheet explosives was considered to be sufficiently regular to excite mainly the first few vibration modes. Also, the durations of the impulses ($T_{op} \approx 0.1 - 0.2$ ms) from the sheet explosives were considerably shorter than the fundamental quarter periods of the shells ($T_p \approx 1 - 3$ ms). From arguments given in Section II.1, we conclude that the response of the prototype shells was dependent only on peak impulse I_{op} .

Each prototype shell was loaded by a series of three or four sheet explosives of increasing impulse level, starting with a load that produced little deformation and ending with one that completely destroyed the shell. The maximum residual deformation U_P^R was measured for each test; in addition, high speed motion pictures provided measurements of maximum transient deformations. Since the levels of impulse applied to the prototype shells were dependent on the loads which each shell could sustain, these loads were estimated from the model test results.

3. Scale Factors

The scale factors were chosen largely on the basis of available materials and available facilities for testing the models. As stated earlier, the present investigation was intended to demonstrate the technique of modeling with dissimilar materials. The development of model materials was discussed in Section IV. Tables I - IV list the properties of the prototype and model materials. The density and stress scale factors

$$\left. \begin{aligned} \gamma &\equiv \frac{\rho_{MAL}}{\rho_{AL}} = \frac{0.285 \text{ pci}}{0.100 \text{ pci}} = 2.85 \\ \mu(\text{dynamic}) &\equiv \frac{E_{MAL}}{E_{AL}} = \frac{10^6 \text{ psi}}{10^7 \text{ psi}} = 0.10 \end{aligned} \right\} \quad (5.3.1)$$

are based on the "dynamic" properties of the primary model and prototype materials, designated MAL and AL, respectively.

The following conditions were recognized as desirable with regard to size of the models. Models should be as large as possible in order to reduce the possibility of geometric distortion, yet models should be small enough to allow inexpensive fabrication. It was expedient to test models in the existing two-foot diameter shock tube. It was considered desirable that prototypes and models be of significantly different size in order to demonstrate the range of the modeling technique.

The diameter of the shock tube limited the largest model dimension to about one foot. For convenience, a mean inner diameter of six inches was finally selected for the models. This choice resulted in a length scale factor of

$$\lambda \equiv \frac{a_m}{a_p} = \frac{3.0 \text{ in.}}{15.0 \text{ in.}} = 0.20 \quad (5.3.2)$$

From Equation (2.3.5) and Equations (5.3.1) and (5.3.2), we can calculate the time scale factor

$$\tau \equiv \lambda \left(\frac{\gamma}{\mu} \right)^{1/2} = 0.2 \left(\frac{2.85}{0.10} \right)^{1/2} = 1.07 \quad (5.3.3)$$

The conical frustrum shells considered in this Section are special cases of the mechanical systems considered in Section II. Each of the variables defined in Section V.1, and listed in Table V, has a counterpart in Section II, as shown by the following comparison.

<u>Section II</u>	<u>Section V</u>
$l_i; \theta_i$	$a, b, h, h_n; a$
$\rho_n; \mu_n; \tau_n$	$\rho_n; E_n; -$
c_{mn}	$E_n / Y_n; E_n / E'_n$
$T_0; I_0; \Psi(\underline{X})$	$T_0; I_0; \Psi(\theta, z)$
$U_j^T; U_j^R; W; T_1$	$U^T; U^R; W; T_1$

Therefore, the modeling analysis of Section II can be used to provide modeling relationships for the prototypes described in Section V.2. These relationships, which can be calculated from Equations (2.3.3) and (2.3.4) of Section II.3, are listed in Table 6.

4. The Model Variables

As mentioned earlier, a total of nine distinct models were tested. The basic dimensions of the models were

$$\left. \begin{array}{l} \text{cone angle, } a_m = 12.5^\circ \\ \text{mean inner radius, } a_m = 3.0 \text{ in.} \\ \text{axial length, } b_m = 6.0 \text{ in.} \end{array} \right\} \quad (5.4.1)$$

Four of the nine models were direct models of the prototypes described in Section V.2. These models were intended to verify the modeling technique and to provide information about the impulse-deformation characteristics of composite shells. The independent variables for these models were determined by substituting values of the prototype independent variables, as given in Table VII (and in Section V.2), into the modeling relationships listed in Table VI.

The resulting model (geometric) variables are listed below and in Table VIII. The model materials, designated MAL, MHS, and MPF, and the methods of fabricating the models, were discussed in Section IV.

Standard cone model M1. A plain shell $h_m = 0.025$ -in. thick made of the basic model material (MAL).

Heat shield cone model M2. A composite shell, consisting of a layer $h_{2m} = 0.050$ -in. thick of model heat shield material (MHS) bonded to a layer $h_{1m} = 0.025$ -in. thick of the basic model material (MAL); total shell thickness $h_m = 0.075$ in.

Sandwich cone model M3. A composite shell consisting of two layers $h_{1m}, h_{3m} = 0.015$ -in. thick of the basic model material (MAL) separated by a layer $h_{2m} = 0.20$ -in. thick of model plastic foam (MPF); total shell thickness $h_m = 0.23$ in.

Foam-filled cone model M4. A plain shell $h_{1m} = 0.025$ -in. thick made of the basic model material (MAL) and completely filled with model plastic foam (MPF).

Because of the relatively small cost of building and testing models compared with the overall cost of the modeling program, it was deemed expedient to perform tests on additional models in order to generate a wider variety of data. The correlations intended with these additional models were mainly between geometric variables. It was decided to consider only plain shells for these tests, made of the basic model material (MAL); and to consider separate variations of the axial length, shell thickness, and cone angle, using the geometric variables of the standard cone model (M1) as the median values.

The five additional models are listed below, and in Table VIII, together with their distinguishing features.

Short cone model M5. A plain shell $b_m = 4.0$ -in. long, $h_m = 0.025$ -in. thick, and with a cone angle of $\alpha_m = 12.5^\circ$.

Thick cone model M6. A plain shell $b_m = 6.0$ -in. long, $h_m = 0.075$ -in. thick, and with a cone angle of $\alpha_m = 12.5^\circ$.

Standard cylinder model M7. A plain shell $b_m = 6.0$ -in. long, $h_m = 0.025$ -in. thick, and with a cone angle $\alpha_m = 0^\circ$.

Short cylinder model M8. A plain shell $b_m = 4.0$ -in. long, $h_m = 0.025$ -in. thick, and with a cone angle of $\alpha_m = 0^\circ$.

Thick cylinder model M9. A plain shell $b_m = 6.0$ -in. long, $h_m = 0.075$ -in. thick, and with a cone angle $\alpha_m = 0^\circ$.

The short cone model M5 was excluded from Table VIII and from the model test results because insufficient data were obtained for this model during the model tests.

We conclude this discussion of model variables with a discussion of loading and response variables. In Section V.2, it was stated that the prototype shells were to be clamped at their bases, and were to be loaded by impulses uniformly distributed over a quadrant of each shell. The impulse durations were stated to be considerably shorter than the natural quarter periods of the prototype shells. For correct modeling, these conditions were required to prevail during tests of the model shells.

Two methods were used for loading the models. The majority of model tests were made using a two-foot diameter shock tube, as illustrated in Figures 5-7, to provide the impulsive loadings. For each test a model was clamped to a rigid framework located at the mouth of the shock tube. The model was then covered by a blast shield which exposed only a quadrant of the model to the shock wave. The shock wave was generated in the shock tube by the sudden release of compressed air caused by the bursting of a mylar diaphragm. Section V.5 gives a more complete description of the shock tube model test facility.

The other method of loading models was by use of a sprayed-explosives technique recently developed at SwRI. This technique consisted of spraying an explosive coating directly onto the model, and subsequently detonating the coating by means of an electrical spark. Figure 8 shows a model with an explosive coating which is ready to be detonated. The sprayed explosives loading technique will be described in detail in Section V.8.

Both the above loading techniques provided impulses which were uniformly distributed over a quadrant of each model. The shock tube provided two separate impulse durations ($T_{om} \approx 1$ ms and $T_{om} \approx 4$ ms) which were of the same order as the natural quarter periods of the models ($T_{1m} \approx 1 - 3$ ms). Therefore, from Section II.1, we conclude that the response of the models to loading in the shock tube was dependent on peak impulse I_{om} and impulse duration T_{om} . The sprayed explosives technique provided impulse durations ($T_{om} = 0.1 - 0.2$ ms) which were considerably shorter than the natural quarter periods. Therefore, the response of the models to the sprayed explosive was dependent only on I_{om} .

The maximum transient displacement U_m^T and the maximum residual displacement U_m^R , as defined in Section V.1, together with the peak impulse I_{om} and the impulse duration T_{om} , were recorded for each model test.

5. The Shock Tube Model Test Facility

The majority of model tests were performed using the existing compressed-air shock tube facility depicted in Figures 5-7. Figure 5 is a schematic diagram which shows the shock tube, the compressed air lines, the test stand and associated apparatus, and the instrumentation for recording transient pressure, impulse, and displacements during the model tests. Figure 6 is a photograph which shows the entire shock tube; the framework at left is the test stand. Figure 7a shows the test stand in detail, and Figure 7b is a closeup view of the model mounted on the test stand.

The shock tube proper is a two-foot diameter steel pipe, twenty feet long, flanged at one end, and mounted on rollers. Beyond the flanged end of the shock tube is another short section of two-foot diameter pipe, called the air reservoir, which is closed at one end and flanged at the other to match the flange on the shock tube. The air reservoir is fastened to a massive block of concrete which absorbs the recoil from the shock tube. For each model test a mylar diaphragm was fitted between the flanges, and twenty-four, one-inch diameter bolts held the diaphragm securely between the shock tube and the air reservoir. An "O-ring" mounted in one of the flanges prevented leakage of air past the diaphragm.

The shock tube was operated by simply increasing the pressure in the air reservoir until the mylar diaphragm ruptured. Pressure in the reservoir at rupture was read from a Bourdon gauge. The burst pressure was controlled by the thickness of the diaphragm. Mylar was selected as the diaphragm material because of its property of bursting abruptly without fragmenting.

Prior to testing models, a series of measurements was made to determine the general characteristics of the pressure waves generated by the shock tube. The pressure transducers used were Kistler piezoelectric-type, connected through low-capacitance cables and special Kistler charge amplifiers to an oscilloscope. Each pressure transducer was mounted flush with the surface in a lead block, and the lead block was shock isolated with foam rubber. These assemblies were found to provide reliable transient (stagnation) pressure records. One of these assemblies was attached to the mounting plate and used to record transient pressures throughout the model tests.

The shock waves were found to be sufficiently plane near the center of the mouth of the shock tube for the purpose of model testing. Throughout the model tests the exposed surfaces of the models were aligned with the

mouth of the shock tube. It was found that peak pressure at the mouth of the shock tube depends on both the burst pressure and the volume of the air reservoir, whereas the duration of the pressure pulse depends primarily on the volume of the air reservoir. Thus by using various thicknesses of mylar diaphragms in conjunction with each of two air reservoirs of different volumes, it was possible to obtain two families of pulses of varying peak pressures but of virtually constant durations. The loading characteristics of the shock tube averaged over a large number of pressure measurements are shown in Table IX.

The large air reservoir utilized the entire volume (~ 8 cubic feet) inside the section of two-foot-diameter pipe behind the shock tube, and provided pulse durations of about $T_{om} = 4$ ms. The small air reservoir was obtained by fitting a slightly concave aluminum disk between the diaphragm and the large air reservoir. This disk can be seen in Figure 6, leaning against the concrete recoil block. The volume inside the small air reservoir (~ 1 cubic foot) provided pulse durations at the mouth of the shock tube of about $T_{om} = 1$ ms. These values of load duration were of the order of the natural quarter periods of the model shells.

The model shells were extended one-half inch beyond their nominal lengths. This extension (called "base" in Figure 3) was clamped securely to a heavy aluminum mounting plate, which in turn was bolted to the test stand. Figure 7b shows a model shell clamped to the mounting plate. The mouth of the shock tube can be seen at the left.

In order to restrict the loading of the shock waves to the forward quadrant of each model, a blast shield was constructed in the form of a sheet metal box, which completely enclosed each model except for a cutout circumscribing the forward quadrant. Clearances of 1/8-inch were maintained between the models and the blast shield as a compromise between excessive leakage of the shock wave into the blast shield and having the blast shield obstruct the model. Two blast shields were constructed; one for the cylinder models and one for the cone models. Figure 7a shows a model mounted on the test stand and shrouded by the blast shield. In this condition the model is ready to be tested.

The nature of the experimental program made it desirable to obtain records of the transient as well as residual displacements of the model shells. It was found that Bentley displacement transducers, which operate on a principle of generating and detecting eddy currents, could be used satisfactorily with the composite model materials. Unfortunately, the transducers were required to operate over distances ranging up to one-half inch, in order to prevent interference with the motion of the model shells. Over such large distances the output of a Bentley transducer is extremely non-linear. This fact necessitated frequent and careful calibrations of the displacement transducers.

A special adjustable fixture was devised which permitted up to three Bentley transducers to be positioned into proximity with the model shells. The device consisted of an L-shaped arm hinged at the corner to a yoke, which was fitted with a positioning dowel as shown in Figure 5. The long arm of the L contained three uniformly spaced holes, tapped to accept the external threads of the displacement transducers, which were fixed in place by lock nuts. The angle between the short arm of the L and the yoke was controlled by a machine screw acting against a spring, which provided the necessary range of adjustments. The dowel fit snugly into a hole drilled through the mounting plate, concentric with the model shells. Figure 7b shows the adjustable fixture, fitted with two Bentley transducers, and positioned to detect displacements in line with the oncoming shock waves.

The instrumentation used in conjunction with each of the Bentley transducers included a Bentley distance detector (D-152), a 22-1/2-volt dry cell battery, and appropriate cables connecting the detectors to a Tektronix oscilloscope, as shown in Figure 5. The box at the top of the test stand in Figure 7a housed the battery for powering the displacement transducers. The devices shown suspended midway between the power supply box and the blast shield are the Bentley detectors.

One oscilloscope was used to display the transient displacement signals (up to three traces simultaneously) and one oscilloscope was used to display the transient pressure signals. The latter was a dual-beam oscilloscope with a built-in integrator circuit, so that for all shock tube tests records were obtained of transient pressure and transient impulse. Both oscilloscopes were fitted with Polaroid cameras which allowed permanent records to be made of the oscilloscope traces.

The oscilloscopes were triggered by a device which consisted of a battery connected in series with a light bulb and a pair of alligator clips mounted inside the mouth of the shock tube. The circuit was completed by fitting two short strips of aluminum foil, which had been twisted together, between the alligator clips. The light bulb was connected across the external trigger inputs of the oscilloscopes through a blocking capacitor. As a shock wave passed down the tube and encountered the aluminum foil, the two strips of foil were untwisted, thus opening the circuit. The abrupt change in voltage across the light bulb caused the oscilloscopes to trigger. This triggering circuit was found to be reliable, and was used throughout the shock tube tests.

6. Model Test Procedure

The models were refrigerated after curing and overnight between tests to prevent changes in the material properties. A large supply of mylar film of various thicknesses was obtained prior to the model tests, and individual diaphragms were cut from the mylar film with holes punched to match those in

shock tube flanges. All the necessary apparatus including piping and electronic equipment were obtained and put into operating condition.

The Kistler pressure transducers are piezoelectric devices, which cannot measure "static" response. Therefore, it was necessary to resort to a dynamic calibration technique. The calibration technique involved fitting the transducer to a dead-weight tester, and dropping a known weight onto the platform of the tester. Special care was taken to exhaust the air from the tester in order to increase its response rate. The transducer was connected to an oscilloscope, which was set to trigger internally off the pressure signal. The first picture in Figure 9 shows two calibration tests; the upper signal is transient pressure, the lower signal is transient impulse. Knowing the sweep rate and the pressure difference represented by the dropped weight, calibrations of the pressure and impulse scales were easily calculated.

The results of numerous calibration tests during the test series indicated that the sensitivity of the pressure transducers was essentially constant in the range of interest (~ 100 cps). However, variations in sensitivity of 20%-30% were noted from time to time. These variations were attributed mainly to the transducer and connecting cables picking up moisture and thus changing capacitance (piezoelectric transducers are sensitive to capacitance changes). The occurrence of this discrepancy during model tests led to adoption of a single set of average loading characteristics for the shock tube, as described below.

Comparison of burst pressures with the thickness of the mylar diaphragms showed good correlation throughout the test series. Comparison of peak pressure and impulse at the mouth of the shock tube with diaphragm burst pressures provided good correlation between tests on any one day. However, the correlation between tests on different days was not good, which indicated the pressure transducer was at fault. Therefore, we felt that the best correlation of test results would be obtained by using average values of peak pressure and impulse, averaged over many tests, rather than using the specific values recorded for each test. Table IX presents the loading characteristics of the shock tube, which were used in plotting the model test results.

Weights and natural frequencies of the models were recorded because of their interest as results in the modeling investigation, and because comparisons of prototype and model natural frequencies afforded a means of obtaining "dynamic" material properties. The natural frequencies of the models were obtained as follows: The model was clamped to the mounting plate, and two of the Bentley transducers were positioned inside the model. The transducers were connected to an oscilloscope, which was set to trigger internally off one of the displacement signals. The model was then rapped lightly with a knuckle or fingertip. The third picture in Figure 9 shows oscilloscope traces from two such tests. The signals are seen to be

of the form of decaying elastic vibrations. Knowing the oscilloscope sweep rate, the predominant natural frequency was easily calculated.

The last preliminary before a model test was calibration of the displacement transducers. Because of the nonlinearity of their signals and the tendency of the signals to drift, the Bentley transducers were recalibrated after every two or three model tests. The Bentley transducers are capable of measuring "static" as well as rapidly varying displacements; thus, a quasi-static calibration technique was used. The transducers were mounted in the L-shaped adjustable fixture (shown in Figure 8), which was positioned inside the model. The adjustment screw was turned until the top of the adjustable fixture was a convenient distance from the top edge of the model, as measured with a graduated rule. (Before each model test, the adjustable fixture was reset to this same distance from the top edge of the model, so that the transient displacement records and the calibration records could be compared directly.)

The transducers were connected to an oscilloscope, which was set to sweep at its slowest rate (~ 5 sec/cm). With the sensitivities set to convenient values, the oscilloscope was triggered manually. Then the distance between the top of the adjustable fixture and the top edge of the model was decreased by steps of ~ .05 in. until the transducers just touched the inside surface of the model. The second picture in Figure 9 shows oscilloscope traces for two such tests. By comparing these calibration records with transient displacement records, the desired maximum transient and residual displacements were obtained.

The procedure of testing a model using the shock tube facility was essentially as follows. The model was clamped to the mounting plate and located plane with the mouth of the shock tube. The Bentley transducers were calibrated and positioned to measure displacements in the direction of the shock tube axis. The blast shield was then clamped in place over the model. A mylar diaphragm was inserted between the flanges of the shock tube, in conjunction with either the large or small air reservoir, as described in the last section. Two strips of aluminum foil were twisted together and inserted between the alligator clips inside the mouth of the shock tube, thus activating the oscilloscope trigger circuit. The oscilloscopes were then set to single sweep, and the valve for admitting compressed air into the air reservoir was opened.

The diaphragm then burst and the oscilloscopes triggered by separation of the strips of aluminum foil. The third and fourth pictures of Figure 9 show oscilloscope traces for four model tests. In each case, the picture at left contains the transient pressure and impulse traces, and the picture at right contains the transient displacement traces. As explained earlier, the transient and residual displacements were correlated with average values of peak impulse, as given in Table IX rather than with values of peak impulse obtained for each individual test.

7. Model Test Results

At least one of each of the models M1-M9, as specified in Table VIII, was tested in the shock tube according to the above procedure. Since the model M1 was chosen as the standard model shell against which the majority of correlations were to be made, it was desirable to accumulate a large quantity of data for this model. Thus a total of four samples of the model M1 were made and tested. Two samples were made of the standard cylinder model M7. After sufficient data had been obtained from these two models, an inch was cut from each end, thus forming two samples of the short cylinder Model M9. The same technique was tried with only marginal success in converting the model M1 into the short cone model M5.

One sample of the thick cone model M6 and two samples of the thick cylinder model M8 were next made and tested. All samples of the plain model shells were tested in the shock tube. Finally, two samples were made of each of the composite shells M2, M3, and M4. One sample of each of these model shells was tested in the shock tube. The other sample of each of these models was tested using the sprayed-explosives technique, as described in Section V. 8.

From five to ten tests, of successively increasing peak impulse, were performed on each model. In each of these tests loads were restricted to the quadrant of the shell which had the least previous deformation history. Since it was discovered early in the tests that the results were quite sensitive to initial eccentricities of the shells and to any slippage that occurred at the clamped edge, special efforts were made to ensure that the cross sections of the shells were circular before each test and that the bases of the shells were clamped securely.

Figures 10 and 11 show the impulse-deformation data for each of the models (except M5, for which insufficient data were obtained). Plotted for each model are maximum transient displacements U^T and residual displacements U^R versus peak impulse I_0 for each of the two impulse durations provided by the large and small air reservoirs. The solid lines are averages drawn through the residual deformation data, and the dashed lines are averages drawn through the maximum transient deformation data.

For each model and for a given impulse duration, U^T and U^R are increasing functions of peak impulse. However, U^R is zero until a finite value - the threshold of permanent deformation - is reached; for an impulse less than this value the deformations of the shell are purely elastic. For each model and for a given impulse, U^T and U^R increase as the impulse duration decreases. The values of U^T and U^R can be expected to approach limits as the impulse duration tends to zero: U^T and U^R will be maximum for a perfect impulse.

The functions $U^T(I_0)$ and $U^R(I_0)$ for a given impulse duration are seen to be nonlinear in such a way that the impulse approaches a constant value for indefinitely large deformations. Since fracture was not included in the material properties modeled during the present investigation, the model tests were not expected to be accurate for extremely large deformations. However, it is felt that the curves presented in Figures 10 and 11 provide fairly accurate indications of impulse-deformation characteristics of shells for moderately large deformations.

The scatter of data for the standard cone model M1 and the standard cylinder model M6 are seen to be considerably greater than for the other models. This scatter of data can be explained by the fact that the mode of deformation for M1 and M6 was partly buckling, whereas the other models deformed simply in the so-called "collapse" mode. Therefore, M1 and M6 were particularly sensitive to initial eccentricities of the shell and inhomogeneity of the material properties. For the particular buckling mode of these shells, the maximum deformations occurred at points on either side of $\theta = 0$, $z = b$ (see Fig. 3) at which U^T and U^R were measured. This fact also contributed to the scatter in data for the models M1 and M6.

Figures 12 and 13 are photographs of the standard cone model M1 and the standard cylinder model M6, respectively, in undeformed, slightly deformed, and moderately deformed conditions. These photographs show the buckling mode of deformation for the models M1 and M6, as mentioned above. Figure 14 shows the heatshield cone model and the thick cone model M6 in undeformed and slightly deformed conditions. These models deformed uniformly in the "collapse" mode, which partially explains the small scatter in data for these two models. A significant fact to note is that all of the models failed by splitting around the front, just above the clamped base. Evidently, for shells loaded transversely, as in the present investigation, the largest stresses in the shells are tensile stresses tending to pull the shell loose from the clamp in front.

Figure 15 shows the sandwich cone model M3 and the foam-filled cone model M4 in undeformed and deformed conditions. The sandwich model was the most resilient of all the models; that is, for a given amount of permanent deformation the sandwich model sustained far greater transient deformations than any of the other models. The foam-filled model was peculiar in that hardly any residual deformations were observed up to the point at which the model sheared off completely at its base.

As stated in the Foreword, one of the primary objectives of the present investigation was to generate information about the impulse-deformation characteristics of conical frustum shells. The model tests were intended to provide correlations between the resistance to deformation by impulsive loads and the following shell parameters: (1) three special composite shell structures; (2) shells of various length, thickness, and cone angle; and (3) load durations.

In order to make these correlations a discrete measure of "resistance-to-deformation-by-impulsive-loads" was required. Suitable measures of this quantity are defined below.

Let the symbol I_0^T represent the peak impulse necessary to produce a maximum transient displacement of $U^T = 0.60$ in. (ten percent of the mean shell diameter); and let the symbol I_0^R represent the peak impulse necessary to produce a residual displacement of $U^R = 0.30$ inch. For a given model, I_0^T and I_0^R are functions only of impulse duration. Thus, two values of I_0^T and two values of I_0^R (corresponding to the two impulse durations $T_0 \sim 4$ ms and $T_0 \sim 1$ ms) can be obtained from Figures 10 and 11 for each of the models.

These values of I_0^T and I_0^R are tabulated in Table X, along with the weights W and the natural frequencies f_1 of the models. The larger values of I_0^T and I_0^R are associated with the models which are more resistant to deformation by impulse. Note that corresponding values of I_0^T and I_0^R are nearly equal: the maximum transient displacements are nearly twice the residual displacements for almost every model. The following correlations are based on the tabulated values of I_0^T and I_0^R given in Table X. The results for each model will be compared with the results of the standard model M1; each of the other models is considered to be a simple variation from M1.

We first compare and correlate the results of the three composite shells (M2-M4). The independent variables for these shells are identical except for the shell compositions, which are listed in Table VIII. From Table X we observe that the heat shield model (M2) is about twice as resistant to deformations as the standard Model (M1); that the sandwich model is about four times as resistant to deformations as the standard model; and that the foam-filled model (M4) is about five or six times as resistant to deformations as the standard model. Thus, of the composite shells, the foam-filled shell is the most resistant to deformations. However, the sandwich shell has the highest strength-to-weight ratio, since it is the lightest of the composite shells, weighing about half as much as the foam-filled shell.

We next compare and correlate the effects of various geometric variables on the impulse-deformation characteristics of the models. The independent variables of the corresponding cylinder models M7 and M9, except for the cone angle α , which is 12.5° for the cone models and 0° for the cylinder models. From Table X we compute the following ratios:

$$\frac{I_{O}^T(M7)}{I_{O}^T(M1)} = \left\{ \frac{7.5}{5.8} = 1.29; \frac{9.0}{7.2} = 1.25 \right\}$$

$$\frac{I_{O}^R(M7)}{I_{O}^R(M1)} = \left\{ \frac{9.5}{5.3} = 1.80; \frac{11}{8.2} = 1.34 \right\}$$

(5.7.1)

$$\frac{I_{O}^T(M9)}{I_{O}^T(M6)} = \left\{ \frac{30.5}{21.5} = 1.42; \frac{43}{27} = 1.59 \right\}$$

$$\frac{I_{O}^R(M9)}{I_{O}^R(M6)} = \left\{ \frac{37}{23.5} = 1.57; \frac{50}{26.5} = 1.89 \right\}$$

We observe from (5.7.1) that the standard cylinder (M7) is about 1.4 times as resistant to deformation as the standard cone (M1); and that the thick cylinder (M9) is about 1.6 times as resistant to deformations as the thick cone (M6). These results indicate that, in general, cylindrical shells are approximately 1.5 times as strong as corresponding 12.5° conical shells.

The independent variables of the standard cylinder model M7 are identical with those of the short cylinder model M8, except that the axial length $b = 6$ in. for M7 compared with $b = 4$ in. for M8. From Table X we compute the following ratios:

$$\frac{I_{O}^T(M8)}{I_{O}^T(M7)} = \left\{ \frac{15.5}{7.5} = 2.07; \frac{18}{9} = 2.00 \right\}$$

(5.7.2)

$$\frac{I_{O}^R(M8)}{I_{O}^R(M7)} = \left\{ \frac{15}{9.5} = 1.58; \frac{19}{11} = 1.73 \right\}$$

Because resistance-to-deformation should increase very rapidly if the length of the shell were to be decreased further, we conclude that the strength of a clamped shell varies approximately as the reciprocal of its length.

The independent variables of the models M1 and M7 are identical with those of M6 and M9, respectively, except that M6 is three times as thick as M1, and M9 is three times as thick as M7. From Table X we compute the ratios:

$$\frac{I_{O}^{T}(M6)}{I_{O}^{T}(M1)} = \left\{ \frac{21.5}{5.8} = 3.7; \frac{2.7}{7.2} = 3.7 \right\}$$

$$\frac{I_{O}^{R}(M6)}{I_{O}^{R}(M1)} = \left\{ \frac{23.5}{5.3} = 4.4; \frac{26.5}{8.2} = 3.2 \right\}$$

$$\frac{I_{O}^{T}(M9)}{I_{O}^{T}(M7)} = \left\{ \frac{30.5}{7.5} = 4.1; \frac{43}{9.0} = 4.8 \right\} \quad (5.7.3)$$

$$\frac{I_{O}^{R}(M9)}{I_{O}^{R}(M7)} = \left\{ \frac{37}{9.5} = 3.9; \frac{50}{11} = 4.5 \right\}$$

We observe from (5.7.3) that the thick cone model (M6) is about 3.75 times as resistant to deformation as the standard cone model (M1); and that the thick cylinder model (M9) is about 4.3 times as resistant to deformation as the standard cylinder model (M7). We conclude that the strength of a conical shell varies approximately as 4/3 times its thickness.

The foregoing conclusions based on comparisons of the model test results should be fairly accurate, since absolute errors tend to cancel in making such comparisons. However, the absolute errors in the model test results are unknown, since the prototype test results could not be used for comparison. Nevertheless, the model test results should provide nearly correct predictions for the response of the prototypes described in Section V.2. To facilitate making such predictions, we have presented the test results, as given in Table X, in dimensionless form in Table XI.

8. The Sprayed Explosive Loading Technique

Concurrent with model tests using the shock tube, an impulsive loading technique was developed whereby a uniform layer of an explosive compound can be spray-deposited directly onto a surface and subsequently ignited by a spark or a strong light source [15]. The compound, silver acetylide-silver nitrate, was finally selected over other explosives because of the ease and safety with which small quantities can be produced from common stable chemicals. This explosive provides ideal low-level and short-duration impulses, as required for model testing. The peak impulse (per unit area) from this sprayed explosive was found to be directly proportional to the thickness or surface density of the deposited layer in the range 1-50 psi-ms. The impulse durations at a point were found consistently to be less than 5 microseconds.

When suspended in water or acetone, silver acetylide-silver nitrate is completely safe and can be sprayed using a hand-held gun. It was found that

the explosive would not detonate unless completely dry, so that thickness measurements were made by hand during the spraying process. Acetone was used as the liquid agent because it evaporates from a layer of explosive in a matter of minutes (under ideal conditions), whereas a layer of explosive which was suspended in water requires several hours to dry. After drying, the explosive is ready to detonate, or, if desired, it can be completely deactivated using dilute hydrochloric acid. Other details of production, application, and calibrations of this explosive are presented in Reference [16].

A limited number of model tests were made using the sprayed explosive technique. The test procedure differed from the shock tube procedure mainly in the application and detonation of the explosive. The explosive was sprayed directly onto the model, with all but a quadrant of the model surface masked off. The explosive thickness was measured periodically using a penetration gauge (of the type used to measure paint layers) until a sufficiently thick layer of explosive had been applied. The excess explosive was then washed off and deactivated, and the explosive coating was allowed to dry. A typical explosive coating appears snow white and has the texture of fine sandpaper.

Figure 8 shows a model clamped to the mounting plate and ready for testing. A Bentley transducer mounted in the same adjustable fixture was used to measure transient displacements. The explosive was detonated by means of an automotive spark coil, which can be seen in the foreground of Figure 8. Results of the model tests using the sprayed explosive technique are shown in Figure 10 for each of the models M1-M4. These data, represented by open circles, are seen to agree fairly well with the shock tube data. Any scatter in these data can be attributed to the relatively inaccurate values of peak impulse, which were obtained by correlating the measured explosive coating thickness with previous calibrations.

9. The Prototype Tests

One of the objectives of this program was to obtain correlation between tests of prototype structures and tests of scale models in order to verify the technique of modeling with "dissimilar" materials. To obtain this correlation, tests were made of the four prototype conical frustrum shells described in Section V.2. In these tests, the prototypes P1-P4, whose characteristics are given in Table VII, were clamped to a massive test block and subjected to impulsive loadings over a quadrant by detonating sheet explosives near or in contact with the outer surface of each shell. Figure 16 shows one of the prototype shells ready for testing.

Measurements of maximum permanent deformations U_R^p were made after each prototype test for comparison with the model test results. In addition, high-speed motion pictures were made of the prototype tests. These motion pictures were intended to provide an indication of the maximum transient response of the prototypes due to the impulsive loads.

Unfortunately, very little useful information was obtained from these tests. The prototype shells failed in either one or both of two modes:

- (1) slippage from the clamping device, and
- (2) tension failure of the welds.

These failures occurred for all prototype shells for scaled loadings considerably less severe than those required to cause significant damage to the corresponding model shells. A typical failure of the first type can be seen in Figure 17, while one of the second type can be seen in Figure 18. Attempts were made to rectify these deficiencies by rewelding and reinforcing the seams, and modifying the clamping device. We eliminated seam failure in this manner, but were not able to eliminate slippage at the clamped edge.

Pretest measurements did yield values of the weights and natural frequencies of the prototype shells, which were used for comparisons with the model characteristics. Also, the general character of the permanent deformations of several shells whose seams remained intact could be observed and compared with the character of deformation of the model shells. Such qualitative comparisons generally showed good agreement.

SECTION VI

CONCLUSIONS AND RECOMMENDATIONS

1. Conclusions

A dynamic modeling analysis for response of RV-type vehicles due to impulsive loads was developed in detail in this report. The analysis included the possibility of constructing models from "dissimilar" materials; that is, model materials which are different but similar to the prototype materials. The report also includes a discussion of errors in modeling, and a program of developing dissimilar materials to model typical RV materials was described. Modeling experiments, involving impulsively loaded conical frustrum shells, undertaken to illustrate the modeling theory, were also described. In addition, the several appendices provide a useful supplement to the text of this report.

The investigation was successful in several respects. The detailed modeling analysis, including the discussion of modeling errors, can be used as a guide for performing similar studies in the future. The program of developing dissimilar materials, first investigated under a previous contract, was refined and expanded to include several prototype materials in the present investigation. Satisfactory model materials were obtained for lightweight core materials and heat shield materials, as well as for the primary structural material (aluminum). A spray technique was developed for fabricating shell-type model structures from these model materials; this spray technique was found to be successful for fabricating composite shells composed of two or more layers of different materials.

The shock tube facility was found to be a reliable —though somewhat clumsy — method of loading models, with load durations on the order of the natural quarter periods of the model shells. Under a concurrent SwRI internal research project, a technique was developed whereby an explosive compound (silver acetylide) could be sprayed directly onto a model, and subsequently ignited by an electrical spark or an intense light pulse. This sprayed-explosive technique was found to be a safe, simple, and reliable method of applying short-duration impulsive loads to models.

The results of testing a series of one-fifth scale model conical frustrum shells made from dissimilar materials provided the following observations. The models were clamped rigidly at the small end and were impulsively loaded over a quadrant using the shock tube facility and the sprayed-explosive technique.

1. To compensate for the effects of strain-rate sensitivity, the "static" properties of the model materials were "corrected" on the basis of measured natural frequencies of the models and the prototypes. Use of the corrected "dynamic" properties instead of the "static" properties resulted in a decrease in the predicted impulse resistance of the models of about 30 percent.

2. Of the three composite model shells tested, the foam-filled shell provided the highest absolute resistance to impulsive loads, while the sandwich cone provided the highest resistance on the basis of ratio of strength-to-weight.

3. From correlations of geometric variables with the impulse-deformation properties of the plain models, it was observed that the cylindrical shells (cone angle $\alpha = 0^\circ$) are about 1.5 times stronger than corresponding conical shells (cone angle $\alpha = 12.5^\circ$). It was also observed that the strength of cylindrical and conical shells varies approximately as the reciprocal of the axial length, and approximately as $4/3$ times the shell thickness, for the range of shell variables considered in the present investigation. Note that these observations hold only for shells with clamped-free boundary conditions.

4. From correlations of impulse-deformation properties of the model shells with the duration of the applied impulse, it was observed that less peak impulse was required to deform a model by a given amount for shorter pulse durations. This effect can be expected to approach a constant value of deformation/impulse for very short pulse durations. The ratio of the deformations obtained for very short duration impulses to the deformations obtained for impulse durations on the order of the natural quarter periods of the model shells was never greater than about 2:1.

5. Two distinct modes of deformation were observed in the model tests. In the first mode, the very thin shells deformed partly by stretching and partly by buckling circumferentially; this mode of deformation was found to greatly reduce the strength of the shells, and provided erratic data. The other mode of deformation was the so-called "collapse" mode, consisting mainly of bending, which was characteristic of the thicker models, and provided much more reliable data.

6. Initial eccentricities and slippage at the clamped edge significantly reduced the strength of the shells — particularly of the thin shells. All models failed by splitting around the clamped edge. This fact indicated that the highest stresses occurred at the base of the shells.

A series of prototype shells was tested using sheet explosives to provide the impulsive loads. These tests produced inconclusive results because of slippage in the clamping device. Consequently, the impulse-deformation characteristics of the prototypes and models could not be compared, and the prototype test results were not used to verify the modeling technique.

2. Recommendations

In retrospect, it is clear that our choice of the type of structure and method of comparing model and prototype results (and thereby either validating or disproving the modeling philosophy) was unfortunate. The full-scale

experiments were very limited in number and were planned and executed late in the program. They proved to be so expensive that deficiencies in the test arrangement, which only became apparent after testing commenced, could not be corrected within the fund limitations of the program. The choice of conical shells as the structural geometry not only dictated high cost for prototype fabrication and test; it also obviated an accurate analysis of the response of the structure to impulsive loading.

A much more appropriate plan for validation of the model laws would have involved testing much simpler structures than truncated cones. Tests of flat plates, or beams, or simple rings would have had a number of advantages over testing of cones. First, for all of the simple shapes, there are available analytical predictions of plastic response to impulsive loading. References 5 through 11 present such treatments. Second, a large number of experiments have been performed in which transient and permanent large deformations have been measured. See, for example, References 5, 6, 8, and 15. Third, suitable experiments, on both prototype and model scale, are much simpler and less expensive to conduct than tests of cones. By an appropriate program of testing of the simpler structures, one could therefore either model existing test results, or conduct a complete model-prototype comparison. One could also compare predicted response for materials exhibiting strain-rate sensitivity [3] with measured response for our somewhat exotic model materials. Problems of proper mounting of the test structures would be lessened, and the costs of prototype tests so reduced that, if necessary, many such tests could be conducted for comparison with model data.

The lack of success in validating the model law during the test program reported here should not lead to the inference that this model law is invalid. The Institute has just completed an extensive test program on response of structural models of a very complex structure (the Apollo command module) to water impact, which required construction using materials having markedly different properties from the prototype. We were able to compare our results with results of full-scale water impact tests, and showed very good correlation [16]. Furthermore, the results of limited tests on beam structures conducted under a previous AFWL program indicated the validity of the law for relatively small permanent deformations.

We feel very strongly that more extensive experiments on simple structures should be conducted to determine the limits of usefulness of the technique of dynamic modeling with dissimilar materials. Also recommended are more detailed investigations into the properties of the model materials developed in this program. Such an investigation could be made using the dynamic biaxial testing machine recently built at Southwest Research Institute [18].

REFERENCES

1. G. E. Nevill, Jr., "Similitude Studies of Re-Entry Vehicle Response to Impulsive Loading," TDR 63-1, Vol. I (unclassified), Air Force Special Weapons Center, January 1963.
2. H. L. Langhaar, Dimensional Analysis and Theory of Models, John Wiley & Sons, Inc., New York, 1951.
3. W. E. Baker (editor), Colloquium on "Use of Models and Scaling in Shock and Vibration," ASME, New York, 1963.
4. W. E. Baker, "Modeling of Large Transient Elastic and Plastic Deformations of Structures Subjected to Blast Loading," J. Appl. Mech., ASME, Vol. 27, No. 3, 1960, pp. 521-527.
5. E. A. Witmer, H. A. Balmer, J. W. Leech, and T. H. H. Pian, "Large Dynamic Deformations of Beams, Rings, Plates and Shells," AIAA Journal, Vol. 1, No. 8, 1963, pp. 1848-1857.
6. S. R. Bodner and P. S. Symonds, "Experimental and Theoretical Investigation of Plastic Deformation of Cantilever Beams Subjected to Impulsive Loading," J. Appl. Mech., ASME, Vol. 29, No. 4, 1962, p. 719.
7. T. C. T. Ting, "The Plastic Deformation of a Cantilever Beam with Strain-Rate Sensitivity Under Impulsive Loading," J. Appl. Mech., ASME, Vol. 31, No. 1, 1964, pp. 38-42.
8. T. C. T. Ting, "Large Deformations of a Rigid, Ideally Plastic Cantilever Beam," J. Appl. Mech., ASME, Vol. 32, No. 2, 1965, pp. 295-302.
9. P. Symonds and T. Mentel, "Impulsive Loading of Plastic Beams with Axial Constraints," J. Mech. & Phys. of Solids, Vol. 6, 1958, p. 186.
10. F. J. Allen, "An Elastic-Plastic Theory of the Response of Cantilevers to Air Blast Loading," BRL Memorandum Report No. 886, Aberdeen Proving Ground, April 1955.
11. J. S. Humphreys, "Plastic Deformation of Impulsively Loaded Straight Clamped Beams," J. Appl. Mech., ASME, Vol. 32, No. 1, 1965, pp. 7-10.
12. L. S. Jacobsen, and R. S. Ayre, Engineering Vibrations, McGraw-Hill Book Co., Inc., New York, 1958.

13. G. Murphy, Similitude in Engineering, Roland Fress, New York, 1950.
14. L. A. Pipes, Applied Mathematics for Engineers and Physicists, McGraw-Hill Book Co., Inc., New York.
15. G. E. Nevill, Jr., and F. O. Hoese, "Impulsive Loading Using Sprayed Silver Acetylide-Silver Nitrate," Tech. Report No. 1, SwRI Project 02-1471, August 1964.
16. C. G. Langner, and F. O. Hoese, "Qualification Tests of Spray-Deposited and Light-Initiated Silver Acetylide-Silver Nitrate Explosive," Final Report, SwRI Project 02-1698, July 1965.
17. W. E. Baker, P. S. Westine, L. R. Garza, and P. A. Hunter, "Water Impact Studies of Model Apollo Command Module," Final Report on NASA Contract NAS9-2984, SwRI Project 02-1541, August 1965.
18. U. S. Lindholm, "Dynamic Deformation of Metals," Presented at ASME Colloquium on the Macroscopic Behavior of Structural Materials Under Dynamic Loads, November 1965.
19. C. Truesdell, "Principles of Continuum Mechanics," Colloquium Lectures in Pure and Applied Science, No. 5, Socony Mobil Oil Co., Field Research Lab., Dallas, 1960.
20. C. Truesdell, and R. A. Toupin, "The Classical Field Theories," Handbuch der Physik, Springer-Verlag, Vol. III, Part I, 1960.
21. L. Brand, "The Pi-Theorem of Dimensional Analysis," Arch. Ratl. Mech. Anal., Vol. 1, 1957, pp. 34-35.
22. J. C. Jaeger, Elasticity, Fracture, and Flow, 2nd ed., John Wiley & Sons, Inc., 1962, pp. 49-54.
23. F. R. Shanley, Strength of Materials, McGraw-Hill Book Co., Inc., New York, 1957.

APPENDICES

APPENDIX A

A BRIEF REVIEW OF CONTINUUM MECHANICS*

Continuum mechanics is the study of motion of continuous bodies in Euclidean space, and is primarily concerned with the mathematical expressions, or laws, which govern such motion. Euclidean space is the three-dimensional space of ordinary experience, in which the notions of straightness, flatness, and parallelism have precise meanings, and for which time is a scalar parameter independent of position. Existence of Euclidean space implies existence of "inertial" Cartesian coordinate systems for use as reference frames.

A continuous body is any finite portion of extended matter whose boundary and interior can be located by (spatial) points in a continuous region of Euclidean space at a particular instant of time, and for which a positive mass density exists as a measure at each (material) interior point. Motion consists of the continuous variations with time of the spatial coordinates of material points in a continuous body with respect to a "fixed" reference frame. Any motion at a material point can be decomposed into translation along an arc, and simultaneous rotation and stretching along three orthogonal axes.

The fundamental concepts of mechanics are density (mass per unit volume) and stress (force per unit area), and the fundamental problems of mechanics involve relating the scalar field of density and the tensor field of stress at material points in a continuous body to kinematical quantities such as deformation, deformation rates, acceleration, and distance from gravitating bodies. The fundamental field equations of mechanics are expressions of balance of mass and momentum, which can be stated as follows.

1. Balance of mass. The mass contained in a material volume V , which is any volume whose boundary consists of a constant set of material points, is constant. Thus, an expression of balance of mass is

$$\frac{d}{dt} \int_V \rho dv = 0 \quad (\text{A. 1})$$

where ρ is the mass density. Equivalently

$$\dot{\rho} + \text{div}(\rho \dot{x}) = 0, \quad [\rho U] = 0 \quad (\text{A. 2})$$

* Most of the material contained in this appendix has been condensed from References [19] and [20].

where $\dot{\underline{x}}$ is the velocity vector, and where the bracket denotes the amount of jump at a singular surface propagating through the material with speed U .

2. Balance of momentum. The rate change of linear and angular momentum of any material volume V is equal to the total force and total moment, respectively, acting on V . Thus expressions for balance of momentum are

$$\left. \begin{aligned} \frac{d}{dt} \int_V \rho \underline{x} dv &= \int_S \underline{t}(\underline{n}) ds + \int_V \rho \underline{f} dv \\ \text{and} \\ \frac{d}{dt} \int_V \underline{r} \times \rho \dot{\underline{x}} dv &= \int_S \underline{r} \times \underline{t}(\underline{n}) ds + \int_V \underline{r} \times \rho \underline{f} dv \end{aligned} \right\} \quad (\text{A.3})$$

where $\underline{t}(\underline{n}) = \underline{T} \cdot \underline{n}$ is the stress vector acting on an element ds of the surface S of V with unit normal \underline{n} , where $\rho \underline{f}$ is an extraneous body force such as provided by gravitational attraction, and where \underline{r} is a position vector with respect to a fixed origin. Equations (A.3) may be written equivalently as

$$\left. \begin{aligned} \rho \dot{\underline{x}} &= \text{div } \underline{T} + \rho \underline{f}, \quad \left[\underline{T} \cdot \underline{n} + \rho \dot{\underline{x}} U \right] = 0 \\ \text{and} \\ \underline{T} &= \underline{T}^T \end{aligned} \right\} \quad (\text{A.4})$$

The stress tensor \underline{T} is symmetric in the absence of body torques.

3. Initial and boundary conditions. In addition to the expressions (A.1) or (A.2) for balance of mass and the expressions (A.3) or (A.4) for balance of momentum, there are required initial and boundary condition equations, and a set of material constitutive equations, in order for a problem involving motion of a continuous body to be well set. Initial and boundary conditions equations can be stated in the form

$$\underline{x}_0 = \underline{x}(X^B, t_0), \quad \dot{\underline{x}}_0 = \dot{\underline{x}}(X^B, t_0), \quad \rho_0 = \rho(X^B, t_0) \quad (\text{A.5})$$

and

$$\underline{T} \cdot \underline{a} = \underline{t}(\underline{a})(X^A, t), \quad \underline{x}(X^A, t) \geq \underline{x}_c(t), \quad t \geq t_0 \quad (\text{A.6})$$

where \underline{x} are spatial coordinates and X^B , X^A are material coordinates of a body B with surface A and unit normal \underline{a} . Here t_0 is the initial time, and \underline{x}_c are rigid constraints which may limit the motion of B .

The following equations, expressed in terms of the coordinates \underline{x} , \underline{X}^B , are equivalent to the balance of mass equations (A. 1) or (A. 2):

$$\rho = \rho_0 J^{-1}(\underline{X}^B, t), \quad J = (g/G)^{1/2} \det \underline{F}, \quad \underline{F} = \text{grad } \underline{x}(\underline{X}^B) \quad (\text{A. 7})$$

Here g , G are determinants of the metric tensors associated with the coordinates \underline{x} , \underline{X}^B , respectively, and \underline{F} is the deformation gradient.

4. Constitutive Equations. Constitutive equations are relationships between stress and deformation, independent of acceleration, and thus distinguish particular materials. A general constitutive equation for deformable solid materials can be written as

$$\underline{C}(\underline{X}^B, t) = \underline{\mathfrak{J}}_{s=t_0}^t \left[\underline{T}(\underline{X}^B, s), \mu, \lambda, \tau, c_m \right] \quad (\text{A. 8})$$

where $\underline{\mathfrak{J}}$ is a functional relationship between the history of stress at the material point \underline{X}^B and the Cauchy-Green deformation tensor

$$\underline{C} = \underline{C}^T = \underline{F}^T \cdot \underline{F} \quad (\text{A. 9})$$

Here μ, λ, τ , and c_m , $m = 1, 2, \dots, M$ are material constants with dimensions of stress, length, time, and unity, respectively.* Let t_0 be the initial time; before t_0 the material is in its uniform reference condition:

$$\underline{C}(\underline{X}^B, t_0) = \underline{1}, \quad \underline{T}(\underline{X}^B, t_0) = \underline{0} \quad (\text{A. 10})$$

If the material is initially isotropic, then the functional $\underline{\mathfrak{J}}$ is subject to the restriction

$$\underline{\mathfrak{J}}_{s=t_0}^t \left[\underline{A} \cdot \underline{T}(s) \cdot \underline{A}^T \right] = \underline{A} \cdot \underline{\mathfrak{J}}_{s=t_0}^t \left[\underline{T}(s) \right] \cdot \underline{A}^T \quad (\text{A. 11})$$

where \underline{A} is an arbitrary orthogonal transformation

$$\underline{A} \cdot \underline{A}^T = \underline{A}^T \cdot \underline{A} = \underline{1} \quad (\text{A. 12})$$

* The constitutive constant with the dimension of length is included because most materials have structure, whether metallic crystals or large organic molecules, etc. It is not clear how this characteristic length parameter would enter into the constitutive equation.

The constitutive Equation (A.8) actually represents a general class of constitutive equations, and as such has little particular information content. The elements of a particular constitutive equation applicable for describing elastic, plastic, and viscous solid material behavior are presented in Appendix D.

Equations (A.4) through (A.9) comprise a system of equations which is sufficient to determine the mass density $\rho(\underline{X}^B, t)$, the stresses $\underline{T}(\underline{X}^B, t)$, the deformations $\underline{C}(\underline{X}^B, t)$, and the motion $\underline{x}(\underline{X}^B, t)$ of the body B for all time $t \geq t_0$. A deformable solid body whose motion is determined by Equations (A.4) - (A.9) is called a mechanical system. The general formulation presented above can easily be generalized to include a mechanical system consisting of several bodies, either in contact with or moving freely about each other. Only with difficulty, however, can the general equations be made to include cleavage of a body, penetration or mixing of two bodies, or rolling of one body on another.

APPENDIX B

DIMENSIONAL ANALYSIS (ABSTRACT TREATMENT)

Dimensional analysis is the method of deducing information about a phenomenon by considering solely relationships between the dimensions of the relevant physical variables. The goal of dimensional analysis is to derive the conditions necessary to insure that certain variables in two or more systems will be similar, that is, exactly proportional for corresponding points of space and time. The following presentation is restricted to mechanical systems, as defined in Appendix A.

Dimensional analysis can be developed from the following fundamental postulates and definitions of mechanics:

1. There exists a set of four fundamental mechanical entities: force [F], mass [M], length [L], and time [T]. Each of these fundamental entities possesses a dimension: F, M, L, and T, respectively; three of which are defined to be independent. Thus

$$[F] = [MLT^{-2}] \quad (B.1)$$

2. Any variable which bears an effect on any mechanical system can be expressed as a product of powers of the unit fundamental concepts, and will possess corresponding dimensions. For example, a loading variable which might produce an effect on a given mechanical system is impulse per unit area; its dimensions are given by

$$[I] = [FL^{-2}T] = [ML^{-1}T^{-1}] \quad (B.2)$$

3. All mechanical variables can be related by a set of field equations expressing balance of mass and momentum, a set of material constitutive equations, and a set of initial and boundary conditions equations, in such a way as to render determinate the response of any (closed) mechanical system. Equations (A.4)-(A.9) of Appendix A represent a set of equations which (theoretically) can be used to determine the behavior of a wide class of deformable solid bodies. In practice these equations are insoluble for all but the simplest cases.*

* The technique of modeling can be used most advantageously for problems in which the techniques of mathematical analysis are inadequate.

4. All equations connecting the mechanical variables of a given mechanical system are dimensionally homogeneous; that is, additive terms in all governing equations must have the same dimensions. This requirement of dimensional homogeneity affords a means of determining the dimensions of all variables in terms of the fundamental dimensions.

Consider a closed mechanical system S which is determined by a finite set of measurable independent mechanical variables

$$\pi_i [M^{P_i} L^{Q_i} T^{R_i}]; i = 1, 2, \dots, I \quad (B.3)$$

Suppose the response of S can be adequately described by a finite set of dependent mechanical variables

$$\pi_j [M^{P_j} L^{Q_j} T^{R_j}]; j = 1, 2, \dots, J \quad (B.4)$$

By postulate 3 above, the response of S can be expressed as a set of functional relationships for π_j depending on π_i . Thus

$$\pi_j = \pi_j (\pi_i); j = 1, 2, \dots, J; i = 1, 2, \dots, I \quad (B.5)$$

The simplest set of dimensionally independent (scalar) variables

$$\pi_s [M^{P_s} L^{Q_s} T^{R_s}]; s = 1, 2, 3 \quad (B.6)$$

are selected from among the independent variables π_i . A precise condition for the π_s to be dimensionally independent is that there exist no constants c_s such that the summations

$$\sum_{s=1}^3 c_s P_s, \quad \sum_{s=1}^3 c_s Q_s, \quad \sum_{s=1}^3 c_s R_s \quad (\neq 0 \text{ for any } c_s) \quad (B.7)$$

vanish simultaneously. The π_s are generally those dimensionally independent (scalar) variables which affect the response of S most directly, and are therefore called primary independent variables. The remaining independent variables

$$\pi_k [M^{P_k} L^{Q_k} T^{R_k}] = \pi_i - \pi_s; k = 1, 2, \dots, I - 3 \quad (B.8)$$

are called secondary independent variables.

The primary independent variables π_s may be used to form two sets of dimensionless products π'_j and π'_k among the dependent variables π_j and the secondary independent variables π_k , respectively.

Thus

$$\left. \begin{aligned} \pi_j' &= \pi_j / (\pi_{s=1})^{c_{j1}} (\pi_{s=2})^{c_{j2}} (\pi_{s=3})^{c_{j3}} \\ \pi_k' &= \pi_k / (\pi_{s=1})^{d_{k1}} (\pi_{s=2})^{d_{k2}} (\pi_{s=3})^{d_{k3}} \end{aligned} \right\} \quad (\text{B. 9})$$

where c_{js} and d_{ks} are integers or rational fractions which must satisfy the following equations

$$\left. \begin{aligned} \sum_{s=1}^3 c_{js} p_s &= p_j, & \sum_{s=1}^3 c_{js} q_s &= q_j, & \sum_{s=1}^3 c_{js} r_s &= r_j \\ \sum_{s=1}^3 d_{ks} p_s &= p_k, & \sum_{s=1}^3 d_{ks} q_s &= q_k, & \sum_{s=1}^3 d_{ks} r_s &= r_k \end{aligned} \right\} \quad (\text{B. 10})$$

By the requirement of dimensional homogeneity (postulate 4) the set of functional relationships (B. 5) can be reduced to a set of functional relationships among the fewer number of dimensionless variables (B. 9). Thus

$$\pi_j' = \pi_j'(\pi_k'); \quad j = 1, 2, \dots, J; \quad k = 1, 2, \dots, I - 3 \quad (\text{B. 11})$$

This important result, known as the Buckingham (Pi) theorem*, can be stated as follows: If the response of a mechanical system is determined by a set of dimensionally homogeneous Equations (B. 5), then these equations can be reduced to Equations (B. 11) among the dimensionless variables.

Mechanical similitude is based on the following interpretation of this theorem. Given a mechanical system S, the variables of which satisfy Equations (B. 11). For every mechanical system which is determined by the same independent variables π_i as S, and for which the dimensionless products π_k' have the same values as S, the dimensionless response variables π_j' will likewise have the same values of S, regardless of the form of the functional relationships governing the π_j' . Mechanical systems for which the dimensionless response variables π_j' are equal are said to be mechanically similar.

* For a simple, rigorous proof of this theorem, see Brand [21].

APPENDIX C

THEORY OF MODELING (ABSTRACT TREATMENT)

The dimensional analysis developed in Appendix B will now be applied to the case of two systems, a prototype and a model. The objectives of the theory of modeling are to determine the conditions under which a model will be similar to a given prototype, and to derive equations for predicting the prototype response from the observed response of the model. As in Appendix B the presentation is restricted to mechanical systems. The only change in notation from Appendix B is that variables associated with a prototype and a model are denoted by the subscripts p and m, respectively.

Consider a prototype and a model which are determined by the same independent variables, as

$$\left. \begin{aligned} \pi_{jp} &= \pi_{jp}(\pi_{ip}) \\ \pi_{jm} &= \pi_{jm}(\pi_{im}) \end{aligned} \right\} j = 1, 2, \dots, J; i = 1, 2, \dots, I \quad (C.1)$$

in analogy with Equation (B.5). If the independent variables π_{ip} , π_{im} are divided into primary and secondary independent variables according to Equations (B.6)-(B.8),

$$\left. \begin{aligned} \pi_{sp}, \pi_{kp} &= \pi_{ip} - \pi_{sp} \\ \pi_{sm}, \pi_{km} &= \pi_{im} - \pi_{sm} \end{aligned} \right\} s = 1, 2, 3; k = 1, 2, \dots, I - 3 \quad (C.2)$$

then by Equations (B.11) there exists a set of functional relationships

$$\pi'_{jp} = \pi'_{jp}(\pi'_{kp}); \pi'_{jm} = \pi'_{jm}(\pi'_{km}) \quad (C.3)$$

among the dimensionless relationships

$$\left. \begin{aligned} \pi'_{jp} &= \pi_{jp} \prod_1^3 (\pi_{sp})^{-c_{js}}, \quad \pi'_{kp} = \pi_{kp} \prod_1^3 (\pi_{sp})^{-d_{ks}} \\ \pi'_{jm} &= \pi_{jm} \prod_1^3 (\pi_{sm})^{-c_{js}}, \quad \pi'_{km} = \pi_{km} \prod_1^3 (\pi_{sm})^{-d_{ks}} \end{aligned} \right\} \quad (C.4)$$

where the exponents c_{js} and d_{ks} satisfy Equations (B.10).

If the dimensionless independent variables of the prototype and the model are equal,

$$\pi'_{km} = \pi'_{kp}; k = 1, 2, \dots, I - 3 \quad (C.5)$$

then by Equations (C.3) the dimensionless dependent variables must also be equal.

$$\pi'_{jp} = \pi'_{jm}; j = 1, 2, \dots, J \quad (C.6)$$

Equation (C.6) is the statement that the model and the prototype are similar, and Equation (C.5) is the condition necessary to insure similarity between the model and the prototype.

Equations (C.5) and (C.6) may be expressed in terms of the scale factors between the corresponding prototype and model variables. Substituting Equations (C.4) into Equations (C.5) and (C.6), we find the following equations which imply similarity between the prototype and the model.

$$\lambda_k \equiv \pi_{km} / \pi_{kp} = (\lambda_1)^{dk1} (\lambda_2)^{dk2} (\lambda_3)^{dk3} \quad (C.7)$$

$$\lambda_j \equiv \pi_{jp} / \pi_{jm} = (\lambda_1)^{-cj1} (\lambda_2)^{-cj2} (\lambda_3)^{-cj3} \quad (C.8)$$

Here $\lambda_s \equiv \pi_{sm} / \pi_{sp}; s = 1, 2, 3 \quad (C.9)$

are defined as the scale factors between the primary independent variables of the prototype and the model.

The scale factors λ_s are independent in the sense that values may be assigned arbitrarily to each of them without affecting the values of the other two. Selection of a specific set of λ_s automatically fixes the scale factors λ_j and λ_k between all corresponding variables of a prototype and a model, by Equations (C.7), (C.8).

In a typical modeling investigation we are given the prototype independent variables π_{ip} and we seek values of the prototype response variables π_{jp} . By constructing a model which depends on the same variables $\pi_{im} \sim \pi_{ip}$ as the prototype, and by requiring that the model be mechanically similar to the prototype, we are led to Equations (C.7)-(C.9), in which $\pi_{sm} \sim \pi_{sp}$ and $\pi_{km} \sim \pi_{kp}$ are appropriately chosen primary and secondary independent variables, respectively. Equations (C.8) express the (ideal) model independent variables in terms of the given prototype independent variables, and so govern construction of the model. Equations (C.9) express the (ideal) prototype dependent variables in terms of the measured model response variables, and thus represent the desired prediction equations.

APPENDIX D

SOLID MATERIAL BEHAVIOR AND CONSTITUTIVE EQUATIONS

This appendix describes the most common stress-deformation phenomena which occur in solid materials, and includes a discussion of constitutive equations for predicting solid material behavior. At the present time, there does not exist a satisfactory theory of solid material behavior - one that predicts a majority of the predominant material effects and that is consistent with the concepts of three-dimensional space. Fundamental elements for constructing such a theory are presented in this appendix.

Materials can be classified by their stress-deformation behavior. Thus, a solid is a material which retains some memory of its initial state as it deforms. A solid can be distinguished from a fluid by the property that a solid can be brought into equilibrium, whereas a fluid continues to deform, under a small externally applied shear stress.

Solid materials encompass the range from relatively rigid materials, which may be idealized by considering the initial state as invariant for all time, to rubber or jelly-like substances, which can elongate several hundred percent before rupturing. Between these two extremes lies the majority of solid materials. The most typical stress-deformation phenomena involve elastic, plastic, and viscous properties. These properties have been described in numerous references, of which we mention only two: Chapter 2 of Jaeger [22] and Chapters 8-12 of Shanley [23]. The following discussion summarizes these stress-deformation properties.

Consider a cylinder of solid material subjected to a history of uniaxial stress (either tension or compression) along the cylinder axis. Suppose that the axial force and the axial and transverse displacements of the cylinder's exterior have been measured and recorded versus time. These quantities can be converted to stress and strain, and plotted as shown in Figure 2, provided the deformation is uniform throughout the cylinder. Below a certain stress σ_0 the cylinder tends to return to its original length. This is the property of elasticity. Within the elastic range, for most materials, stress is nearly proportional to strain. The ratio of axial stress to axial strain in the elastic range is called Young's modulus E , and the ratio of transverse strain to axial strain is called Poisson's ratio ν .

If the material is stressed beyond the yield stress σ_0 and then unloaded, the cylinder will not return to its original length, but will sustain a permanent deformation. This is the property of plasticity. The yield stress is the stress at which curvature of the axial stress-axial strain curve first becomes apparent. As the cylinder is stressed further, the strain continues to increase and, for a typical stress-strain curve, asymptotically approaches

a straight line of slope E' for large strains, as shown in Figure 2. The quantity E' might well be called the plastic modulus. Meanwhile, a typical transverse strain-axial strain curve asymptotically approaches a straight line of slope $\nu' \approx 1/2$ for large strains. The quantities Y and Y' shown in Figure 2 are also characteristic of the plastic deformation.

Not all materials exhibit smooth stress-strain curves such as shown in Figure 2. For example, some ductile materials exhibit a sharp yield point, followed by a brief interval of strain in which stress remains constant or even decreases slightly before beginning again to increase with strain. Other materials exhibit a smooth stress-strain curve with two or more distinct yield points. The characteristic feature of a brittle material is that it can sustain very little plastic deformation before rupturing.

We return to our discussion of a typical ductile solid material. If the yielded material is unloaded from a stress σ_1 greater than σ_0 , and reloaded in the same sense (tension or compression), then the stress-strain curve follows the initial slope E until the stress returns to σ_1 , at which time the stress-strain curve resumes its post-yield slope E' . A similar phenomenon occurs for the curve of transverse strain versus axial strain. This property whereby the yield stress increases with plastic deformation is called workhardening. If the unloaded material is reloaded in the opposite sense, then the material remains elastic until a stress of approximately $2\sigma_0 - \sigma_1$ (compression or tension) is reached, at which time the material yields in the opposite sense as before. This property whereby the yield stress decreases with plastic deformation for loading in the opposite sense is called the Bauschinger effect.

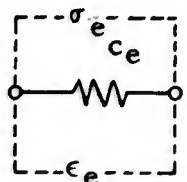
The elastic and plastic properties described above occur regardless of loading rate. However, there are certain material properties, called viscous properties, which are dependent on loading rate. "It is found that when a load is applied suddenly, the resulting strain is not taken up instantaneously, but is approached asymptotically, and also that the work-hardening portion of the stress-strain curve is raised as the rate of strain increases" [22]. Other viscous phenomena include creep, which is a slow, steady deformation under a constant load, and relaxation, by which stress gradually decreases under constant strain. We mention here that temperature usually has a pronounced effect on the viscous properties of a material. For the remainder of this appendix we assume that temperature and all material properties are constant.

The foregoing discussion of solid material behavior dealt strictly with the response of a cylinder to uniaxial stress. Obviously, more complicated tests could be performed with the material subjected to more complicated states of stress. However, the discussion of uniaxial stress brought out the essential features of the stress-deformation behavior of typical solid materials. Any theory which predicts the elastic, plastic (including

workhardening and the Bauschinger effect), and viscous properties – as described above – for a history of uniaxial stress, and which predicts similar properties for a general history of stress, should be a good theory, worthy of careful consideration as a general constitutive equation for solids.

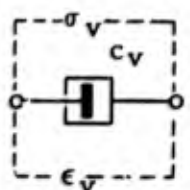
We next develop a mechanical model which can be used to relate stress and strain magnitudes in such a way as to predict the elastic, plastic, and viscous properties described above. Two advantages of developing a mechanical model to predict the desired properties are: (1) mechanical models provide definite material constants which can be evaluated from single material tests, and (2) mechanical models provide an economical means of visualizing rather complicated material behavior. The mechanical model will be considered as an element to be used in constructing a general constitutive equation.

We first introduce the mechanical elements from which the mechanical model can be developed. A spring is an idealization for the mechanical concept of elasticity. The relationship between a stress magnitude σ_e and a strain magnitude ϵ_e for a linear spring is



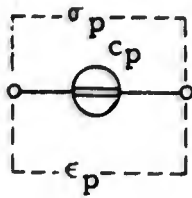
$$\left. \begin{aligned} \sigma_e &= \mu c_e \epsilon_e \\ \epsilon_e &= (\mu c_e)^{-1} \sigma_e \end{aligned} \right\} \quad (D.1)$$

where μ is a representative stress constant and c_e is the dimensionless elasticity constant of the spring. A dashpot is an idealization for the concept of viscosity. The relationship between a stress magnitude σ_v and a strain magnitude ϵ_v for a linear dashpot is



$$\left. \begin{aligned} \sigma_v &= \mu \tau c_v \dot{\epsilon}_v, \quad \dot{\epsilon}_v \equiv d\epsilon_v/dt \\ \epsilon_v &= \int_{t_0}^t \dot{\epsilon}_v dt = (\mu \tau c_v)^{-1} \int_{t_0}^t \sigma_v dt \end{aligned} \right\} \quad (D.2)$$

where τ is a representative time constant and c_v is the viscosity constant of the dashpot. A yield element is an idealization for the concept of plasticity. The relationship between a stress magnitude σ_p and a strain magnitude ϵ_p for a yield element is:



$$\left. \begin{aligned} \sigma_p &= \mu c_p U(\tau \dot{\epsilon}_p), \quad \dot{\epsilon}_p \equiv d\epsilon_p/dt \\ \epsilon_p &= \int_{t_0}^t \dot{\epsilon}_p dt = \epsilon_{pN} + \int_{t'_N}^t \dot{\epsilon}_p dt \end{aligned} \right\} \quad (D.3)$$

where c_p is the plasticity constant and $U(x)$ is the yield function defined by

$$\left. \begin{aligned} U(x) &= 1 \quad \text{for } x > 0 \\ |U(x)| &< 1 \quad \text{for } x = 0 \\ U(x) &= -1 \quad \text{for } x < 0 \end{aligned} \right\} \quad (D.4)$$

We assume that the yield element is initially unstrained,

$$\epsilon_{p0} = 0 \quad \text{at time } t = t_0 \quad (D.5)$$

and that subsequent yielding occurs in N finite time intervals

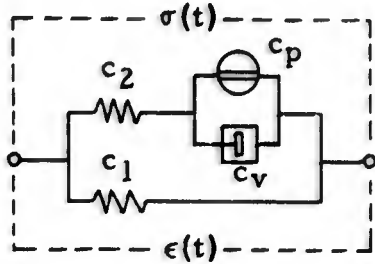
$$\left. \begin{aligned} \dot{\epsilon}_p &= 0 \quad \text{from } t_0 \text{ to } t_1, t_1' \text{ to } t_2, \dots, t_{N-1}' \text{ to } t_N \\ |\dot{\epsilon}_p| &> 0 \quad \text{from } t_1 \text{ to } t_1', t_2 \text{ to } t_2', \dots, t_N \text{ to } t_N' \end{aligned} \right\} \quad (D.6)$$

Thus the strain at the end of the time interval from t_N to t_N' is

$$\epsilon_{pN} = \sum_{n=1}^N \int_{t_n}^{t_n'} \dot{\epsilon}_p dt \quad (D.7)$$

where $t_0 < t_n < t_n' \leq t_N' \leq t$ (t being the current time).

Consider the mechanical model composed of a yield element c_p in parallel with a dashpot c_v , this combination connected in series with a spring c_2 , and this combination connected in parallel with another spring c_1 . The symbolic representation, and the equations expressing balance of stress and compatibility of strains are given as:



Balance of stress

$$\sigma = \sigma_1 + (\sigma_2 = \sigma_p + \sigma_v)$$

Compatibility of strain

$$\epsilon = \epsilon_1 = \epsilon_2 + (\epsilon_p = \epsilon_v)$$

(D.8)

Define the following constants

$$c_d = c_1 + c_2, \quad \epsilon_N \equiv (c_2/c_d)\epsilon_{pN}$$

(D.9)

$$\sigma_N' \equiv \sigma(t_N') = \sigma(t_{N+1}), \quad \epsilon_N' \equiv \epsilon(t_N') = \epsilon(t_{N+1})$$

The gross behavior of this mechanical model can be obtained by substituting Equations (D.1) - (D.7) into Equations (D.8). Thus

For $t_N' < t < t_{N+1}$: $|\sigma_p| < \mu c_p, \quad \dot{\epsilon}_p = \dot{\epsilon}_v = 0, \quad \epsilon_p = \epsilon_v = \epsilon_{pN}$

(D.10)

$$\sigma/\mu = c_d \epsilon - c_2 \epsilon_{pN} = c_d(\epsilon - \epsilon_N), \quad c_d \epsilon = \sigma/\mu + c_d \epsilon_N$$

For $t = t_N'$ or t_{N+1} : $\sigma_p = \pm \mu c_p, \quad \dot{\epsilon}_p = \dot{\epsilon}_v = 0, \quad \epsilon_p = \epsilon_v = \epsilon_{pN}$

$$\sigma_N'/\mu = c_1 \epsilon_{pN} \pm c_p c_d / c_2 = (c_p / c_2)(c_1 \epsilon_N \pm c_p) = c_1 \epsilon_N' \pm c_p$$

$$\epsilon_N' = \epsilon_{pN} \pm c_p / c_2 = (c_d \epsilon_N \pm c_p) / c_2 = (\sigma_N' / \mu \mp c_p) / c_1 \quad (D.11)$$

For $t_{N+1} < t < t_{N+1}'$: $\sigma_p = \pm \mu c_p, \quad \epsilon_p = \epsilon_v = \epsilon_{pN} + \int_{t_{N+1}}^{t_N} \dot{\epsilon}_v dt, \quad |\dot{\epsilon}_v| > 0$

$$\mu^{-1} (c_v \sigma + c_2 \tau^{-1} \int_{t_{N+1}}^t \sigma dt) = c_v c_d (\epsilon - \epsilon_N) + c_1 c_2 \tau^{-1} \int_{t_{N+1}}^t \epsilon dt \quad (D.12)$$

$$\pm c_2 c_p \tau^{-1} (t - t_{N+1})$$

$$\text{or } \mu^{-1} (c_2 \sigma + \tau c_v \dot{\sigma}) = c_1 c_2 \epsilon + \tau c_v c_d \dot{\epsilon} \pm c_2 c_p$$

Equations (D.10) - (D.12) can be used to determine the complete history of strain $\epsilon(t)$ for the mechanical model when the history of stress $\sigma(t)$ is known, or vice versa. These equations predict the effects of initial elasticity, yield, plastic flow including workhardening and the Bauschinger effect, and post-yield dependence of stress on the strain rate. Because this mechanical model qualitatively predicts all of the predominant stress-deformation properties discussed earlier, it should have value for describing the constitutive behavior of solid materials.

We remark that the simple linear dashpot is probably the most drastic source of discrepancies between predictions with this mechanical model and the behavior of actual materials. The dependence of stress on strain rate is usually much less for actual materials than that predicted by a simple dashpot. Therefore, in devising a more realistic mechanical model, we should replace the simple dashpot with a more sophisticated linear dashpot or with an appropriate nonlinear dashpot.

We next present a complete and consistent set of variables for describing the states of stress and strain at a point, which can be used in constructing a general constitutive equation for solid materials. We recognize that it is merely an algebraic exercise to translate a constitutive equation, once postulated in terms of given "state variables," into equivalent "state variables." Equation (A.8) of Appendix A represents a very general constitutive equation, which is written in terms of the stress tensor and the Cauchy deformation tensor. However, Equation (A.8) has little information content, and the general stress and deformation tensors are not well suited for the purpose at hand. We consider a simpler and more explicit representation of stress and strain.

The stress tensor $\underline{\sigma}$ is symmetric in the absence of body torques, and the strain tensor $\underline{\epsilon}$ is symmetric by definition. Any symmetric second-order tensor \underline{A} is completely described by three orthogonal vectors \underline{A}_i , called principal vectors, whose magnitudes A_i are roots of the determinantal equation

$$\det(\underline{A} - A_i \underline{1}) = 0, \quad i = 1, 2, 3 \quad (\text{D.13})$$

and whose directions can be determined by solving for the unit vectors $\underline{\bar{A}}_i$ in the algebraic equations

$$(\underline{A} - A_i \underline{1}) \cdot \underline{\bar{A}}_i = 0, \quad i = 1, 2, 3 \quad (\text{D.14})$$

Therefore, instead of the stress and strain tensors we consider simply the orthogonal principal stress and strain vectors

$$\underline{\sigma}_j = \bar{\sigma}_j \underline{\bar{A}}_j; \quad \underline{\epsilon}_k = \bar{\epsilon}_k \underline{\bar{A}}_k, \quad \epsilon_k = \sum_1^{\infty} \beta_n (\delta_k)^n \quad (\text{D.15})$$

where $\bar{\sigma}_j$ and $\bar{\xi}_k$ are unit vectors in the direction of σ_j and ξ_k , respectively. The principal strains ϵ_k are defined by a power series in terms of the principal extensions δ_j , so as to permit "fitting" of the theory to stress-strain data.

The single deficiency of the principal stress and strain vectors (in the spatial description) for use as "state variables" is the failure of these variables to include any information about the orientation of the material. This deficiency can be corrected by introducing an arbitrary rectangular triad of unit vectors in the material description, and by referring the principal stress and strain vectors to the material description.

A constitutive equation is then required to depend on only twelve independent scalar variables: the magnitudes σ_j and ϵ_k of the principal stress and strain vectors, and the components of two orthogonal unit "rotation tensors" $\underline{\underline{A}}$ and $\underline{\underline{B}}$ which specify the directions of the principal stress and strain vectors with respect to the unit triad. Only three of the components of $\underline{\underline{A}}$ or $\underline{\underline{B}}$ are independent because $\underline{\underline{A}}$ and $\underline{\underline{B}}$ are each restricted by six orthogonality conditions. In addition to the above variables, a constitutive equation may be dependent upon certain "preferred directions," indicating anisotropy of the material. One form of a general constitutive equation would involve relating the variables σ_j , ϵ_k , $\underline{\underline{A}}$, $\underline{\underline{B}}$ by the mechanical model discussed earlier.

We conclude this discussion of constitutive equations by deriving a specific constitutive equation for the case of uniaxial stress - for which the directions of the principal stress and principal strain vectors coincide and remain constant with respect to the material. In this case the "rotation tensors" $\underline{\underline{A}}$ and $\underline{\underline{B}}$ are constant, and can be equated to the unit tensor $\underline{\underline{1}}$ by a proper choice of the unit triad. In the general case, the directions of the principal stress and strain vectors neither coincide nor remain constant with respect to the material.

We consider a unique transformation from the principal stress and strain vectors to an orthogonal set of mean and deviatoric stress and strain vectors, defined by the following formulae

$$\underline{\underline{\sigma}}_m = (\underline{\underline{\sigma}}_1 + \underline{\underline{\sigma}}_2 + \underline{\underline{\sigma}}_3) \sigma_m / \sqrt{3}, \quad \sigma_m = (\sigma_1 + \sigma_2 + \sigma_3) / \sqrt{3}$$

$$\underline{\underline{\sigma}}_d = \underline{\underline{\sigma}}_1 + \underline{\underline{\sigma}}_2 + \underline{\underline{\sigma}}_3 - \underline{\underline{\sigma}}_m, \quad \underline{\underline{\sigma}}_d \cdot \underline{\underline{\sigma}}_m = 0 \quad (\text{D. 16})$$

$$\sigma_d = (2/3)^{1/2} (\sigma_1^2 + \sigma_2^2 + \sigma_3^2 - \sigma_1\sigma_2 - \sigma_2\sigma_3 - \sigma_3\sigma_1)$$

For uniaxial stress

$$\sigma_l = -P/\pi a^2, \sigma_m = \sigma_l / \sqrt{3}, \sigma_d = \sigma_l \sqrt{2/3} \quad (D.17)$$

where P is a compressive force on a cylinder of radius a, as shown in Figure 2. For small strains

$$\epsilon_m = (\epsilon_l + 2\epsilon_t)/\sqrt{3}, \epsilon_d = (\epsilon_l - \epsilon_t)\sqrt{2/3} \quad (D.18)$$

The mean and deviatoric stress and strain vectors for the case of uniaxial stress are shown in Figure 19.

As a specific constitutive equation, we consider mean stress and strain to be related elastically

$$\sigma_m = \mu c_m \epsilon_m \quad (D.19)$$

and we consider the deviatoric stress and strain to be related by the mechanical model considered earlier. As a specific material test we assume the cylindrical specimen to be mounted in a testing machine of resilience k, with an overall testing machine motion given by

$$d_T/b = \delta_T = \dot{\delta}_T (t - t_N'') \quad (D.20)$$

where b is the length of the specimen, t_N'' is the instant the test begins, and $b\dot{\delta}_T$ is the constant speed of the testing machine.

The initial elastic response of the specimen is given by

$$\left. \begin{aligned} \sigma_l / \mu &= \delta_T / \beta' = \dot{\delta}_T (t - t_N'') / \beta' \\ \epsilon_l - \epsilon_{lN} &= (2/c_d + 1/c_m)(\sigma_l / 3\mu) \\ \epsilon_t - \epsilon_{tN} &= - (1/c_d - 1/c_m)(\sigma_l / 3\mu) \end{aligned} \right\} \quad (D.21)$$

where

$$\beta' = \frac{\beta}{c_v c_d} = \frac{1}{K} + \frac{1}{3c_m} + \frac{2}{3c_d}, \quad K = \frac{kb}{\pi \mu a^2}$$

$$\epsilon_{lN} = -2\epsilon_{tN} = \sqrt{\frac{2}{3}} \left(\frac{c_2}{c_d} \right) \epsilon_{pN}$$

At the yield point ($t = t_{N+1}$) we have:

$$\left. \begin{aligned}
 \sigma'_{lN} &= \sqrt{3/2} (c_1 \epsilon_{pN} \pm c_p c_d / c_2) \\
 t_{N+1} - t'_N &= (\beta' / \dot{\delta}_T) (\sigma'_{lN} / \mu) \\
 \epsilon'_{lN} - \epsilon_{lN} &= (2/c_d + 1/c_m) (\sigma'_{lN} / 3\mu) \\
 \epsilon'_{tN} - \epsilon_{tN} &= - (1/c_d - 1/c_m) (\sigma'_{lN} / 3\mu)
 \end{aligned} \right\} \quad (D. 22)$$

After yielding the response of the cylindrical specimen is

$$\left. \begin{aligned}
 \sigma_l / \mu &= \sigma'_{lN} / \mu + \left(\frac{\dot{\delta}_T}{a'} \right) t' + \left(\frac{\gamma}{a'} \right) \left[1 - \exp \left(- \frac{at'}{\beta\tau} \right) \right] \\
 \epsilon_l &= \epsilon'_{lN} + \left(a' - \frac{1}{K} \right) \left(\frac{\dot{\delta}_T}{a'} \right) t' - \left(\frac{\gamma}{Ka'} \right) \left[1 - \exp \left(- \frac{at'}{\beta\tau} \right) \right] \\
 \epsilon_t &= \epsilon'_{tN} + \left(\frac{1}{c_m} - \frac{1}{c_1} \right) \left(\frac{\dot{\delta}_T}{3a'} \right) t' + \left(\frac{1}{c_m} + \frac{1}{K} \right) \left(\frac{\gamma}{2a'} \right) \left[1 - \exp \left(- \frac{at'}{\beta\tau} \right) \right]
 \end{aligned} \right\} \quad (D. 23)$$

where

$$t' = t - t_{N+1}, \quad a' = \frac{a}{c_1 c_2} = \frac{1}{K} + \frac{1}{3c_m} + \frac{2}{3c_1}, \quad \gamma = \left(\frac{2c_v}{3c_1^2} \right) \left(\frac{\tau \dot{\delta}_T}{a'} \right)$$

The above expressions provide remarkably good predictions for the response of a cylindrical specimen to a uniaxial compression test. In particular, all the material properties discussed at the beginning of this appendix are predicted by these expressions.

We can relate the properties E , E' , Y , Y' , ν , and ν' , as defined in Figure 2 for a uniaxial compression test, to the material constants μ , τ , c_m , c_1 , c_2 , c_p , and c_v , which appear in the inelastic constitutive equation. Substituting Equation (D. 21) into the definitions of Young's modulus and Poisson's ratio results in

$$\left. \begin{aligned}
 E &\equiv \left(\frac{d\sigma_l}{d\epsilon_l} \right)_{\text{elastic}}^{\text{small}} = \left(\frac{\dot{\sigma}_l}{\dot{\epsilon}_l} \right)_{t'_N < t < t_{N+1}} = 3\mu \left(\frac{2}{c_d} + \frac{1}{c_m} \right)^{-1} \\
 \nu &\equiv - \left(\frac{d\epsilon_t}{d\epsilon_l} \right)_{\text{elastic}}^{\text{small}} = \left(\frac{\dot{\epsilon}_t}{\dot{\epsilon}_l} \right)_{t'_N < t < t_{N+1}} = \left(\frac{1}{c_d} - \frac{1}{c_m} \right) \left(\frac{2}{c_d} + \frac{1}{c_m} \right)^{-1}
 \end{aligned} \right\} \quad (D. 24)$$

which can be solved for μc_m and μc_d as

$$\mu c_m = E/(1 - 2\nu), \quad \mu c_d = E/(1 + \nu) \quad (D.25)$$

Likewise, substituting Equation (D.23) into the definitions of the plastic moduli results in

$$\left. \begin{aligned} E' &= \left(\frac{d\sigma_l}{d\epsilon_l} \right)_{\text{plastic}}^{\text{large}} = \lim_{t' \rightarrow \infty} \left(\frac{\dot{\sigma}_l}{\dot{\epsilon}_l} \right) = 3\mu \left(\frac{2}{c_1} + \frac{1}{c_m} \right)^{-1} \\ \nu' &= \left(\frac{d\epsilon_t}{d\epsilon_l} \right)_{\text{plastic}}^{\text{large}} = \lim_{t' \rightarrow \infty} \left(\frac{\dot{\epsilon}_t}{\dot{\epsilon}_l} \right) = \left(\frac{1}{c_1} - \frac{1}{c_m} \right) \left(\frac{2}{c_1} + \frac{1}{c_m} \right)^{-1} \end{aligned} \right\} \quad (D.26)$$

which can be solved for μc_m , μc_1 , and μc_2 as

$$\left. \begin{aligned} \mu c_m &= \frac{E'}{1 - 2\nu'} = \frac{E}{1 - 2\nu} \\ \mu c_1 &= \frac{E'}{1 + \nu'} = \left(\frac{2E'}{3} \right) \left[1 - (1 - 2\nu) \left(\frac{E'}{3E} \right) \right] \\ \mu c_2 &= \mu(c_d - c_1) = \left(\frac{E}{1 + \nu} \right) \left[\frac{1 - E'/E}{1 - (1 - 2\nu)(E'/3E)} \right] \end{aligned} \right\} \quad (D.27)$$

The stress-strain curves asymptotically approach straight lines with slopes E' and ν' for large plastic deformations. These asymptotes can be expressed as

$$\left. \begin{aligned} \sigma_l &= Y + E' (\epsilon_l - \epsilon_{lN}) \\ \epsilon_t - \epsilon_{tN} &= -\nu' (\epsilon_l - \epsilon_{lN}) \end{aligned} \right\} \quad (D.28)$$

where Y is the intercept of the asymptote to the curve $\sigma_l(\epsilon_l)$ with the σ_l -axis, and Y' is the intercept of the asymptote to the curve $\epsilon_t(\epsilon_l)$ with the ϵ_l -axis. Substituting Equations (D.23) into Equations (D.28) yields

$$\frac{Y}{E'} = Y' \left(\frac{2\nu'}{1 - 2\nu'} \right) = \frac{2c_v}{3c_1^2} \left(\frac{\tau \delta T}{a'} \right) + \sqrt{\frac{2}{3}} \left[\left(\frac{c_2}{c_d} \right) \epsilon_{pN} - \left(\frac{c_p}{c_1} \right) \right] \quad (D.29)$$

Results of tests at two distinct loading rates can be used to solve for the remaining material constants, by the following formulae:

$$\left. \begin{aligned} \pm \mu_{c_p} &= \sqrt{\frac{3}{2}} \left(\frac{\mu_{c_1}}{E'} \right) \left(\frac{Y_2 \dot{\delta}_{T1} - Y_1 \dot{\delta}_{T2}}{\dot{\delta}_{T1} - \dot{\delta}_{T2}} \right) + \frac{(\mu_{c_1})(\mu_{c_2})}{(\mu_{c_d})} \left(\frac{\epsilon_{p1} \dot{\delta}_{T2} - \epsilon_{p2} \dot{\delta}_{T1}}{\dot{\delta}_{T1} - \dot{\delta}_{T2}} \right) \\ \mu_{\tau_{c_v}} &= \frac{3(\mu_{c_1})^2}{2(\dot{\delta}_{T1} - \dot{\delta}_{T2})} \left(\frac{1}{E'} + \frac{\pi a_0^2}{kl'} \right) \left[\left(\frac{Y_1 - Y_2}{E'} \right) - \sqrt{\frac{2}{3}} \left(\frac{\mu_{c_2}}{\mu_{c_d}} \right) (\epsilon_{p1} - \epsilon_{p2}) \right] \end{aligned} \right\} \quad (D.30)$$

TABLES AND ILLUSTRATIONS

TABLE I

MEASURED PROPERTIES OF THE PROTOTYPE MATERIALS

Material designation	Weight density ρ_g (pci)	Uniaxial compression test data					
		$\dot{\epsilon} \approx 0.2 \text{ min}^{-1}$			$\dot{\epsilon} \approx 2.0 \text{ min}^{-1}$		
		E (kpsi)	Y (kpsi)	E' (kpsi)	E (kpsi)	Y (kpsi)	E' (kpsi)
AL. 6061-T6 aluminum	.100	10^4	40	300	10^4	40	300
HS. C-124 ablator	.042	320	10	0			
PF. FPH-10H foam	.005	8.7	.27	0			

TABLE II

"STATIC" PROPERTIES OF THE MODEL MATERIALS

Material designation	Weight density ρ_g (pci)	Uniaxial compression test data					
		$\dot{\epsilon} \approx 0.2 \text{ min}^{-1}$			$\dot{\epsilon} \approx 2.0 \text{ min}^{-1}$		
		E (kpsi)	Y (kpsi)	E' (kpsi)	E (kpsi)	Y (kpsi)	E' (kpsi)
MAL. Model of AL	.285	550	2.0	14			
MHS. Model of HS	.132	8.2	.10	5.2	16	.19	5.6
MPF. Model of PF	.006	.55	.012	.020	.65	.012	.020

TABLE III

"DYNAMIC" PROPERTIES OF THE MODEL MATERIALS

Material designation	Weight density ρ_g (pci)	Uniaxial compression test data					
		$\dot{\epsilon} \approx 20 \text{ min}^{-1}$			$\dot{\epsilon} \approx 200 \text{ min}^{-1}$		
		E (kpsi)	Y (kpsi)	E' (kpsi)	E (kpsi)	Y (kpsi)	E' (kpsi)
MAL. Model of AL	.285	1000	3.64	25.5			
MHS. Model of HS	.132	15	.18	9.5	29	.35	1.02
MPF. Model of PF	.006	1.0	.022	.036	1.18	.022	.036

TABLE IV
COMPOSITIONS OF PROTOTYPE AND MODEL MATERIALS

Prototype materials		Corresponding Model Materials	
		Material compositions (percentage by weight)	
AL	6061-T6 aluminum alloy	MAL	90.0 Lead powder 5.45 Epon 828 resin 3.64 Epon 871 resin 0.91 Curing agent CL
HS	C-124 heat shield material (or Epon 828 resin and curing agent D)	MHS	78.1 Lead powder 15.6 Epon 871 resin 3.9 Epon 828 resin 2.0 Curing agent CL 0.4 Cab-O-Sil
PF	FPH-10H (Emerson and Cummings) plastic foam	MPF	80.8 Lead powder 10.8 FPH-4H foam 7.0 FPH-4H catalyst 1.4 Water

TABLE V
PERTINENT SHELL VARIABLES

Independent Variables

Geometric Variables	Symbol	Physical Dimension
cone angle	α	-
mean inner radius	a	L
axial length	b	L
shell thickness	h, h_n *	L
Material Variables		
mass density	ρ_n	ML^{-3}
elastic modulus	E_n	$ML^{-1}T^{-2}$
yield stress	Y_n	$ML^{-1}T^{-2}$
plastic modulus	E'_n	$ML^{-1}T^{-2}$
Impulse Load Variables		
impulse duration	T_0	T
peak impulse	I_0	$ML^{-1}T^{-1}$
normalized impulse distribution	$\psi(\theta, z)$	-

Dependent Variables

Dependent Variables	Symbol	Physical Dimension
total weight	W	MLT^{-2}
fundamental quarter period	T_1	T
peak transient displacement	U^T	L
residual displacement	U^R	L

* Variables with a subscript n refer to the nth layer of a composite shell.

TABLE VI

SCALE FACTORS AND MODELING RELATIONSHIPS

Scale Factors

$$\begin{aligned}\lambda &= \frac{a_m}{a_p} = \frac{3.0 \text{ in}}{15.0 \text{ in}} = 0.20 && \text{(length scale)} \\ \gamma &= \frac{\rho_m}{\rho_p} = \frac{0.285 \text{ pci}}{0.100 \text{ pci}} = 2.85 && \text{(mass density scale)} \\ \mu &= \frac{E_m}{E_p} = \frac{10^6 \text{ psi}}{10^7 \text{ psi}} = 0.10 && \text{("dynamic" pressure scale)} \\ \tau &= \frac{T_{om}}{T_{op}} = \lambda(\gamma/\mu)^{1/2} = 1.07 && \text{(time scale)}\end{aligned}$$

Similarity of Space and Time Coordinates

$$\frac{\theta_m}{\theta_p} = 1, \quad \frac{z_m}{z_p} = \lambda = 0.20, \quad \frac{t_m}{t_p} = \tau = 1.07$$

Geometric Similarity

$$\frac{\alpha_m}{\alpha_p} = 1, \quad \frac{a_m}{a_p} = \frac{b_m}{b_p} = \frac{h_m}{h_p} = \frac{h_{nm}}{h_{np}} = \lambda = 0.20$$

Similarity of Material Properties

$$\frac{\rho_{nm}}{\rho_{np}} = \gamma = 2.85, \quad \frac{E_{nm}}{E_{np}} = \frac{Y_{nm}}{Y_{np}} = \frac{E'_{nm}}{E'_{np}} = \mu = 0.10$$

Similarity of Impulsive Loads

$$\frac{T_{om}}{T_{op}} = \tau = 1.07, \quad \frac{I_{om}}{I_{op}} = \lambda(\gamma\mu)^{1/2} = 0.11, \quad \frac{\psi_m(\theta_m, z_m)}{\psi_p(\theta_p, z_p)} = 1$$

Similarity of Dependent Variables

$$\begin{aligned}\frac{W_p}{W_m} &= \frac{1}{\gamma\lambda^3} = 44, \quad \frac{T_{ip}}{T_{im}} = \frac{f_{im}}{f_{ip}} = \frac{1}{\tau} = 0.94 \\ \frac{U_p^T}{U_m^T} &= \frac{U_p^R}{U_m^R} = \frac{1}{\lambda} = 5.0, \quad \frac{I_{op}^T}{I_{om}^T} = \frac{I_{op}^R}{I_{om}^R} = \frac{1}{\lambda(\gamma\mu)^{1/2}} = 9.4\end{aligned}$$

TABLE VII
PROTOTYPE SPECIFICATIONS

Prototype designation and shell composition	Cone angle	Mean radius	Axial length	Shell thick.
	α (deg)	a (in)	b (in)	h (in)
P1. Standard cone .125-in AL plain shell	12.5	15.0	30.0	.125
P2. Heat shield cone .125-in AL covered with .25-in HS	12.5	15.0	30.0	.375
P3. Sandwich cone 2-.075-in AL separated by 1.00-in PF	12.5	15.0	30.0	1.15
P4. Foam-filled cone .125-in AL completely filled with PF	12.5	15.0	30.0	—

TABLE VIII
MODEL SPECIFICATIONS

Model designation and shell composition	Cone angle	Mean radius	Axial length	Shell thick
	α (deg)	a (in)	b (in)	h (in)
M1. Standard cone .025-in MAL plain shell	12.5	3.00	6.00	.025
M2. Heat shield cone .025-in MAL covered with .050-in MHS	12.5	3.00	6.00	.075
M3. Sandwich cone 2-.015-in MAL separated by .20-in MPF	12.5	3.00	6.00	.230
M4. Foam-filled cone .025-in MAL completely filled with MPF	12.5	3.00	6.00	—
M6. Thick cone .075-in MAL plain shell	12.5	3.00	6.00	.075
M7. Standard cylinder .025-in MAL plain shell	0	3.00	6.00	.025
M8. Short cylinder .025-in MAL plain shell	0	3.00	4.00	.025
M9. Thick cylinder .075-in MAL plain shell	0	3.00	6.00	.075

TABLE IX
SHOCK TUBE LOADING CHARACTERISTICS

diaphragm thickness (mils)	burst pressure (psi)	Small Reservoir (~ 1 cubic foot) Duration \approx 1 ms		Large Reservoir (~ 8 cubic feet) Duration \approx 4 ms	
		peak pressure (psi)	peak impulse (psi-ms)	peak pressure (psi)	peak impulse (psi-ms)
2	6.5	3.0	1.2	5.0	3.0
3	9	5.0	1.8	7.5	5.0
5	14	7.5	3.0	11.5	9.0
7.5	20	10	4.5	16	15
10	25	12.5	6.0	20	20
15	35	17.5	9.0	28	32
20	45	22	12	35	44
30	65	30	18	50	70

TABLE X
MODEL TEST RESULTS

Model designation	W (lb)	f_1 (cps)	T_o (ms)	I_o^T * (psi-ms)	I_o^R * (psi-ms)
M1. Standard cone	.83	100	.05	—	—
			1	5.8	5.3
			4	7.2	8.2
M2. Heat shield cone	1.50	120	.05	—	10
			1	12	12.7
			4	17	17.5
M3. Sandwich cone	1.20	146	.05	10	18
			1	12	23.5
			4	19.5	28.5
M4. Foam-filled cone	2.10	—	.05	—	35
			1	—	30
			4	—	—
M6. Thick cone	2.48	200	1	21.5	23.5
			4	27	26.5
M7. Standard cylinder	.81	130	1	7.5	9.5
			4	9.0	11
M8. Short cylinder	.54	200	1	15.5	15
			4	18	19
M9. Thick cylinder	2.42	270	1	30.5	37
			4	43	50

* The quantity I_o^T is defined to be the impulse necessary to produce a maximum transient displacement of $U^T = 0.60$ -in;
 I_o^R is the impulse necessary to produce a maximum residual displacement of $U^R = 0.30$ -in.

TABLE XI
MODEL TEST RESULTS IN DIMENSIONLESS FORM

Model designation	$\frac{W}{\rho g a^3}$	$f_1 a \sqrt{\frac{\rho}{E}}$	$\frac{T_0}{T_1}$	$\frac{10^5 I_0^T}{a \sqrt{E \rho}}^*$	$\frac{10^5 I_0^R}{a \sqrt{E \rho}}^*$
M1. Standard Cone	.108	.008	.02 0.4 1.6	— 7.1 8.8	— 6.5 10.0
M2. Heat shield cone	.195	.010	.025 0.5 1.9	— 14.5 21	12 15.5 21.5
M3. Sandwich cone	.156	.012	.03 0.6 2.3	12 14.5 24	22 28.5 35
M4. Foam-filled cone	.273	—	<<1 —	— —	43 37
M6. Thick cone	.322	.016	0.8 3.2	26 33	28.5 32.5
M7. Standard cylinder	.105	.011	0.5 2.1	9.2 11.0	11.6 13.5
M8. Short cylinder	.070	.016	0.8 3.2	19 22	18.5 23
M9. Thick cylinder	.314	.022	1.1 4.4	37 52	45 61

* Values of impulse $I_0^T/a\sqrt{E\rho}$ and $I_0^R/a\sqrt{E\rho}$ correspond to maximum transient displacements of $U^T/a = 0.20$, and maximum residual displacements of $U^R/a = 0.10$, respectively.

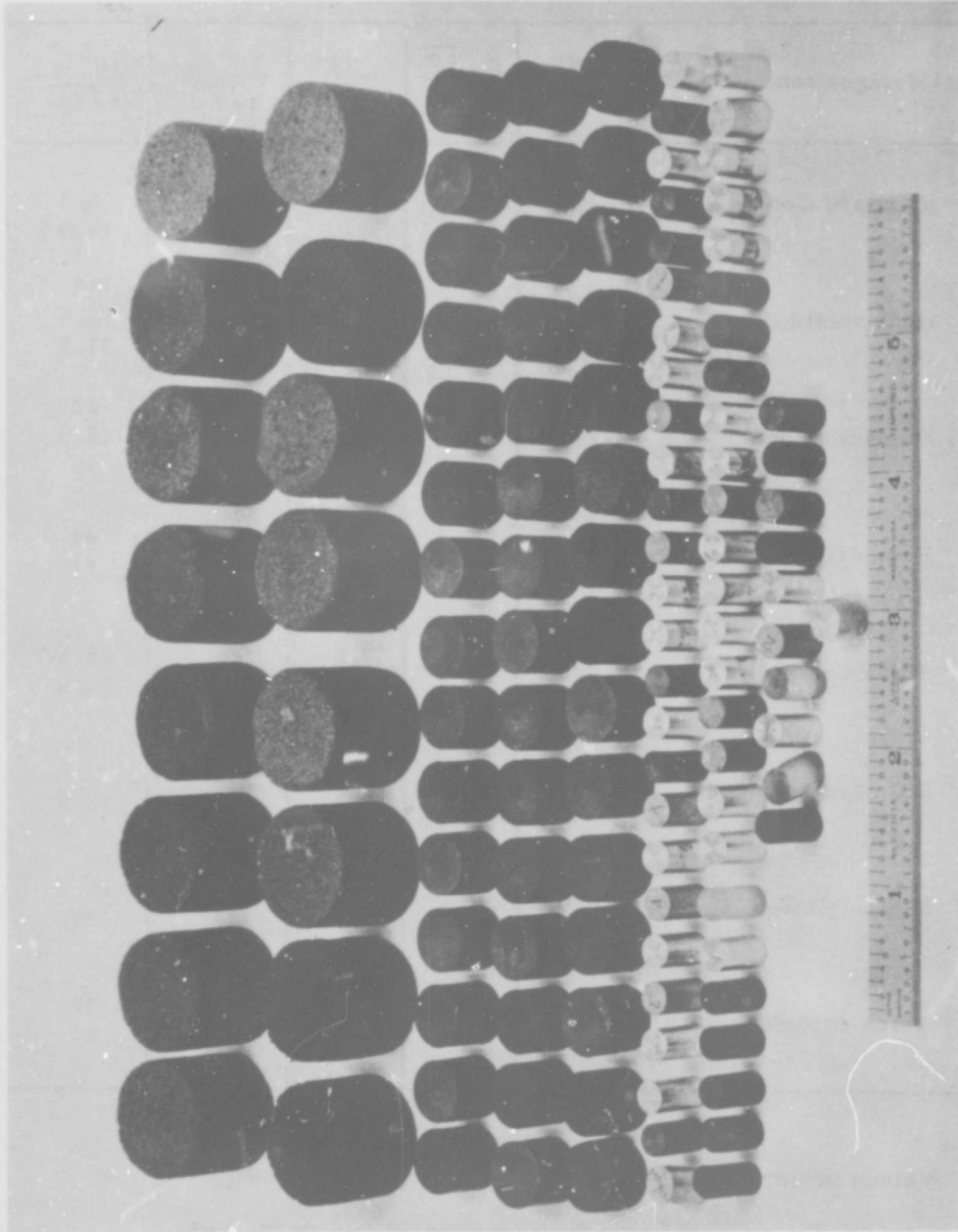
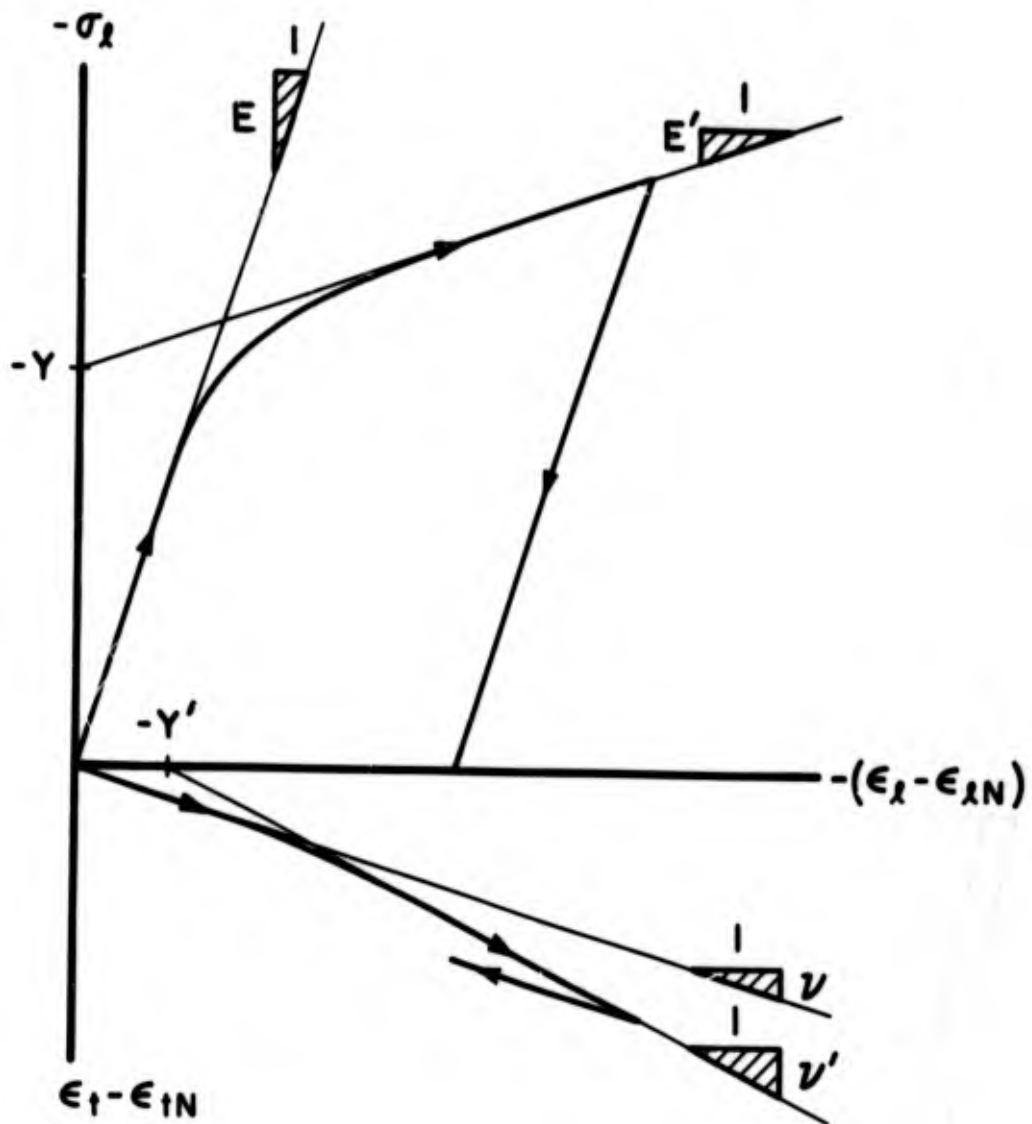
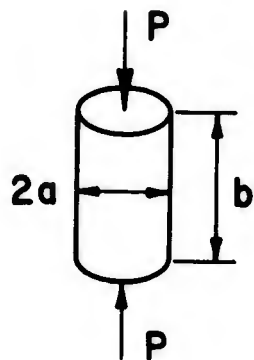


FIGURE 1. COMPRESSION TEST SPECIMENS

TYPICAL STRESS - STRAIN DIAGRAM



DEFINITION OF MATERIAL PROPERTIES



$$-\sigma_L = P / \pi a^2$$

$$\epsilon_{L,t} = \sum_1^{\infty} \beta_n (\delta_{L,t})^n$$

$$\delta_L = b / b_0 - 1$$

$$\delta_t = a / a_0 - 1$$

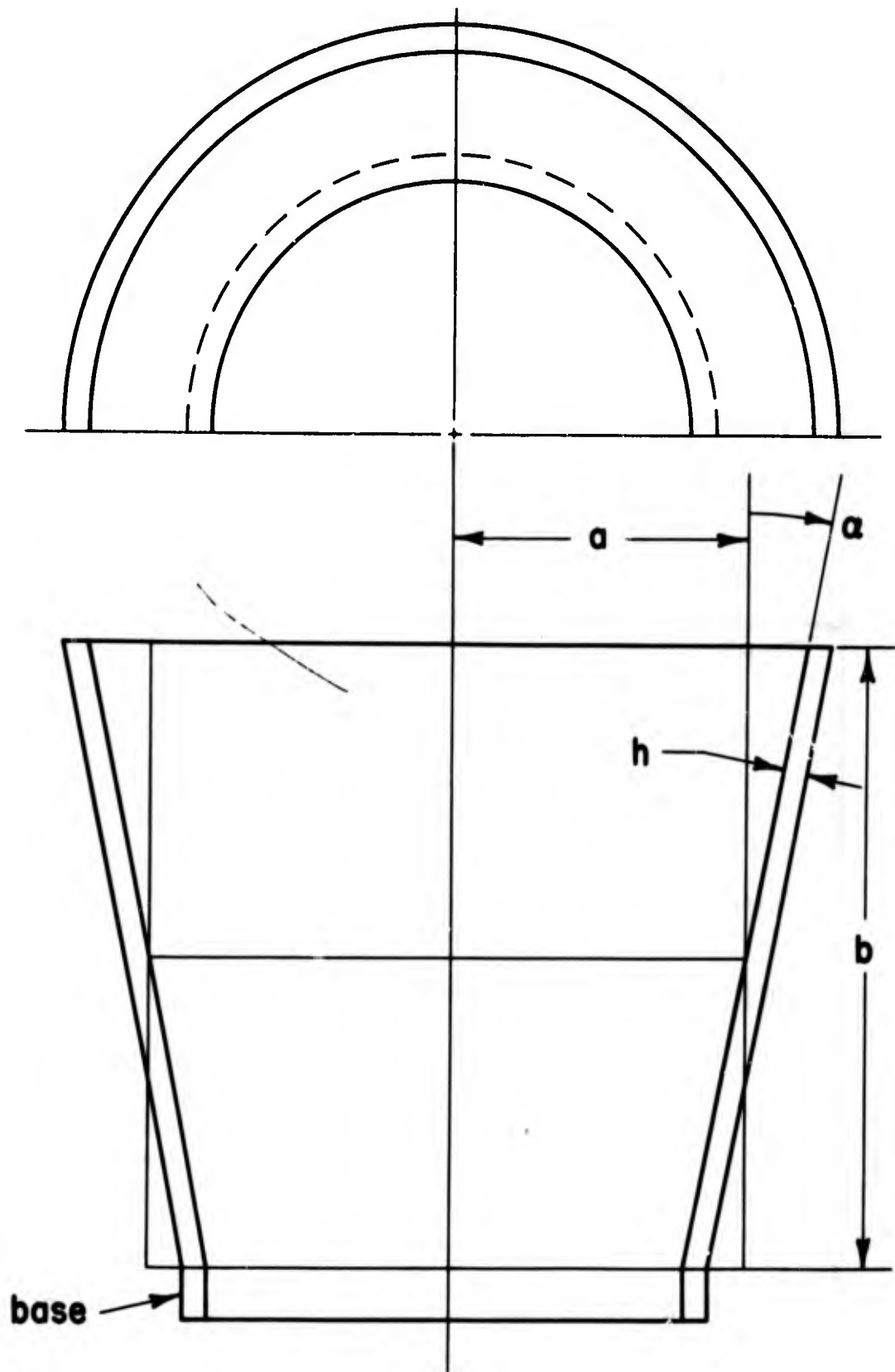
$$E \equiv \left(\frac{d\sigma_L}{d\epsilon_L} \right)_{\epsilon_L \text{ small}}$$

$$E' \equiv \left(\frac{d\sigma_L}{d\epsilon_L} \right)_{\epsilon_L \text{ large}}$$

$$-\nu \equiv \left(\frac{d\epsilon_t}{d\epsilon_L} \right)_{\epsilon_L \text{ small}}$$

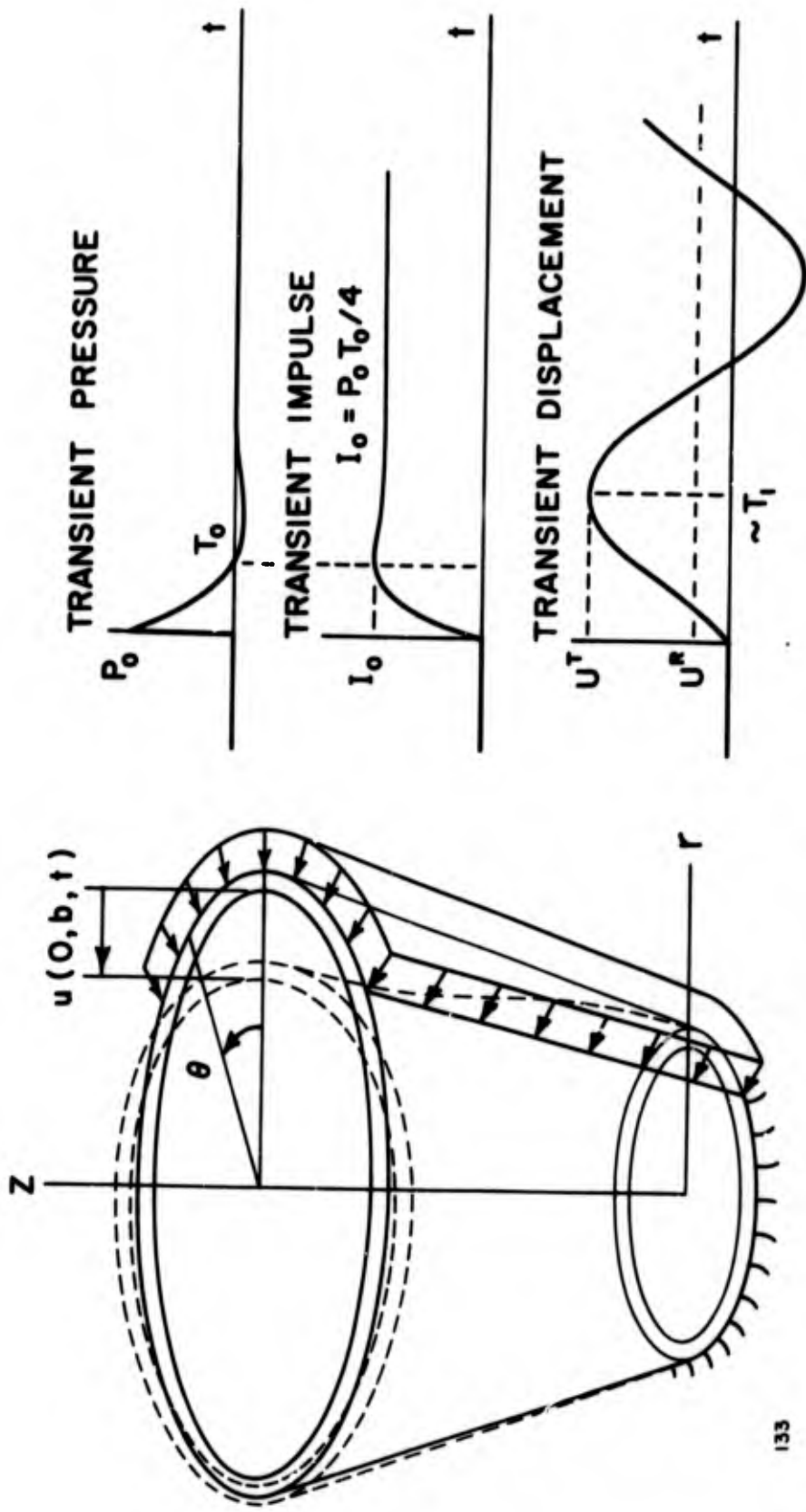
$$-\nu' \equiv \left(\frac{d\epsilon_t}{d\epsilon_L} \right)_{\epsilon_L \text{ large}}$$

FIGURE 2. INTERPRETATION OF UNIAXIAL COMPRESSION TEST DATA



128

FIGURE 3. SHELL GEOMETRY



133

FIGURE 4. IDEALIZED IMPULSIVE LOAD DISTRIBUTION AND TRANSIENT DISPLACEMENTS OF A CONICAL FRUSTUM SHELL

KEY TO NUMBERED ITEMS IN FIGURE 5

Shock Tube

1. Recoil Block
2. Large Volume Air Reservoir ($\sim 8 \text{ ft}^3$)
3. Partition for Small Volume Air Reservoir ($\sim 1 \text{ ft}^3$)
4. Mylar Burst-Diaphragm
5. Shock Tube Barrel
6. Oscilloscope Triggering Mechanism

Test Stand

7. Kistler Pressure Transducer Mounted in Rubber-Supported Lead Block
8. Motor for Rotating Displacement-Probe Fixture
9. Model Mounting Plate
10. Model Conical Shell
11. Three Bentley Displacement Transducers Mounted in Adjustable Fixture
12. Switch for Controlling Motor (8)
13. Blast Shield
14. Bentley Distance Detectors
15. Test Stand
16. Power Supply Box

Compressed Air Supply

17. Pipe to Air Compressor
18. Reservoir Feed Pipe
19. Reservoir Gauge Pipe
20. Pressure Gauges
21. Exhaust Valve
22. Pressurization Valve

Instrumentation

23. Electrical Cables
24. Dry-Cell Battery for Triggering Oscilloscope
25. Oscilloscope for Recording Displacements of Model Shells
26. Oscilloscope for Recording Transient Pressure and Impulse
27. Kistler Amplifier



FIGURE 6. SHOCK TUBE MODEL TEST FACILITY



FIGURE 7. MODEL SHELL MOUNTED ON THE TEST STAND

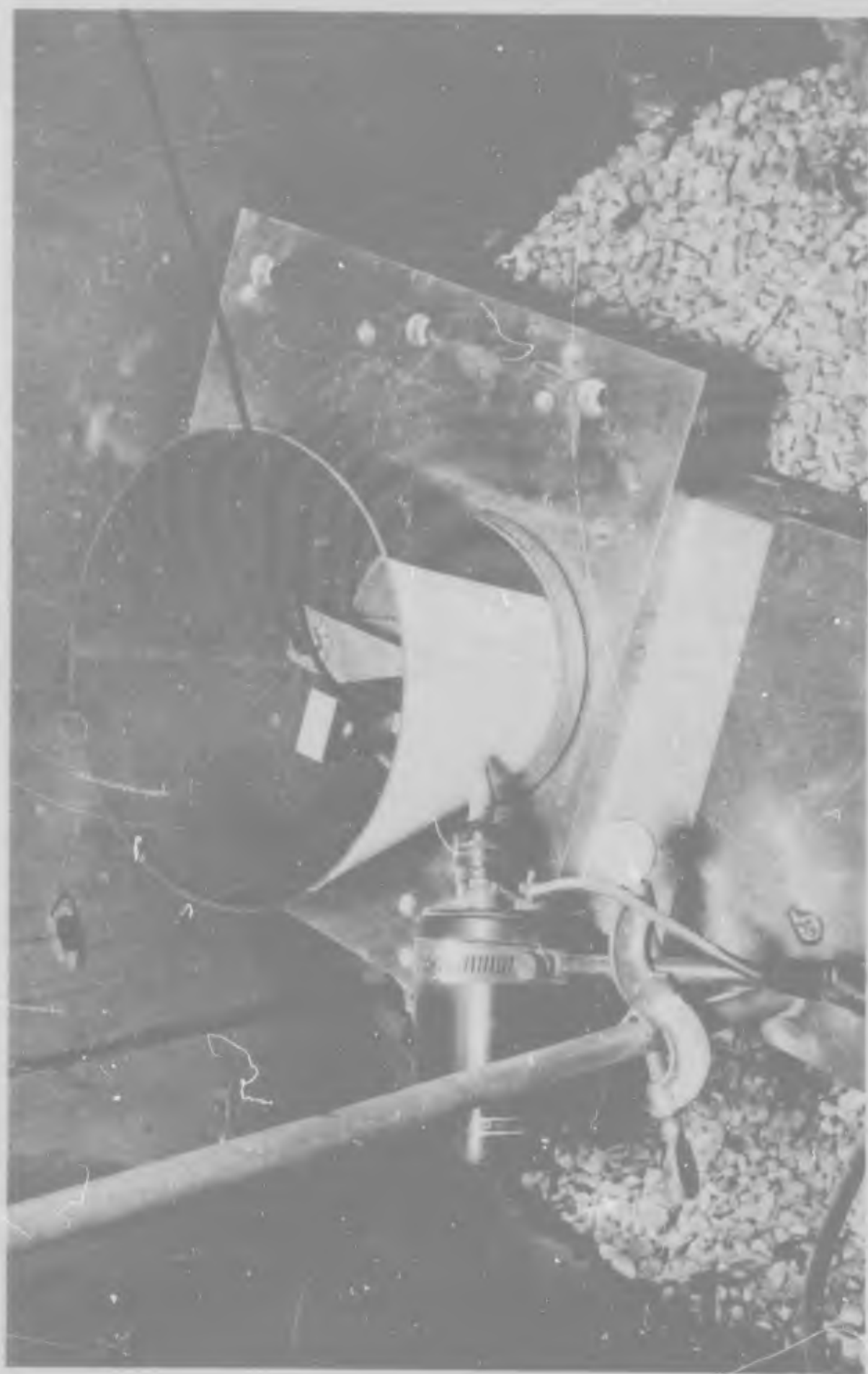
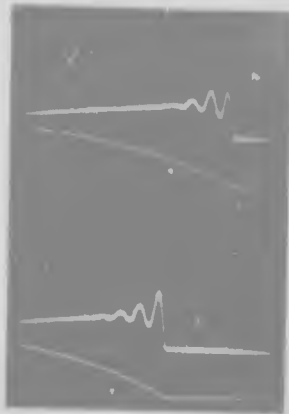


FIGURE 8. SPRAYED EXPLOSIVES TEST FACILITY



CALIBRATION OF
PRESSURE AND
IMPULSE SIGNALS

$k_T = 100 \text{ ms/cm}$
 $\delta_P = 4 \text{ psi}$



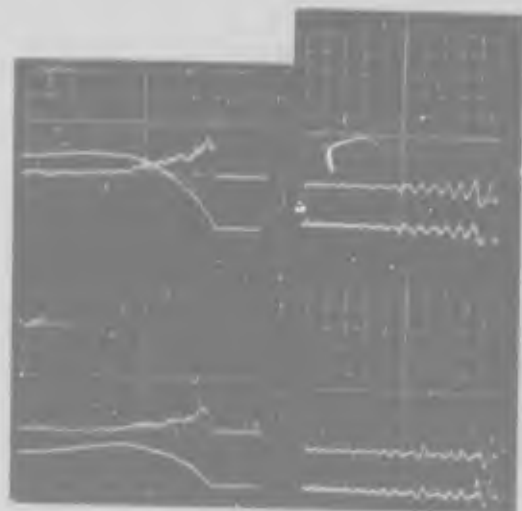
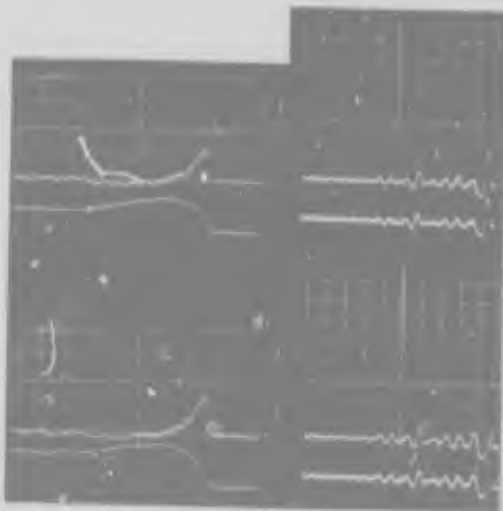
CALIBRATION OF
DISPLACEMENT
TRANSDUCERS

$C_T = 5 \text{ sec/cm}$
 $\delta_X = .05 \text{ in}$



RECORDS FOR
DETERMINING THE
NATURAL FREQUENCY

$C_T = 10 \text{ ms/cm}$
 $C_X \approx .01 \text{ in/cm}$



RECORDS OF TRANSIENT PRESSURE, IMPULSE, AND DISPLACEMENTS

LEFT : UPPER SIGNAL IS TRANSIENT PRESSURE, LOWER SIGNAL IS IMPULSE
RIGHT : SIGNALS CORRESPOND TO UPPER AND LOWER DISPLACEMENT PROBES

$k_T = 1 \text{ ms/cm}$, $k_P = 5 \text{ psi/cm}$, $k_I = 5 \text{ psi-ms/cm}$, $C_T = 10 \text{ ms/cm}$

FIGURE 9. CALIBRATION AND TEST RECORDS

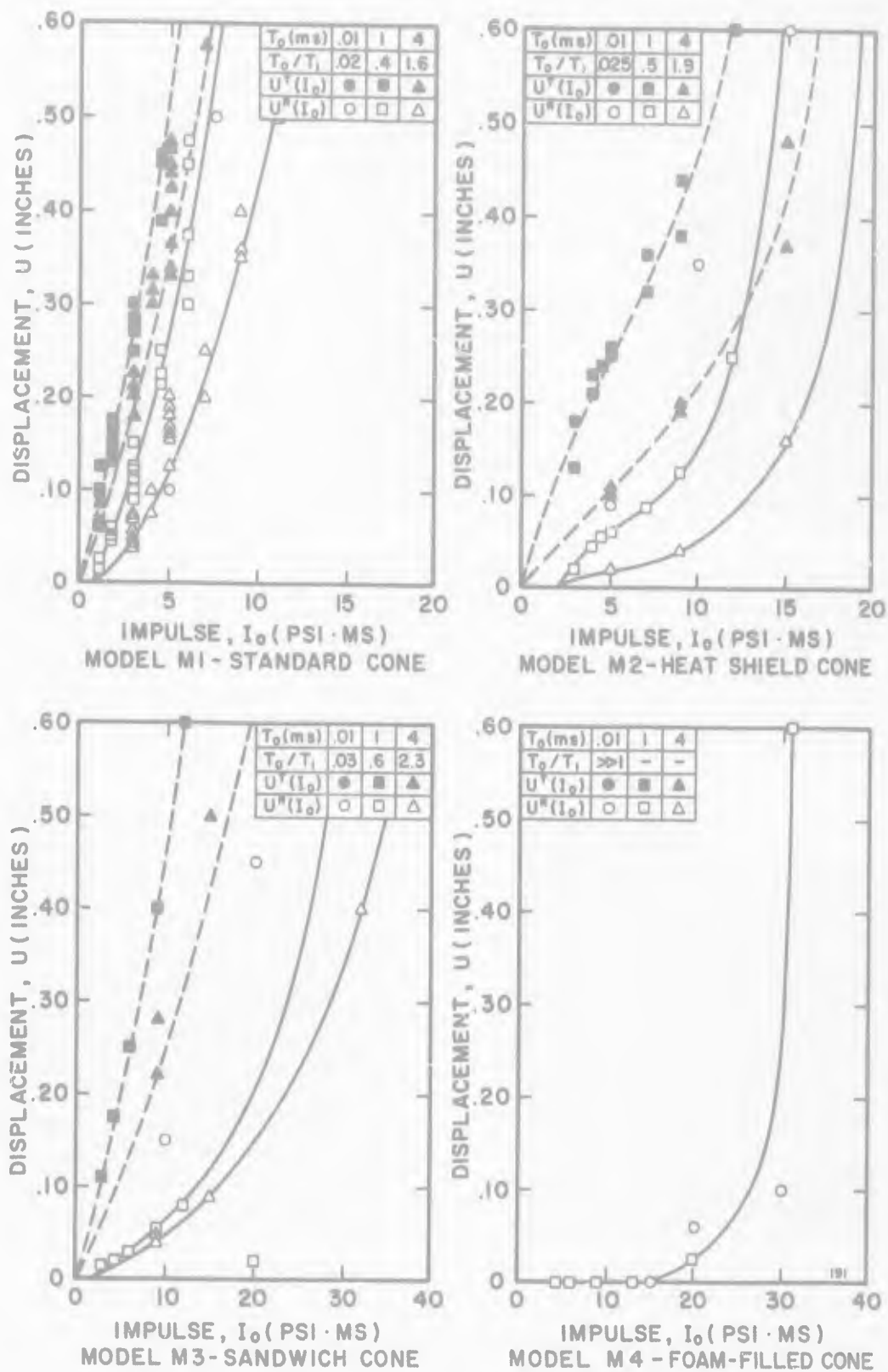


FIGURE 10. IMPULSE-DEFORMATION CHARACTERISTICS OF THE MODELS, I

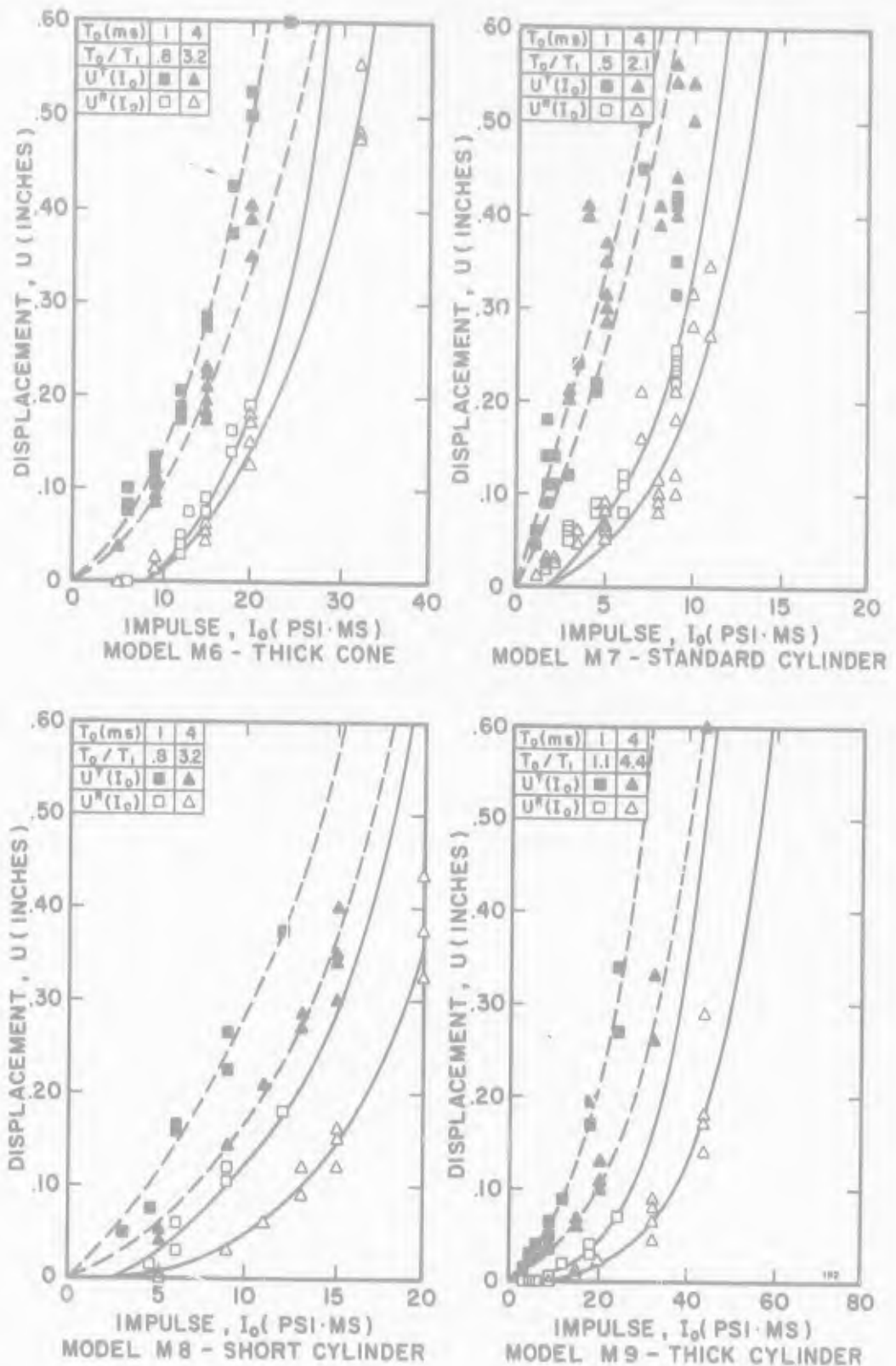


FIGURE II. IMPULSE-DEFORMATION CHARACTERISTICS OF THE MODELS, II

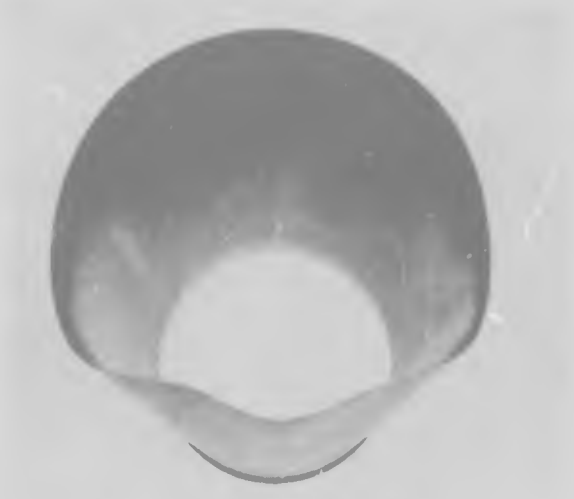
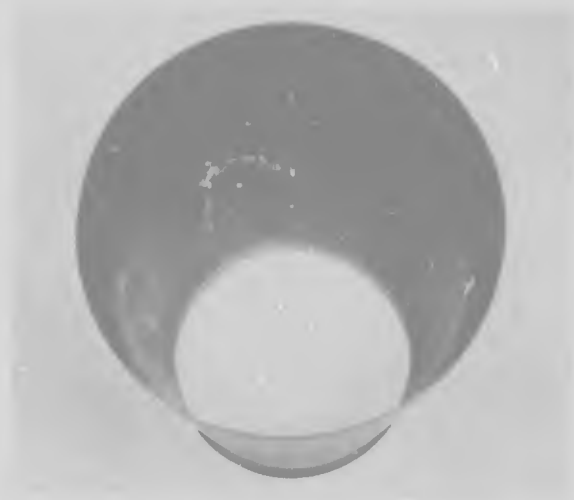


FIGURE 12. STANDARD CONE MODEL M1
BEFORE AND AFTER TESTING



FIGURE 13. STANDARD CYLINDER MODEL M7
BEFORE AND AFTER TESTING

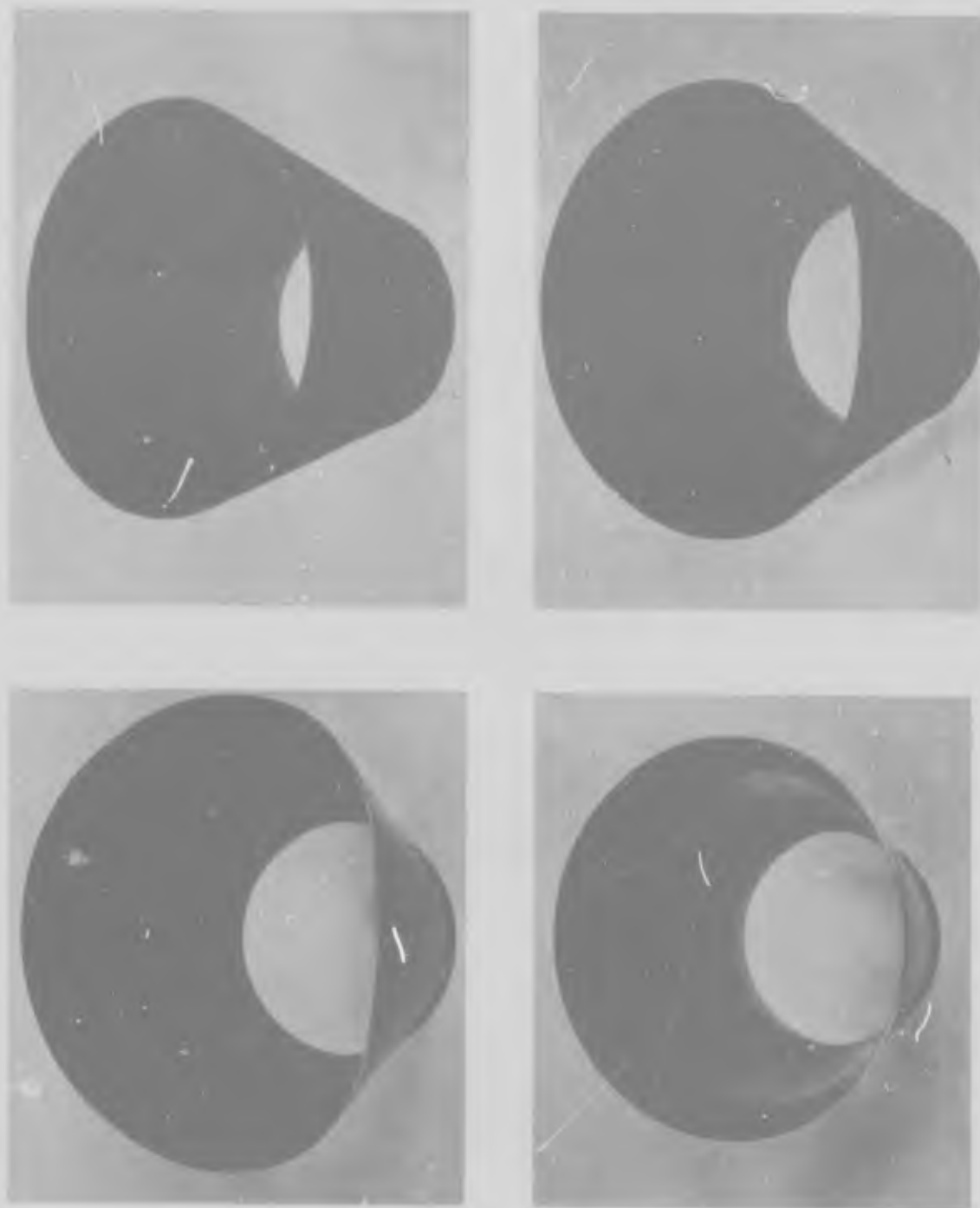


FIGURE 14. THICK CONE MODEL M6 AND HEAT SHIELD MODEL M2

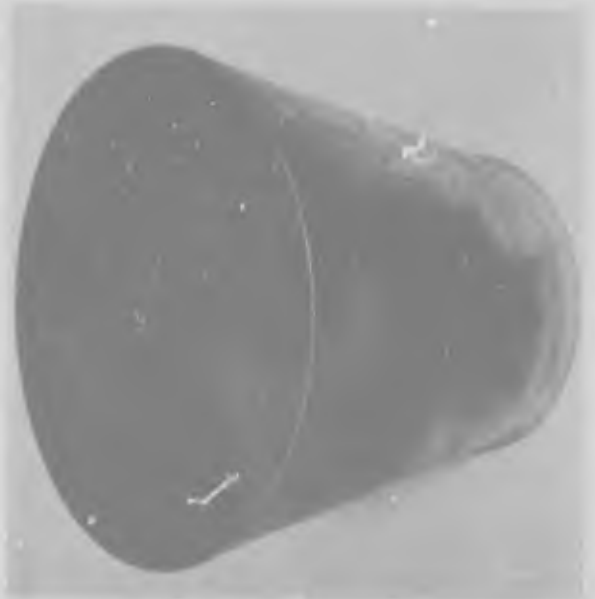
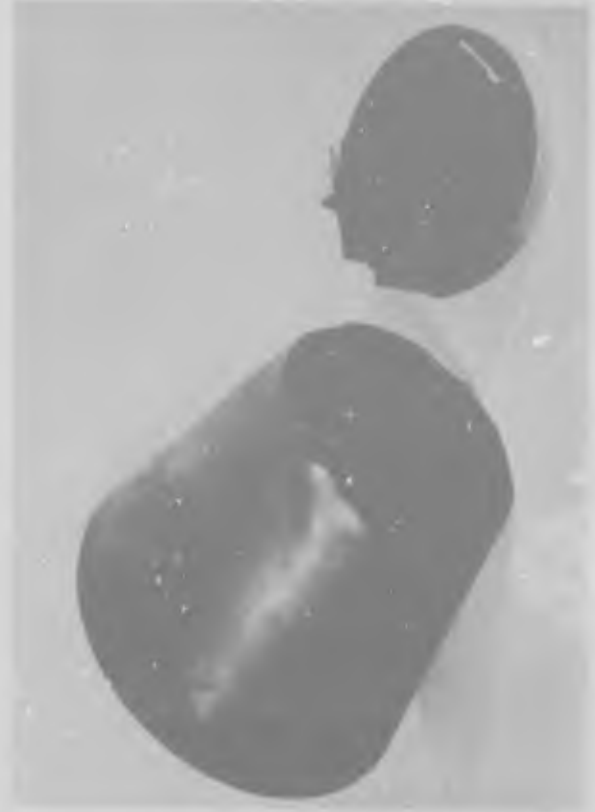


FIGURE 15. SANDWICH MODEL M3 AND FOAM-FILLED MODEL M4



FIGURE 16. PROTOTYPE TEST FACILITY

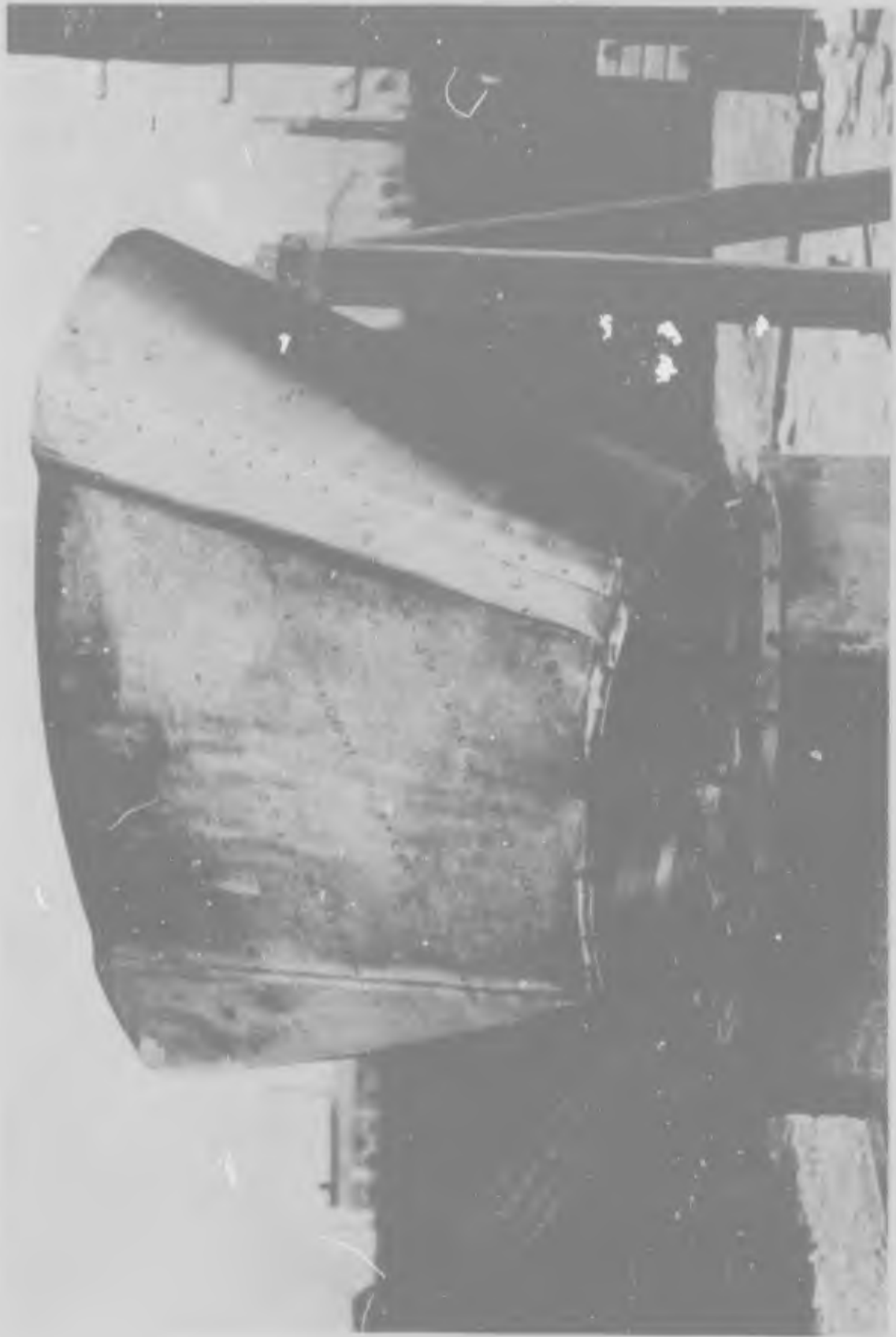


FIGURE 17. SANDWICH PROTOTYPE SHELL, AFTER RECEIVING
AN IMPULSE OF $14,000 \text{ DYNE} \cdot \text{SEC} / \text{CM}^2$



FIGURE 18. HEAT - SHIELD PROTOTYPE SHELL, AFTER RECEIVING
AN IMPULSE OF 3500 DYNE - SEC / CM²

